MEASUREMENTS OF the α PARTICLE INDUCED CURRENT IN METAL FOILS

by

Brian Steward

A thesis submitted to the Faculty and the Board of Trustees of the Colorado School of Mines in partial fulfillment of the requirements for the degree of Masters of Science
(Applied Physics)

Golden, Colorado

Date_____

Signed:_____

Brian Steward

Signed:_____

Dr. Kyle Leach
Thesis Advisor

Golden, Colorado
Date_____

Signed:_____

Dr. Jeff Squier
Professor and
Department Head of Physics

ABSTRACT

We have investigated the use of a 1.3 mCi ^{244}Cm source as a reproduction of a lost α particle flux from high temperature fusion plasma. The purpose of the experiment was to allow the testing of thin-foil Faraday collectors as a lost α particle diagnostic. Many sets of measurements were made: the first with a single thick Al sheet and subsequently with a thin (2.5 μm) Ni foil backed by a thick Al sheet under varying conditions. The measurements were made with a commercial Keithley picoammeter and with a custom built high precision current integrator. Measurements were made at pressures between 1 mTorr and atmosphere. At higher pressures, above 1 Torr, the measured current was greatly exceeded by the predicted current. At lower pressures, less than 0.1 Torr, the measured current was observed to be in rough agreement with the expected current. A new technique to measure pressure in the regime of 1 to 50 Torr with an accuracy of about 1% at the lower pressures is explored.

TABLE OF CONTENTS

LIST OF FIGURES

CHAPTER 1

INTRODUCTION AND BACKGROUND

Many types of fusion reactors use strong magnetic fields which confine charged radiation such as α particles. It is desirable to contain as much of this charged radiation as possible because it contributes to the heating of the plasma, ultimately leading to a more efficient reaction. A characterization of the flux of α particles escaping the magnetic confinement of this fusion reaction would be useful as a diagnostic tool.

A model detection apparatus capable of detecting both the number and energy of incident α-particles has been researched. Specifically, this model detector is designed for use in Tokamak fusion reactors for the purpose of lost α particle detection and diagnostic. Finding the flux of α particles incident on the detector is of primary importance, but the energy of each of the α particles is also important information.

The Tokamak fusion reactor environment in which the detection apparatus must function is important to consider. Tokamak reactors utilize strong magnetic fields to heat and confine plasma and these fields will also affect the radiation incident on the detector, demonstrated by F.E. Cecil et al. [1]. Tokamak reactors are operated in an ultra-low pressure regime, as is discussed by M.J. Loughlin et al [2]. The reaction in question is explored in order to illuminate the radiation fluxes which the detector must be able cope with in a fusion reaction environment.

1.1 Reaction

The reaction which dominates in fusion reactions in modern Tokamak reactors is the deuterium tritium fusion reaction, or d-t reaction, according to J.C. Barbour et al[3]. The nuclear reaction's equation is shown in equation 1.1, taken from Krane [4].

$$ {}^{2}_{1}H + {}^{3}_{1}H \rightarrow {}^{4}_{2}He(3.5MeV) + {}^{1}_{0}n(14.1MeV) \tag{1.1} $$

The by products of the d-t reaction are α particles and fast neutrons, where fast neutrons refer to neutrons with energies ranging from about 1-20 MeV according to Carron[14]. The average energy of the products are also shown in equation 1.1. Only considering equation 1.1 one might expect the equal number of each species of product per reaction to indicate that the detector should observe an equal flux of each species of products. In actuality this is far from the case due to the magnetic method of plasma confinement utilized in Tokamak reactor design.

1.2 Tokamak Reactors

Tokamak reactors use large magnetic fields to confine and heat deuterium tritium plasma until d-t reactions occur. Broadly speaking, Tokamak reactors consume plasma fuel inside of an evacuated torus shaped coil. The coil has a large current driven through it to create a large magnetic field inside of the torus according to Bondarenko [15]

Because Tokamak reactors rely on strong magnetic fields to confine the nuclear reaction, the large majority of the α particle products of the reaction will be contained in the plasma due to the α particles charge, and never make it to the detector. The containment of the α particles is essential to Tokamak plasma heating. The more α particles confined in the plasma, the higher the temperature of the plasma, and the more reactions will occur as is shown in $Plasma\ Science$ [5]. Finding how many α particles escape from confinement is of interest in Tokamak reactors. The neutrons produced in the d-t reaction are uncharged and will not be affected by the strong magnetic field, meaning that the neutron particle flux at the detector will be much larger than the flux of α particles. The detector must be able to discriminate between signals from a potentially small α particle flux and signals from a much larger neutron flux.

1.3 Background Radiation as a Noise Source

The main type of radiation that could overwhelm the detector, given the detectors environment, is a large unconfined fast neutron flux. The current from the generally confined α particles that escape and become incident on the detectors surface must be greater than the current induced by non-confined fast neutrons. The current induced by a neutron flux in a simple sheet of nickel can be described as,

$$I_N \approx \Phi_N * N_T * \sigma_n * e \tag{1.2}$$

in which Φ_N is the flux of neutrons, N_T is the number of targets in a volume of nickel, σ_n is the cross section of reaction for fast neutrons in nickel, and e is the fundamental charge with a value of $1.602{*}10^{-19}$ C. This quantity must be much lower than the current induced by α particles incident upon the same sheet of nickel if the detector is to accurately diagnose lost α fluxes. The induced current due to α particle flux can be approximated by,

$$I_\alpha \approx \Phi_\alpha * 2e \tag{1.3}$$

in which the nickel sheet is assumed to have absorbed the incident α particles as current with 100% efficiency. Dividing the values of I_α by I_N will yield the effective signal to noise ratio of the detector. This calculation, with constants input, and assuming an α particle flux which is .1%

of the neutron flux is,

$$\frac{I_\alpha}{I_N} = \frac{\Phi_\alpha * 2e}{\Phi_N * N_T * \sigma_n * e} = \frac{1}{500 * N_T * \sigma_n} \approx 241 \tag{1.4}$$

The assumption of an approximate .1% flux ratio, $\frac{\Phi_\alpha}{\Phi_N}$, is supported by Cecil et al[6]. The cross section of the reaction between a projectile 14.5 MeV neutron and a target of nickel is taken from the National Nuclear Data Center[7] and has a very small value of σ_n=.46 barnes. The 14.5 MeV energy of the neutron is very close to the 14.1 MeV expected neutron energy from equation 1.1. The number of targets is calculated using 8.908 $\frac{g}{cm^3}$ as the density of nickel, taken from $Density\ of\ elements$[8]. This sets the value of N_T to $2.06 * 10^{19}$ targets for a 1 cm by 1 cm by 2.5 μm sheet of nickel. This signal-noise ratio indicates that the current induced by α particles is 241 times greater than the current induced by the neutron flux. This high signal to noise ratio indicates that a nickel sheet would make a good detection device for α particles in a high neutron flux environment.

1.4 Radioactivity

One curie is defined as 3.7×10^{10} decay events per second. Each of the decay events experienced by the ^{244}Cm source used in these experiments will result in an α particle being produced, as ^{244}Cm decays only via α radiation. This 1.3 mCi source therefore emits 4.81×10^7 alpha particles every second.

Every emitted alpha particle will carry a charge of $2e$ where e is the charge of a single proton. The numeric value of e is 1.602×10^{-19}. The expected value of the current due to α particle capture assuming perfect collection of all incident α particles can be calculated using equation 1.5.

$$I_{detector} = \frac{Q_{incident}}{t} \tag{1.5}$$

The amount of charge incident on the detectors surface will depend on the flux of α particles at the detector, which will depend on the chamber pressure.

When the incident charge is in question a key factor to consider is the geometry of the detector and of the source. Geometric setups in which the radiation source is farther away from the detector should correspond to a decrease in the current collected by the detector. Many trials of the experiment utilized a point blank style setup in which the radiation source and detector were very close together. Using a typical assumption of isotropic radioactive decay the point blank setup case is approximated by half of the solid angle being covered by the detector, and thus half of the total charge being captured. In this case equation 1.5 is shown to be equal to equation 1.6

$$I = \frac{1}{2} * 2 \times 1.602 \times 10^{-19} \times 4.81 \times 10^{-7} \approx 7.7 \times 10^{-12} A \tag{1.6}$$

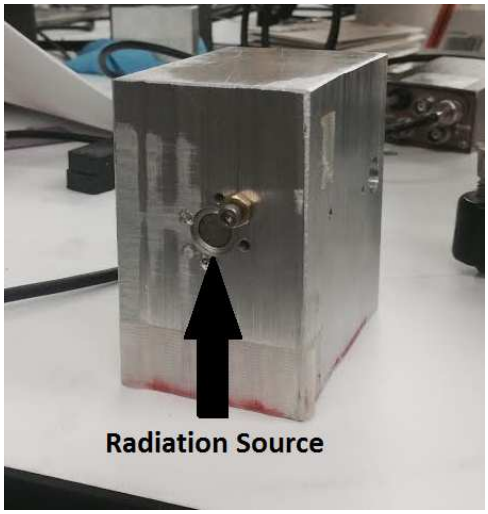

Figure 1.1: The radiation source

or about 7.7pA. This can be challenging to measure accurately.

1.5 α Particle Source

A well described source of α particles is vital to demonstrate the feasibility of using this style of detector. With a well known source of radiation the behavior of the detector can be classified and investigated without having to worry about uncertainty in observed current due to the source of the α radiation. Well characterized α particles can be produced at accelerator beams. Using an accelerator beam as an α particle source has the advantage of having a tunable initial α particle energy. Accelerator beams also allow for the flux of incoming α particles to be changed. These benefits would make it easier to explore the workings of the detector. The main issue with using an accelerator as an α particle source is the costly operation and sparse availability of accelerators in general.

A radioactive source for testing the detector which only emitted α particle radiation and produced monoenergetic α particles, or at least close to monoenergetic particles would be best for reducing potentially confounding radiation sources. This means that a radioactive source with a single decay pathway would be best, or if an isotope decayed via several pathways the energies of emitted α particles should be close together. Several radioactive sources would work well, but the experiments described in this report were run with Curium 244, denoted ^{244}Cm. There are two significant pathways for the decay of ^{244}Cm, both via α particle emission. Approximately a quarter of emitted α particles have an initial energy of 5.76 MeV, and virtually all of the other emitted α particles have an initial energy of 5.80 MeV, according to the National Nuclear Data Base[9]. A picture of the radiation source can be seen in figure 1.1.

To investigate the detector with the ^{244}Cm source, a chamber was evacuated to better simulate a Tokamak reactor environment.

1.6 Stopping and Ranges of Ions in Matter

A program called Stopping and Ranges of Ions in Matter, better known by its acronym SRIM, was used in the analysis of the data obtained from the detector setups [11]. This program is able to calculate the distance an ion, in this case an α particle, travels through a medium before it is stopped. In the process of doing this many other useful bits of information are determined including the number of ion pairs produced, the number of transmitted ions and the lateral range of the ions in the medium. Information on the initial conditions that one must provide to SRIM to get these calculations include the composition of the medium, the initial energy and species of ion and depth of the medium.

The inner workings of the mathematics of SRIM are thoroughly discussed in the SRIM handbook by Ziegler[11], and will not be considered in this paper. Suffice it to say that SRIM is a well respected and often used tool in nuclear physics circles.

1.7 Custom Charge Integrating Circuit

A custom charge integrating circuit was used in some of the experimental trials. The custom current detection circuit essentially consists of an operational amplifier grounded on its positive terminal and with its output connected to its negative input terminal via a capacitor.

The use of an amplifier helped to relieve some of the challenges of detection by changing the variable to be measured to voltage and boosting the signal. Instead of trying to detect picoamps of current the circuit output voltage will be on the order of millivolts. The schematic design of the current detection circuit can be seen in appendix D .

The output voltage of this circuit is

$$V_0 = \frac{-1}{C} \int I(t)dt \tag{1.7}$$

in which C is the capacitance of the capacitor, $I(t)$ is the current running through the detector, and V_0 is the output voltage. This equation can be obtained from a simple analysis of the circuit diagram. Equation 1.7 suggests that the current collected in the detector is stored in the capacitor. As the capacitor charges, the output voltage increases. Thus the maximum voltage reached over a known collection time indicates the current observed.

In the radioactive decay of ^{244}Cm the flux of emitted α particles is approximated to be constant for the duration of the very small collection time. If the current $I(t)$ is constant then equation 1.7

reduces to

$$V_0 = I\frac{t}{C} \tag{1.8}$$

where t is the time period over which current was integrated in the circuit. In practice the collection time is very small so that the voltage, and thus current, can be measured quickly. The components of the detection circuit were chosen carefully so that the resolution of the detector would be robust. The circuit's performance was compared to that of a more traditional Keithley picoammeter to ensure its validity as a current detection apparatus. The statistical measure used for this comparison is the Pearson correlation coefficient taken from $Pearson\ Correlation$ [12].

1.8 Bethe Formula

The Bethe formula is used to describe the energy lost by a heavy ion moving through a medium. Ion pairs are created in the medium which the heavy ion moves through. These ion pairs which are created can affect the current measured by the detector. The Bethe formula is useful in determining the energy loss along the path traveled by an ion. The usefulness of the Bethe formula is limited to situations in which the energy of the projectile ion is in the range of keV to MeV and to situations where the ion is much heavier than an electron. For the analysis done in this project the ion is an α particle, which starts with an initial energy of approximately 5.8 MeV. α particles are nearly 8000 times as massive as electrons and 5.8 MeV is comfortably in the range of Bethe formula ion energy validity, indicating that this formula will work well in the analysis. The Bethe formula in this case is applied to α particles moving through air on their way to the detector. The Bethe formula is

$$-\left(\frac{dE}{dx}\right) = \left(\frac{4\pi}{m_e c^2}\right) * \left(\frac{N_T * Z_p^2 * Z_t}{\beta^2}\right) * \left(\frac{e^2}{4\pi\epsilon_0}\right)^2 * \left(\ln\left[\frac{2m_e v^2}{I(1-\beta^2)}\right] - \beta^2\right) \tag{1.9}$$

where $\frac{dE}{dx}$ refers to the amount of energy a projectile ion loses in a differential step of length dx. The mass of an electron is denoted m_e, the speed of light is denoted c, Z_p represents the atomic number of the projected ion, Z_t is the atomic number of the medium through which the ion is moving, ϵ_0 is the vacuum permittivity constant, v is the relativistic velocity of the heavy ion, β is equal to $\frac{v}{c}$ and I is the ionization energy for the given atom in the material, called the mean excitation potential. This version of the Bethe formula is taken from Sigmund [13].

1.9 Solid Angle Emission

The Bethe formula describes the position dependent energy loss due to the ionization of a medium through which a heavy ion travels. If the electrons ionized by the incoming α particles are assumed to be emitted isotropically from the point of interaction we can develop a simple solution for the number of electrons incident on the detector based on the portion of the solid angle covered

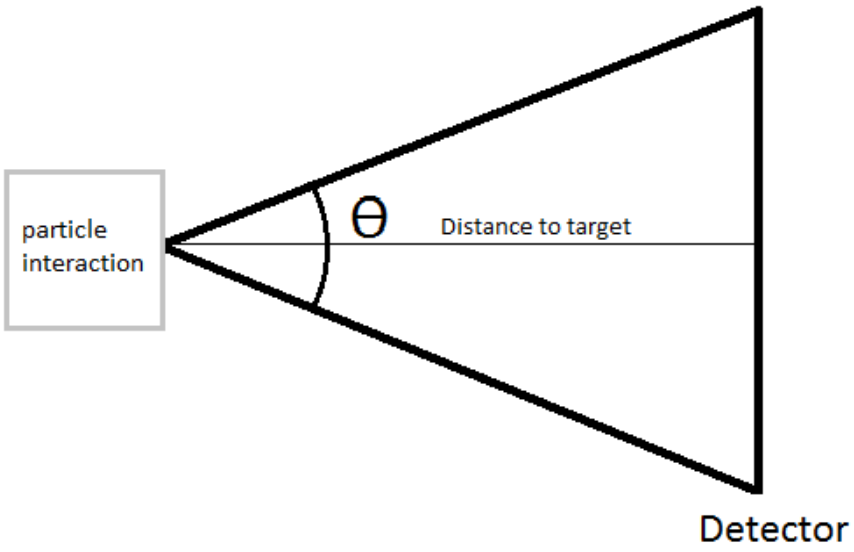

Figure 1.2: The geometry of emitted electrons

by the detector. The geometry of this angle can be seen in figure 1.2. The value of θ in figure 1.2 is associated with the spread of electrons in the plane of the detector. The other angle describing the spread of the emitted electrons, ϕ, is assumed to be equal to θ due to the symmetry of the detector and the process. Using the geometry presented in figure 1.2, and integrating over θ and ϕ the solid angle covered by the detector can be expressed as

$$\Omega = 2 * \arctan\left(\frac{l}{2d}\right) * \left(1 - \cos\left(2 * \arctan\left(\frac{w}{2d}\right)\right)\right) \tag{1.10}$$

in which l is the length of the detector, w the width of the detector and d is the distance between the ionization interaction and the detector. The solid angle formula is useful in analysis because it indicates the relative size of the detector as seen by an electron which has become ionized by the α particle and may end up being collected by the detector as current.

CHAPTER 2

EXPERIMENTAL PROCEDURES

A ^{244}Cm Source was placed in a vacuum chamber in front of an α particle detector apparatus. The signal from the detector was read on either a commercial Keithley picoammeter or using the detection circuit described in section 1.7. The pressure in the chamber was varied and the output of the detection apparatus was measured. Two iterations of detector were examined in this setup. Other additions and slight changes were also made to the setup. The distance between detector and source was changed, voltage biases were applied to the layers of the detectors, magnetic fields were applied and the orientation of the detector was changed. In all cases data relating the pressure in the chamber and the current in the detector was recorded. Each apparatus was constructed to help answer a potential question about the functioning of the detector.

2.1 Design

Obtaining information on the depth into a metal an α particle has traveled can be found by layering thin foils of the metal and collecting the current from each of theses foils individually. If an α particle hits the first thin layer and is not stopped, it will lose some of its initial energy and will continue on to the second thin metal layer. The α particle will continue to lose energy until it stops in one of the thin foils and current is collected in that foil. Because the number of and thickness of each of foils the α particle moved through before it was stopped is known, the total energy lost, and thus the initial energy, can be solved for. The aggregate current from all of the foils will still reveal the total flux of the incident α particles, but the layer in which current is collected will give a range of possible initial energies of each incident α particle.

Ideally the detector would be a series of thin layers of metal, each of which are electrically isolated from all of the others and are each of which are connected to a current detector. The layers would alternate between nickel and aluminum, starting with a 2.5 μm thick nickel foil. This technique has been demonstrated before by Cecil et al[1].

For the purpose of testing, a simplified version of this multi-layer detector was constructed and used to test the main principles of detection in this set up. This simplified detector consisted of a 2.5 μm thick foil of nickel connected to a current detection device in front of an aluminum sheet thick enough to stop every α particle incident on its surface, also connected to a current measurement device. A picture of the actual device can be seen in figure 2.1. The simplified detector set up should give two categories for possible incoming α particle energies because there are two layers in which an α particle could embed. To test this configuration of detector a suitable source of α particles is required. While performing the experiments some interesting pressure current relations

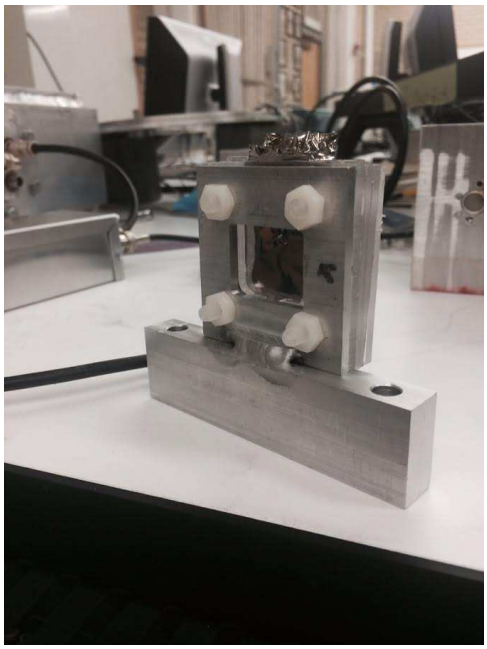

Figure 2.1: The detection apparatus in the multi-layer case

were observed by the detector. This being the case some pressure measurement techniques are discussed.

2.2 Pressure Measurement

An interesting technique for the measurement of air pressure was found while testing a single layer detector. The pressure in the vacuum chamber is linearly correlated with the current induced by the radioactive source. At pressures on the order of 10 Torr the strength of the correlation between pressure and α-particle current is very high. The relation between pressure and current is a new way to measure pressure in vacuum chambers, using a radioactive source and a current meter.

Pressure measurements taken during the experiments were taken with a Convectron pressure gauge. These gauges work by measuring heat loss in a circuit. The sensor is one section of a wheatstone bridge. This ensures that the current in the sensor will change to maintain a balance. Heat is removed via both conduction and convection in a Convectron pressure gauge. The heat losses due to conductive effects measure pressures in the mTorr range and convective heat losses measure high pressure ranges according to Bertolini[10].

2.3 Apparatus

Several related lab setups were used to thoroughly measure the radioactively-induced current in the metal foil style detector used in the experiments. In all of these different setups a 1.3 mCi

source of ^{244}Cm was used to simulate lost α-particle flux from fusion reactions in Tokamak style reactors. The ^{244}Cm was prepared in a vacuum chamber, and the vacuum chamber was evacuated via a mechanical roughing pump. The pressure in the vacuum chamber was measured with a Convectron pressure gauge, capable of reporting pressures in the range of 950 Torr to 1 millitorr.

2.3.1 Single Sheet Detector

In the first setup a thick aluminum sheet was placed inside the vacuum chamber, approximately 3 cm away from the ^{244}Cm source of α-particles. This is visualized in figure 2.2. The aluminum

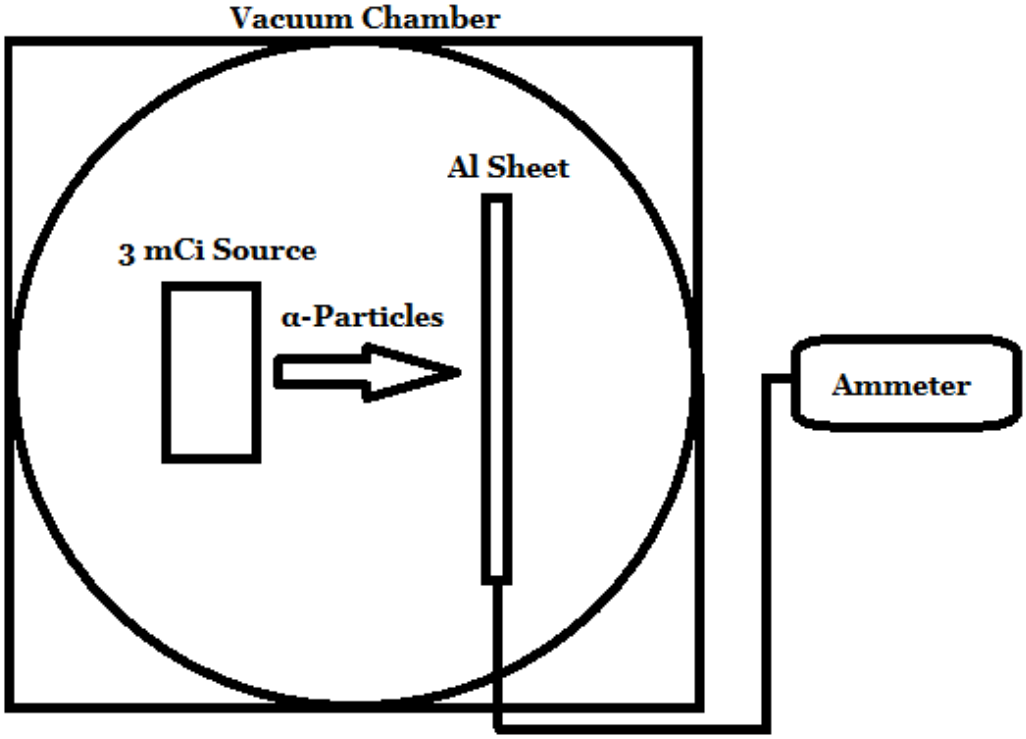

Figure 2.2: The experimental setup in the single metal case

sheet was electrically connected via coaxial cable to a Keithley picoammeter, as is shown in figure 2.3. The ammeter was used in the first experimental setup in place of the current integration circuit used in later trials. The single metal sheet style detector was tested first in this simple setup. This simple setup was intended to clarify the basic pressure current relation in the detector system. Variations on the single metal sheet style detector experiment were run to further probe the system.

In a setup related to the simple single metal sheet detector apparatus the aluminum sheet was voltage biased either positively or negatively at an intensity of 18 V. These biases were achieved by using two 9 V batteries wired in series. The voltage biased setup for the single aluminum sheet style detector can be seen in figure 2.4. This bias was added in order to attempt to discriminate between

Figure 2.3: The Keithley picoammeter

different types of incoming radiation. A positive voltage bias would be expected to push more incident electrons as current and a negative voltage bias would be expected to facilitate positive charged particle flow, namely α particles. Some interesting data was obtained in this alternate single sheet detector setup.

A second setup involved utilizing a different current measurement device. The new current detection device was used in a setup very similar to the first setup described. The second setup still included a 1.3 mCi ^{244}Cm source of α-particles; however, the current collected in this arrangement was run through an ORTEC research amplifier, differing from the previous experiment's layout. The ORTEC amplifier was used to help reduce electronic noise in the data. The biggest difference between the first and second setup was the replacement of the Keithley picoammeter with a new current measurement device. The new device is a specialty current integration device. The output of this device was connected to an oscilloscope, which facilitated measurements and checked on the operation of the circuit. The Keithley picoammeter was replaced by the current integrator circuit in order to increase the resolution of the current measurements in the picoamp range. The integrating circuit uses the connection between the charging time of a capacitor and that capacitors output voltage, as is described in equation 1.8, to determine the current collected by the aluminum sheet. The data obtained using a single aluminum sheet as a detector indicated important detection principles in this setup. To learn more information about the incoming α particles the detector must be improved from a single metal sheet style. A multi-layer device is ultimately required, in this detection scheme, to get information on incident α particle energy.

2.3.2 Multi-Layer Detector

A set of measurements was taken using an improved detection device. In this experimental variation a thin foil of nickel was placed just in front of the aluminum sheet, impeding the α particles coming from the ^{244}Cm source on their way to the thick aluminum sheet. This nickel foil

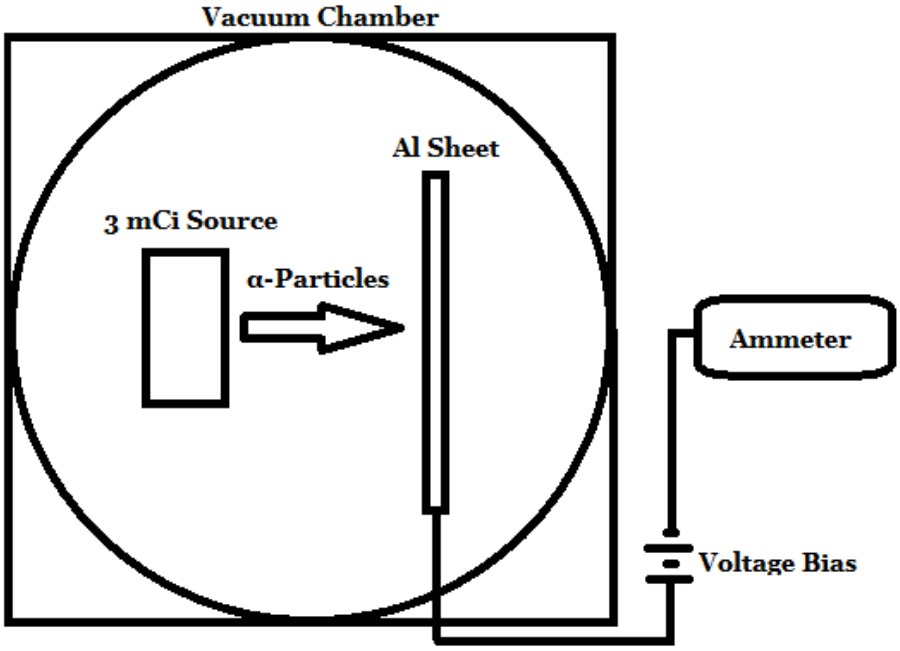

Figure 2.4: The experimental setup with the aluminum sheet and a voltage bias

is $2.5\mu m$ thick. A visual representation of the simplest layout of the experiment with the more sophisticated detector can be seen in figure 2.5. A picture of the actual detector can be seen in figure 2.1.

The thin nickel foil, the aluminum sheet, and the ^{244}Cm source were once again all contained in a vacuum chamber which was evacuated in 42 steps, with pressures ranging from 999 Torr to 2 mTorr, by a mechanical roughing pump. The output data from the aluminum sheet in this setup was taken with both the Keithley picoammeter, and the current integration circuit. Current collected by the thin nickel foil was also recorded. Data was taken using many different variations of the multi-layer detector experiment.

The first variation on the multi-layer detector experiment was the distance between the source and the detector. Trials were run at a distance of either 7 mm $\pm$ 1 mm or at a distance of 45 mm $\pm$ 2 mm. This experiment was run in order to help assess the component of the flux of ionized electrons contributing to current measurements in the device. A source further from the target should increase the electron flux, as more air targets should be available along the longer α particle track. The α particle induced current should decrease with a larger distance between source and detector because the detector covers a smaller solid angle at a greater distance.

Another variation on the multi-layer detector experiment involved voltage biasing the detectors. The combinations of voltage biases were explored thoroughly, with either a positive, negative or no bias applied to each of the layers of the detector. The intensity of these biases were either positive or

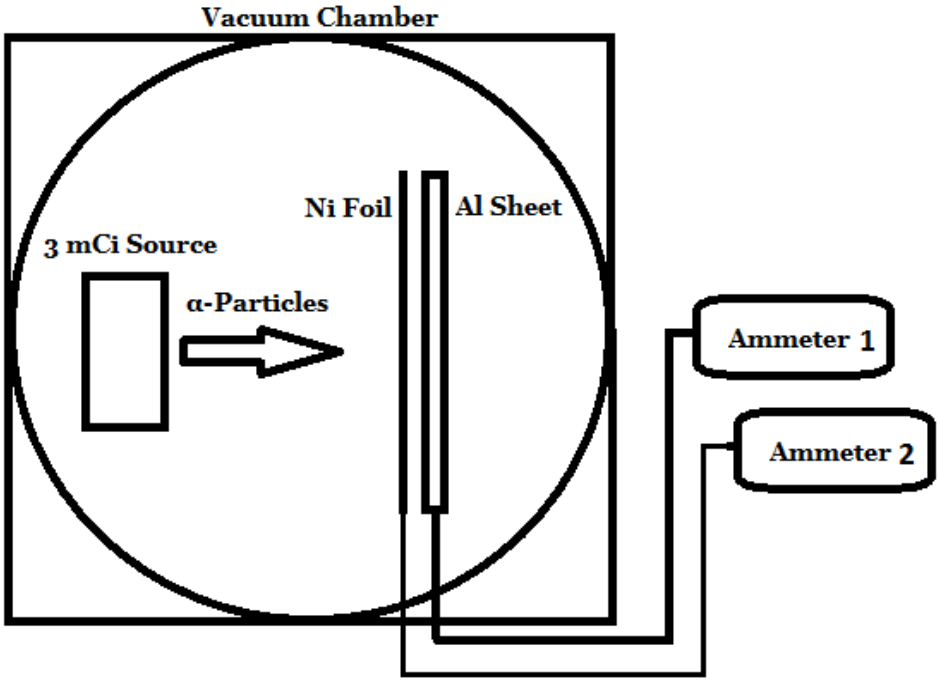

Figure 2.5: The setup for the multi-layer current detector

negative 18 V, supplied by two 9 V batteries in series. A simple schematic of this setup can be seen in figure 2.6. The bias applied to each of the detectors was meant to help discriminate between positive charge carriers causing current and negitive charge carriers doing the same. Electrons should be helped by a positive voltage bias on a detector.

To probe the characteristics of the detector, the orientation of the source and of the detector were varied. Figure 2.7 shows the case where the source was aimed at the thin edge of the detector. This orientation was used to study the electron flux. In this orientation the flux of ionized electrons incident on the thin detectors edge should be small, and the electron flux on the thick sheet should still be small but greater than the electron flux on the thin sheet due its greater exposed surface area. Another orientation scheme had the source aimed at the back side of the detector, so that incoming α particles would encounter the aluminum sheet before the thin nickel foil. The backwards detection arrangement was expected to show a large flux of current in the aluminum sheet, and no current in the nickel foil. All incident α particles and all incident ionized electrons should be collected in the aluminum sheet.

The experiment was also tweaked with the addition of a magnetic field. Strong magnetic fields are present in Tokamak style fusion reactors, so the inclusion of a magnetic field in the apparatus seems natural. The magnetic field was induced by opposing rare earth bar magnets as is depicted in figure 2.8. These bar magnets had a strength of approximately .01 T [16]. The magnetic field was added so that electrons could potentially be screened from the detector. A magnetic field will curve

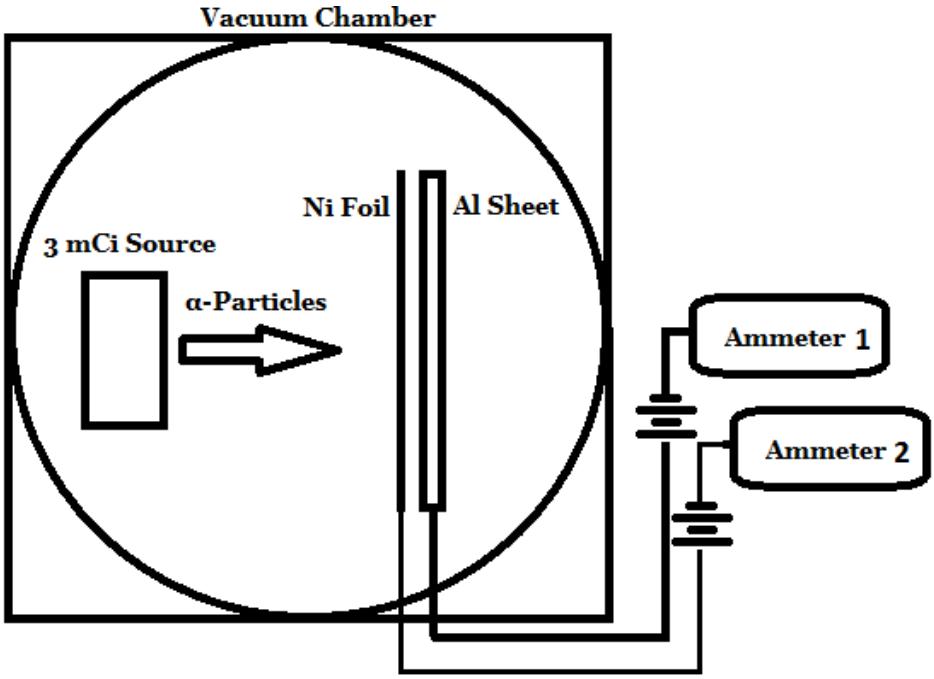

Figure 2.6: The setup for the multi-layer current detector with voltage biases applied to the detectors

the trajectories of charged particles moving through them, according to the well known Lorentz force, $F = (q * v) \times B$. Because electrons are much lighter than α particles they should be curved much more for a given magnetic field. This means that the flux of electrons should be reduced by an applied magnetic field and the flux of α particles should remain relatively unchanged because of their large mass.

These setups were not exclusive. For instance trials were done with both an altered orientation and with voltage biases on the detectors. These combinations of apparatus were useful in determining a more comprehensive picture of the multi-layer detection system. In each setup case data was taken relating the pressure in the chamber housing the experimental apparatus to the current detected by the multi-layer detector. Many of the setups used the current detection circuit to measure this current.

2.4 Current Integrator Design

The current integrating detection circuit was designed to measure very small currents. The schematic of the current integrating circuit can be seen in appendix D, along with a simple expression for the output voltage of the circuit. The incoming current can be found by using the simplified form of equation 1.8. This current integrating circuit has a total integration time of 100 ms. This means that the capacitor is filled every 100 ms and the voltage recorded. The approximate output

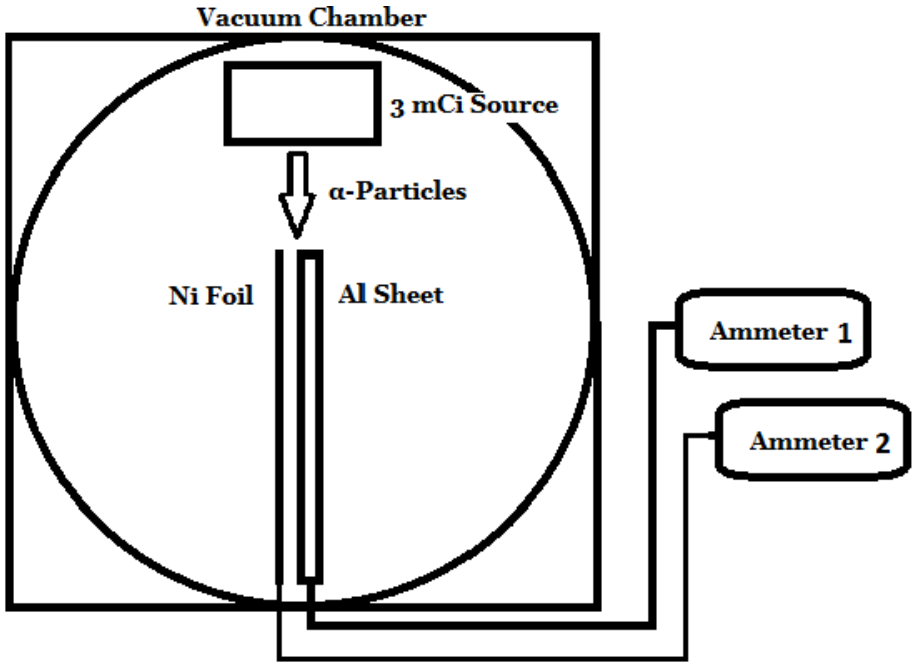

Figure 2.7: The setup for the multi-layer current detector with the orientation changed

voltage that was recorded is dependent on the flux of detected radiation, but was on the order of 100 mV for most of the data points. The capacitor used had a capacitance of 100 pF, thus the current detected is on the order of picoamps. The resolution of the integrating circuit detector is limited by the resolution to which one can distinguish voltage changes in the millivolt range. The output of the circuit was measured using an oscilloscope which had highly reliable resolution, indicating a high resolution in the current measured.

2.5 Operation

The vacuum chamber which housed the experimental setup was always evacuated in steps. At each step the current measured in each detector was recorded. Each layer of the multi-layer detector was connected electrically to the current outside of the chamber via coaxial cable, so as to minimize electric noise in the line. The pressure in the vacuum chamber was initially measured to be 950 Torr, which defines one atmosphere of 668 Torr, and was lowered in steps going through the Torr range all the way to a minimum pressure in the single digit mTorr range. At each pressure step, time had to be taken to wait for the fluctuations in the value of the measured current to stabilize. After values of current were recorded at representative pressures from approximately atmospheric to mTorr the chamber was vented. A new arrangement for the setup was constructed and the current pressure relation in the detector system was investigated with the new setup, in much the same way

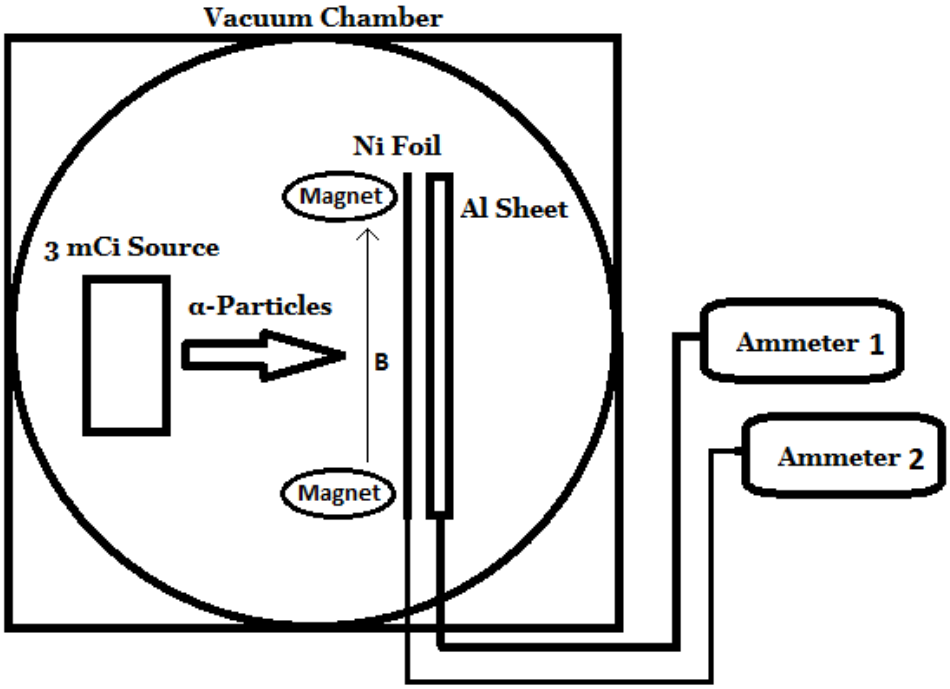

Figure 2.8: The setup for the multi-layer current detector with a magnetic field applied

as it was for the previous experimental arrangement. A picture of the experimental setup can be seen in figure 2.9, and a top down view can be seen in figure 2.10.

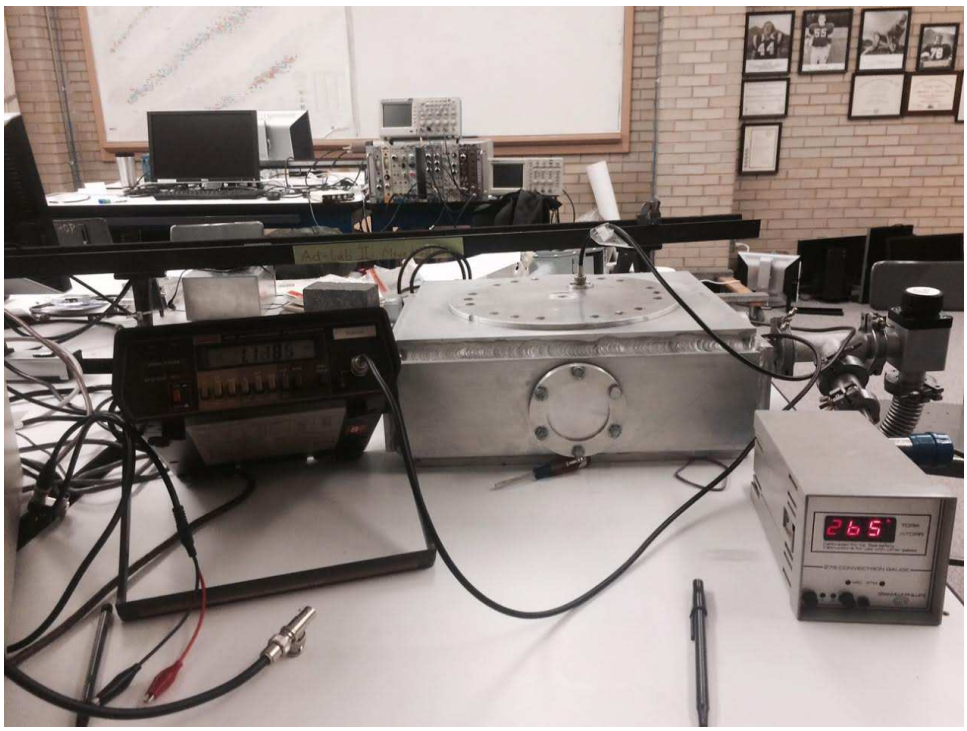

Figure 2.9: The setup for the multi-layer current detector

Figure 2.10: The setup for the multi-layer current detector as viewed from above

Some of the data collected while using the Keithley picoammeter to detect current extends further into the mTorr range than does the data coming from the integrating circuit because the Keithley picoammeter could measure current at lower pressures than the integration circuit could, due to an instability in the value measured by the current integrating circuit when the pressure at which the measurement was taken became to low. The most interesting section of the data occurred at pressures that were easily accessible to both current measuring devices.

CHAPTER 3

RESULTS

Many sets of data were recorded because the number of experimental variations was large. In many cases the results were very much what was expected. In other cases, even utilizing some of the simplest detector setups, effects were observed which were not anticipated. Some of the cases which display the most interesting odd behaviors were further investigated, analyzed and alternative hypotheses about the systems in question were explored in order to better describe the radiation environment and the detector apparatus. The simplest class of setup's which were explored are the cases in which the detector is a single sheet of aluminum connected to a current detector, with no thin metal foil acting as part of the detector.

3.1 Single Metal Sheet Type Detector Measurements

The most simple of the detection arrangements is a single thick sheet of aluminum. The current measured in this case is not exposed to an electrical bias as in other experiments. In this run the commercial Keithley picoammeter was used to take the current data. A graph showing the interesting detector current as a function of pressure in the vacuum chamber on a logarithmic-logarithmic scale can be seen in figure 3.1. There is a small but positive detector current of about 2.5 pA in the pressure range from mTorr to 0.1 Torr. The solid angle in this geometry is about half the value in equation 1.10 and hence the expected current would be about 3.9 pA. This is in very rough agreement with the measured current of 2.5 pA. In the intermediate range of pressures from about one torr to 100 torr there is a sharp rise in current that appears to be linear in nature. At pressures near atmospheric levels the current began to level off, and eventually drop.

The single metal sheet detector apparatus was reused in the next experiment, but with both positive and negative voltage biases applied to the single aluminum sheet detector. This bias was intended to discriminate between currents carried by positive charge carriers such as α particles and more traditional currents carried by negativity charged electrons. The data from the positively and negatively biased trials, overlaid upon the original data can be seen in figure 3.2. The results from positively and negatively biasing the detector data are strikingly similar to one and other. Both the positively biased detector and negatively biased detector show much higher current at all pressures than the non-biased detector setup. At low pressures the negatively biased detector setup had a larger observed current than the positively biased detector setup. This difference in observed current was reduced as pressure in the chamber was increased. The data obtained in these biased single aluminum sheet detector trials was procured using the commercial Keithley picoammeter.

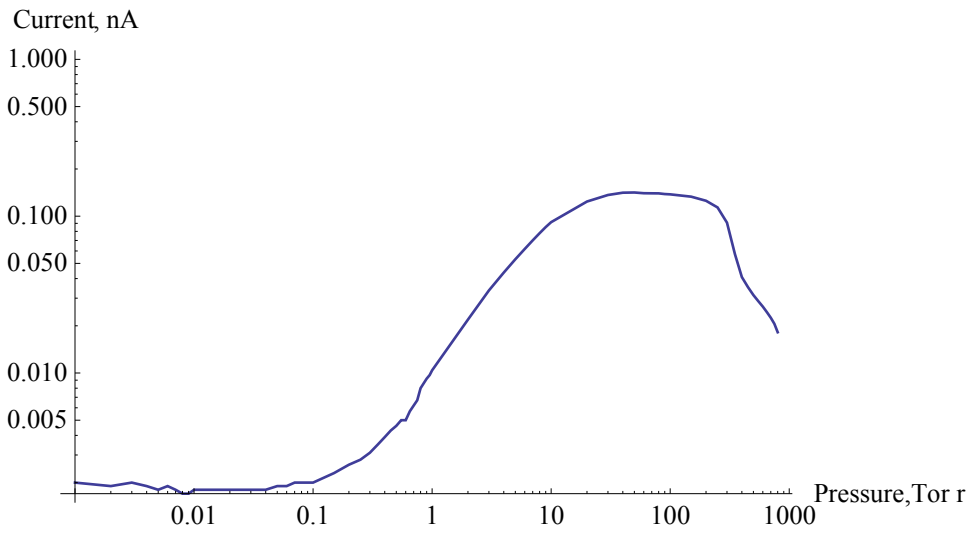

Figure 3.1: The data obtained using the Keithley picoammeter and an Al sheet collector

A variation on the previous experimental setup involved replacing the Keithley picoammeter with an alternate device for measuring current. The alternate current measuring device was a circuit with an output measured on an oscilloscope. The data obtained when feeding the output of the circuit directly to the oscilloscope can be seen in figure 3.3; to reduce the noise in the output of the circuit, the signal was first run through an ORTEC research amplifier. For comparison the amplified oscilloscope waveform can be seen in figure 3.4. The result of using the ORTEC amplifier was a much cleaner signal coming from the circuit. The waveform observed on the oscilloscope in figures 3.3 and 3.4 show the voltage of the signal on the vertical axis and time on the horizontal axis. The form in either case is a decaying function. The integration time of the circuit is represented by the horizontal distance between decaying peaks. The maximum voltage reached by the function is the voltage used to determine the current in equation 1.8

Data was recorded using the amplified signal from the current integrating circuit. The amplified data had a profile shown in figure 3.5. The data obtained directly from the ORTEC amplifier was run through a multiple channel analyzer, and used to generate a pulse height spectrum using the Maestro program. The Maestro spectrum can be seen in figure 3.6. The Maestro spectrum displays distinct peaks, with no reading in between the peaks. The width of the peaks correlates to the resolution of the measurement, the less the full width half max of the peaks, the better the resolution.

Data taken directly from the output of the integrating circuit was also collected. The output voltage taken from the circuit is related to the current as is described by equation 1.8. The voltage data collected is used to solve for the current in the detector. The resulting data overlaid with the results from the Keithley in the same setup is shown in figure 3.7.

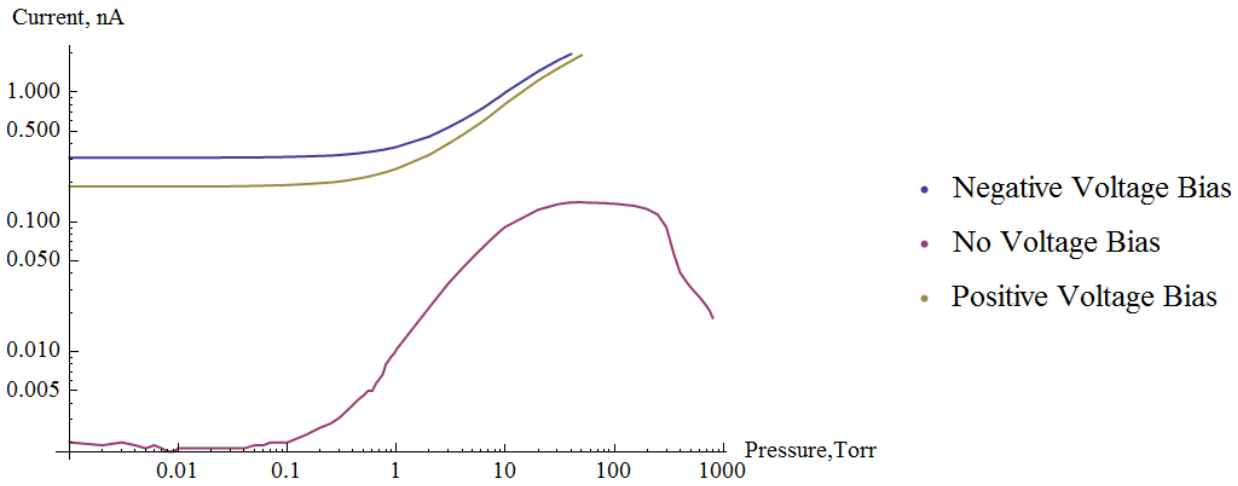

Figure 3.2: The data obtained using the Keithley picoammeter and an Al sheet with positive and negative voltage biases

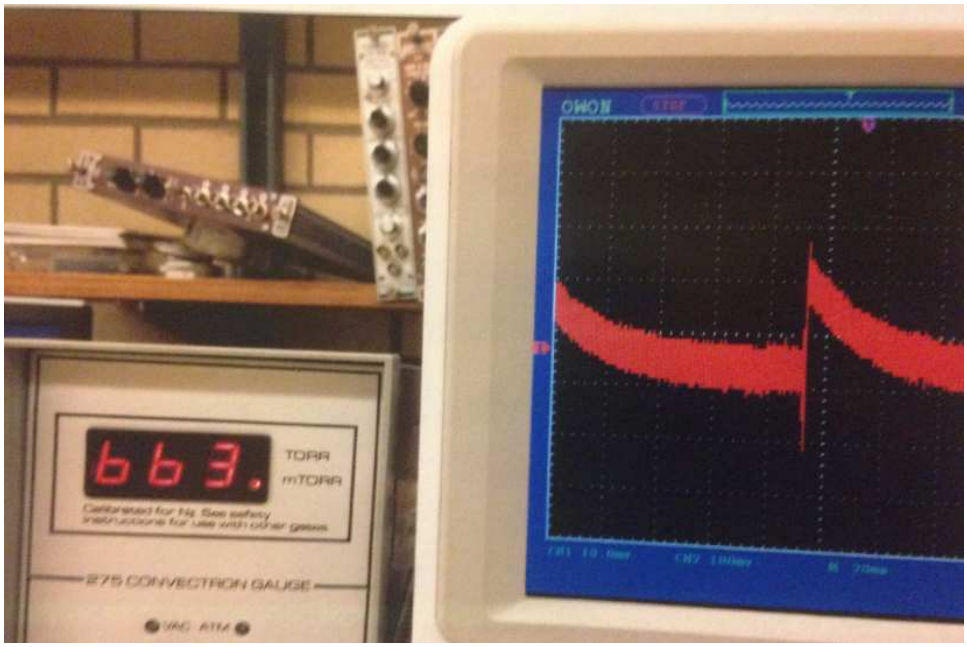

Figure 3.3: Waveform at 663 Torr, without the ORTEC amplifier

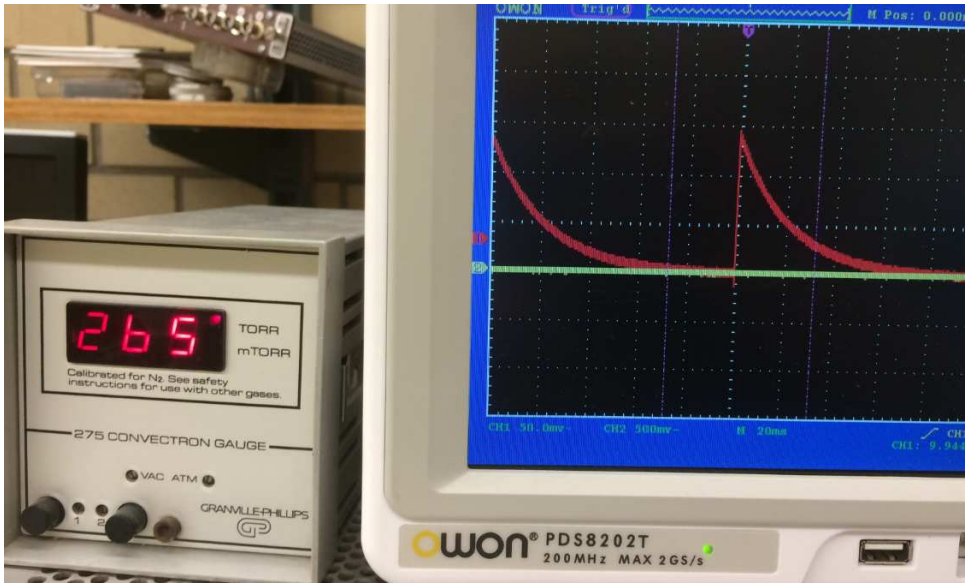

Figure 3.4: Waveform at 265 Torr, with the ORTEC amplifier

The data set acquired with the current integration circuit had a similar shape to the measurements taken with the Keithley picoammeter. The data acquired using the detection circuit rises slightly in the 10 to 100 torr range, just like the data acquired with the Keithley picommeter. The current observed by the integrating circuit also drops off much more quickly in the high pressure range than the current observed by the Keithley picoammeter does at the same pressure. The commercial Keithley picoammeter consistently displays larger current values than the current integrator circuit does for the same pressures. Using only a single sheet of aluminum as a detector allowed for the testing of the most basic detector collection principles. Questions involving the pressure regime in which α particles can be reliably detected can be answered with these data sets. Some ideas about the types of charge carriers in the system may be explored by looking at the sets of measurements which included a bias on the aluminum sheet detector. Examining the data taken from the single aluminum sheet style detector setup cannot answer all of the questions about the environment in which the detector is operating. Interesting and unexpected effects dominate the intermediate pressure regime in this setup. To further elucidate these anomalous effects a more advanced detector had to be constructed and tested.

3.2 Multi-Layer Metal Foil Type Detector Measurements

The multi-layer detector is a detector which adds a thin nickel foil to the aluminum slab style detector from the previous section. In this detector current is measured in both the thin nickel foil in front, and in the thick aluminum sheet behind it. In every experimental variation of the multi-layer detector setup the current measured in each layer is measured using the same current detection

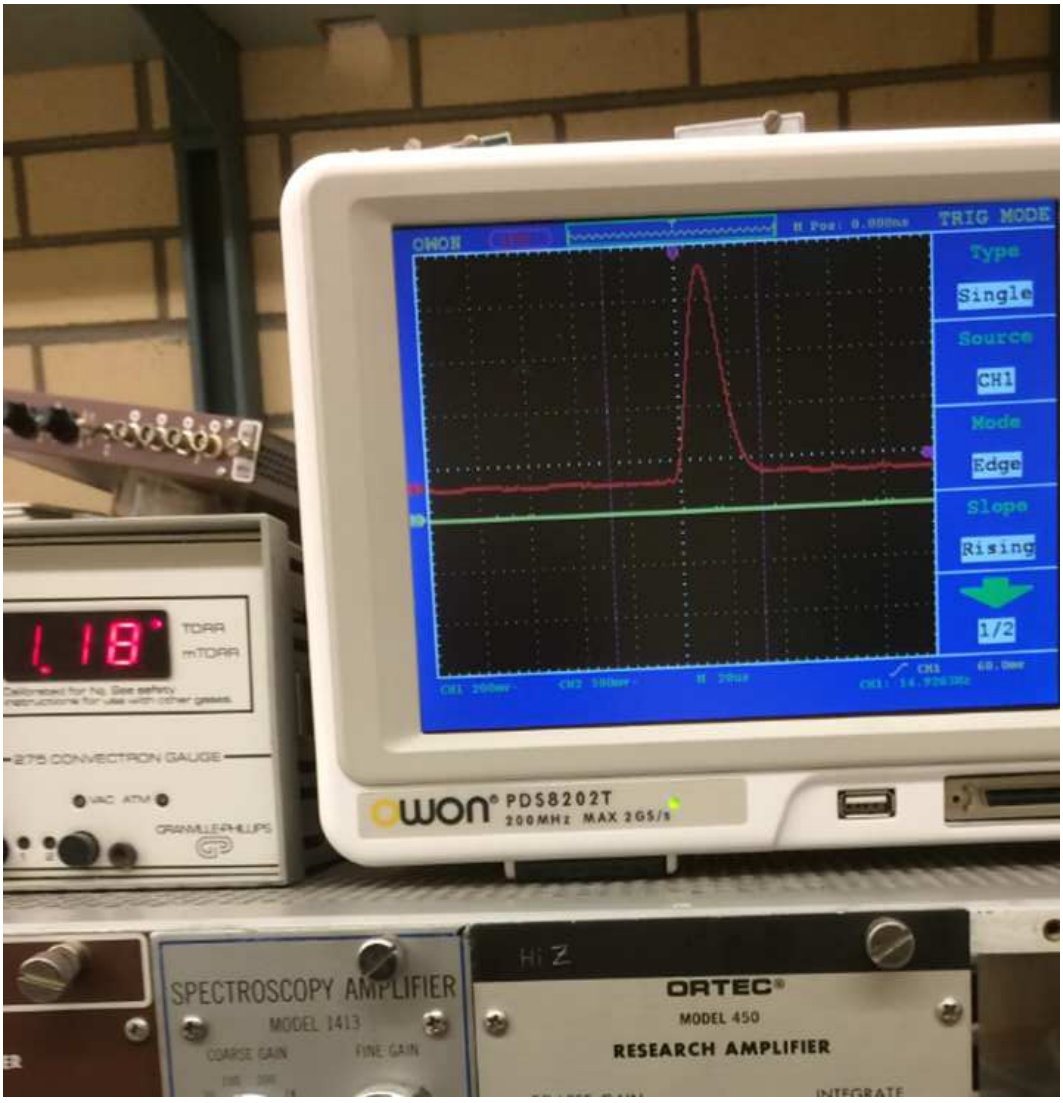

Figure 3.5: The output of the ORTEC amplifier at 1.18 Torr

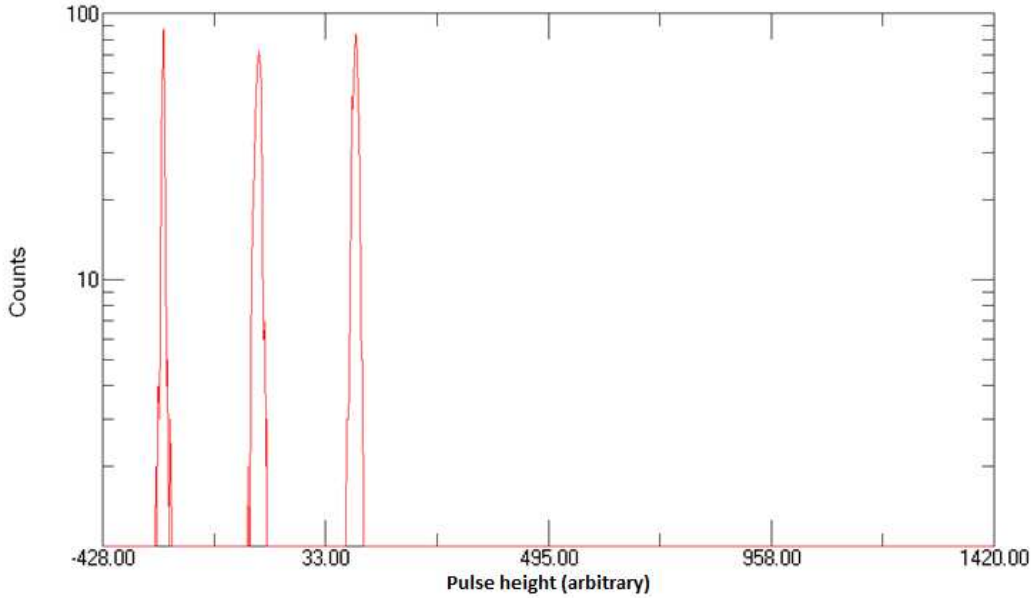

Figure 3.6: The Maestro spectrum of three peaks at varying pressure

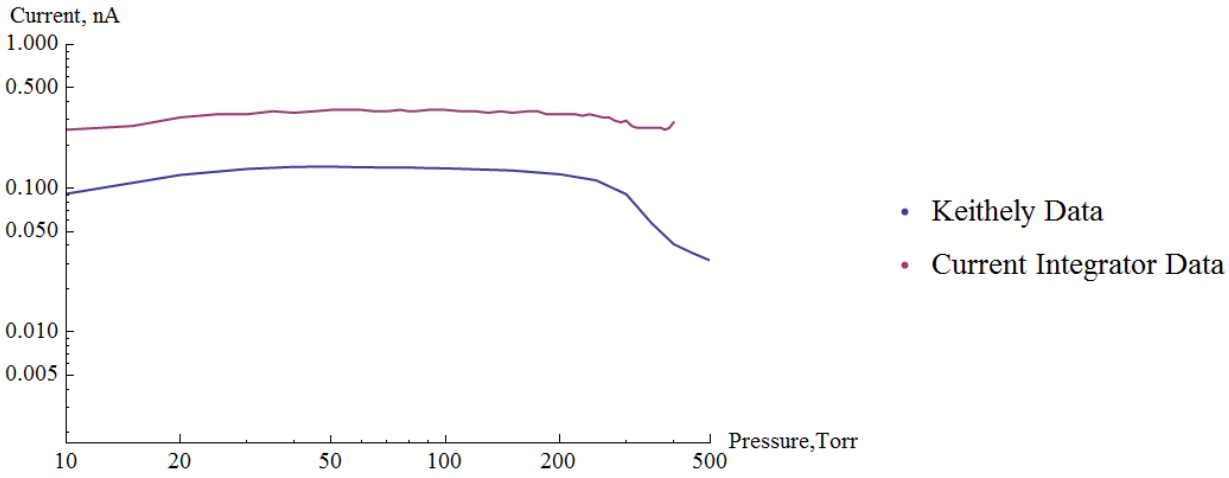

Figure 3.7: Comparison of data from Keithley picoammeter and integrating circuit.

device to avoid mismatches in the current observed. Most often the current in each of the layers was measured with the commercial Keithley picoammeter, due to the Keithley picoammeters ease of use. The first experimental variation tested with the multi-layer detector was the most simple case of direct α particle radiation with no electrical or magnetic fields applied.

3.2.1 Simple Set Up

The first setup explored is visualized in figure 2.5. The collected data which corresponds to the simple case of a multi-layer detector 7mm $\pm$ 1 mm in front of an α particle source can be seen in figure 3.8. The current in each of the layers increases with an increase in the pressure in the chamber up to a point, at which point the trend reverses. The thin nickel foil collects more current than the aluminum sheet, which is behind the nickel, at any given chamber pressure. The general pattern of current in each of the layers matches the pattern of current observed in the single aluminum sheet style detector. At low pressures the currents drop to a small steady value for both the thin nickel layer and the thick aluminum layer. With intermediate pressure in the chamber the current in each of the layers increases. When the pressure in the chamber is at its highest recorded values the current in both of the layers begins to decrease. The next variations considered are applied electrical biases to the detectors.

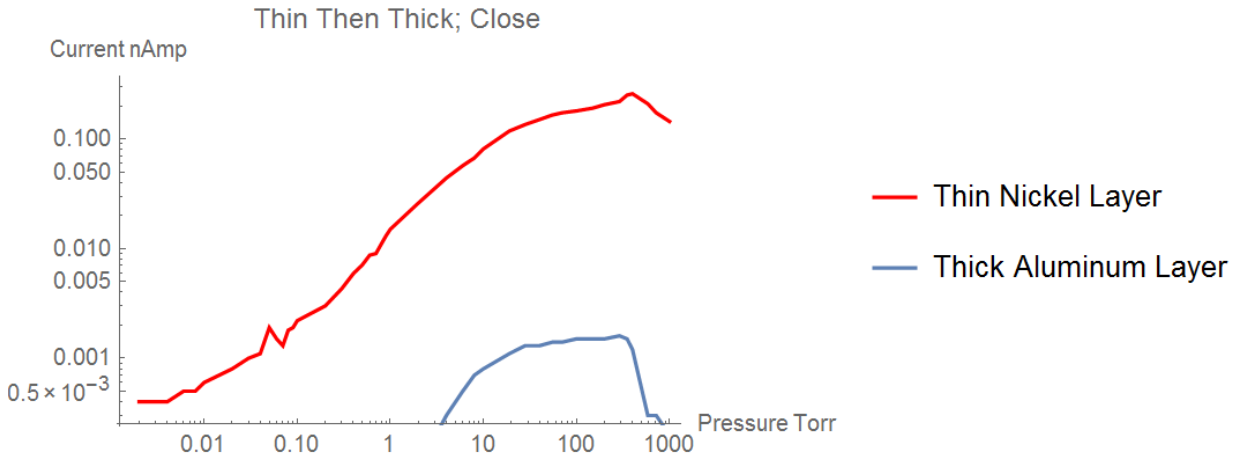

Figure 3.8: The current from both the front and back layers.

3.2.2 Electrically Biased Set Ups

The situation in which the layers of the detector have a voltage applied to them, but the orientation of the detector is unchanged, is visualized in figure 2.6. Relationships between the pressure in the chamber and the current in the detector were explored with many combinations of biases applied to both the thin nickel layer and the thick aluminum layer. The data from the situation

in which both layers are negatively biased is shown in figure 3.9. In this situation the currents detected in each layer are increased dramatically when compared to the currents detected in the unbiased case. The average maximum value of current in the case of a negative bias on the nickel layer was 7.58 $\pm$ .003 times as large as the current detected when there was no bias on the nickel layer. In the case of a negatively biased aluminum layer the average current detected was 35.32 $\pm$ 2.21 times larger than the current detected without a bias applied. When a positive bias was applied to the nickel layer the average magnitude of the detected current was 7.28 $\pm$ .003 times the magnitude of the current detected in the unbiased nickel layer. When positively biasing the aluminum layer the average magnitude of the current increased by 35.63 $\pm$ 2.23 times. The method of error propagation is discussed in section 4. The shape of the pressure current relationship stays fairly similar to the shape of the pressure current relationship in unbiased case however. The pressure

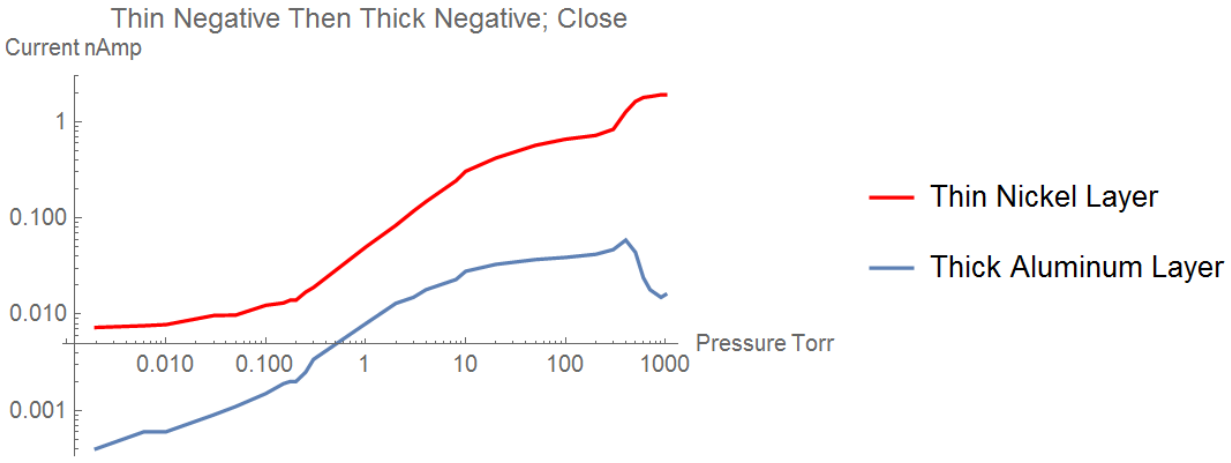

Figure 3.9: The current in both layers. Each has a negative voltage biases applied.

current relationship in the case in which each of the layers has a positive bias applied to them can be seen in figure 3.10. The most notable feature in this case is the reversed direction of current in the layers, shown by negative currents in the figure. The current values are not only negative in the positively biased detector case, but the currents are also large in magnitude when compared to the magnitude of current observed in an unbiased detector case. The shape of both of the pressure current relations remained similar to the shape of the pressure current relationship in the unbiased case. To check these effects trials were run in which only one of the two layers were biased. The data shown in figure 3.11 corresponds to an experimental setup in which only the front thin nickel layer had a bias applied to it. The bias on the nickel layer is positive. Only the layer with the positive bias detected a negative current. The current detected in the unbiased aluminum layer remained positive. Interestingly there was an increase in the magnitude of the current detected in both the nickel layer and the aluminum layer even though only the nickel layer had an electrical

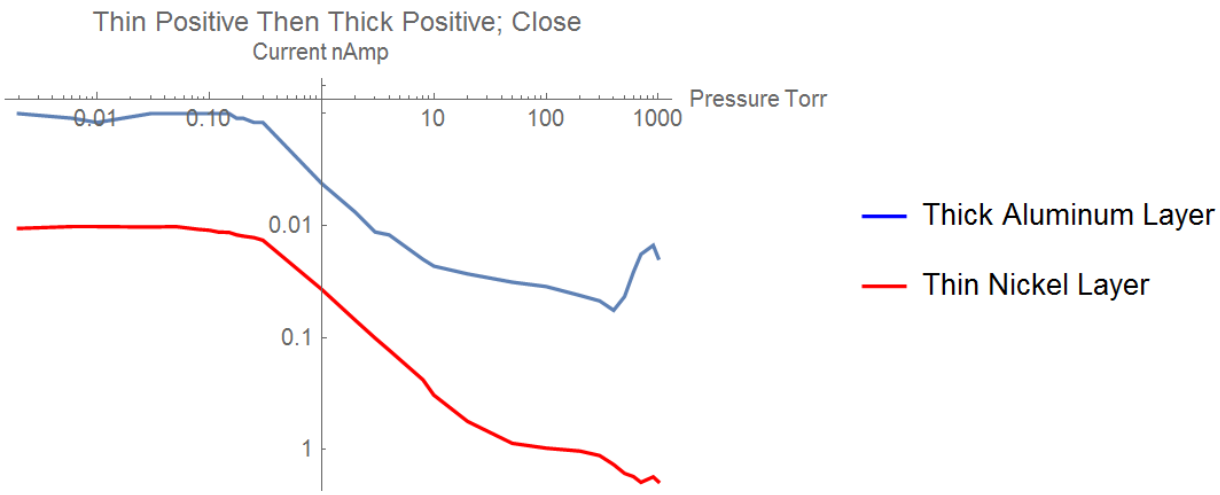

Figure 3.10: The current in both layers. Each has a positive voltage bias applied.

bias applied to it. All of the biases that were applied to either of the layers had a magnitude of 18 V from two 9 V batteries wired in series.

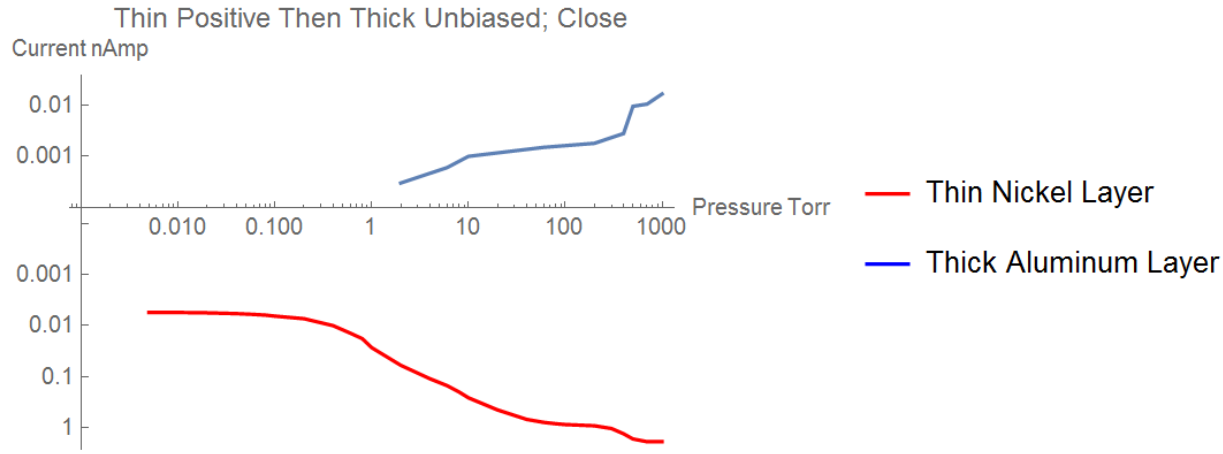

Figure 3.11: The current in both layers with only the thin front layer positively biased

3.2.3 Set Ups With Magnetic Fields Applied

One variation on the experimental setup involved applying a magnetic field to the detection apparatus (figure 2.8). Tokamak fusion reactor environments, in which the detector must be able to function, are dominated by extremely strong magnetic fields. The application of a magnetic field to the detector is therefore a more similar operating environment. It was hopped that the application of a magnetic field would deflect some of the electrons that would have otherwise been incident on

the detectors surface. The data acquired when the source was 7 mm $\pm$ 1 mm from the detector and this magnetic field was applied can be seen in figure 3.12. The application of this magnetic field has very little effect on the current detected in either of the layers. The approximate magnitude of the currents detected did not change with the application of a magnetic field. The direction of current and shape of the pressure current relationship also remained unchanged.

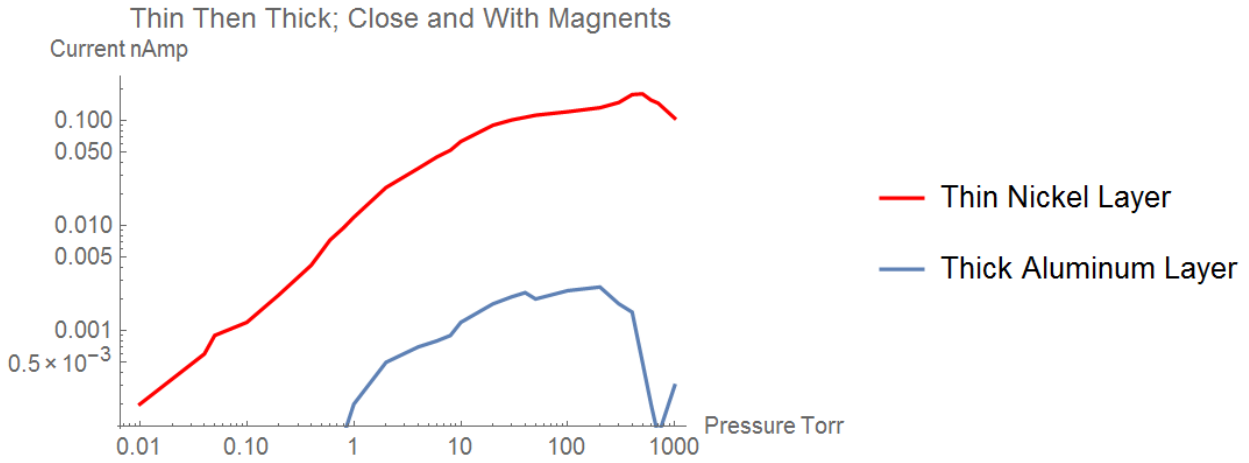

Figure 3.12: The current in both the front and back layers with an applied magnetic field

3.2.4 Orientation Change Set Ups

The simplest change that can be made to the orientation of the experimental setup is to increase the distance between the detector and the source. In all of the trials run on the multi-layer detector discussed up until this point the source was positioned 7 mm $\pm$ 1 mm away from the detector in an almost point blank style. The data collected when the source was moved to a distance of 45 mm $\pm$ 2 mm away from the detector can be seen in figure 3.13. The most obvious feature of this data is the sharp rise and fall in the current detected in the backing aluminum layer in the tens of mTorr pressure range. This is not the only oddity of this data set however. The magnitude of the current that is measured in the aluminum layer is greater than the magnitude of the current measured in the nickel layer, by 2.81 times. The detection layer that is furthest removed from the α particle source actually has the greater detected current in the increased distance setup. The setup shown in figure 2.7 shows a situation in which the flux of α particles is parallel to the surface of the detector. The current in this case should be drastically reduced from the point blank orientation because the area of the detector facing the α particle source is very small. The data that was taken in the case in which the source faced the edge of the detector can be seen in figure 3.14. The magnitude of the currents detected in the thin nickle layer and thick aluminum layer are approximately equal, with the aluminum layer detecting slightly more current. When the detector is positioned parallel to the

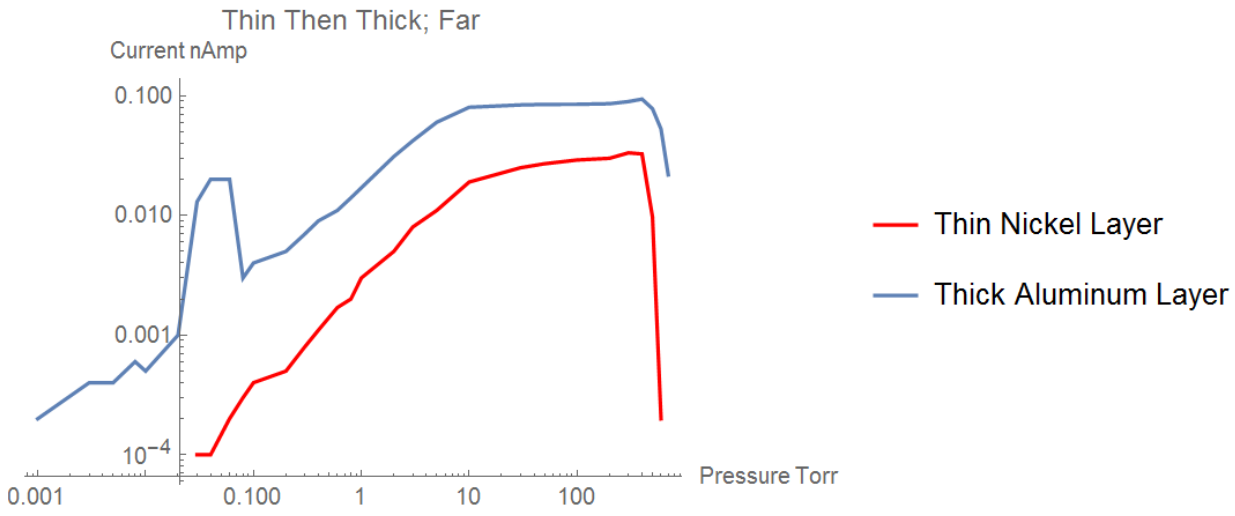

Figure 3.13: The current in both layers when the source is further from the detector

α particle flux both of the layers detect much less current than in the case of an α particle flux perpendicular to the detectors surface. The general shape of the pressure current relationship in the changed orientation case remains strikingly similar to the shape seen in most of the data sets. The

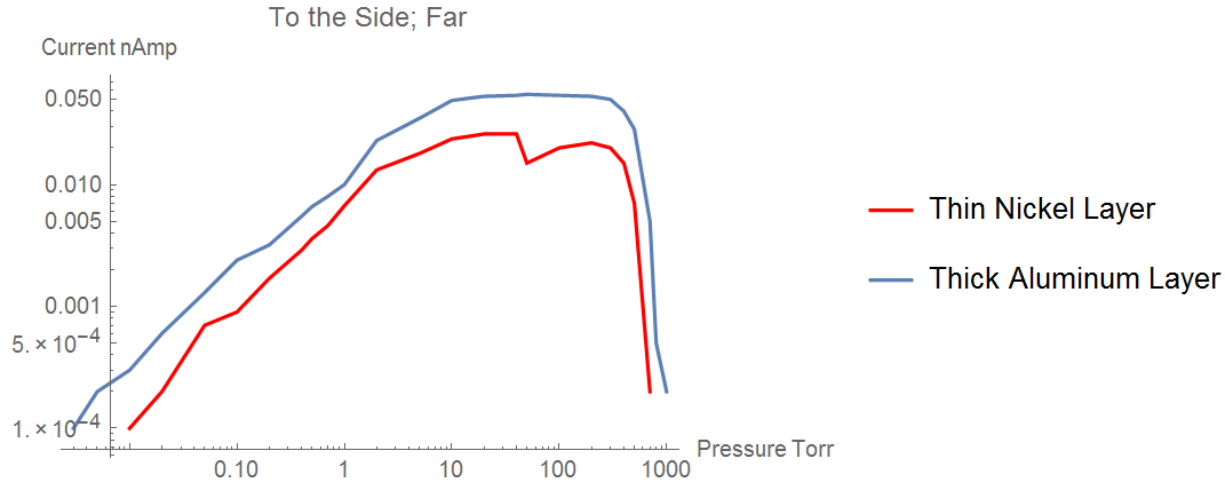

Figure 3.14: The current in both layers with α particle source parallel to detectors face

final orientation change considered is the reversal of the two layers. In the reversed layer geometry the α particle source is closest to the thick aluminum layer and furthest from the thin nickel layer. In this geometry the α particles emitted from the source would first encounter the thick aluminum layer, indicating that the aluminum layer should have a larger detected current than the thin nickel layer. The data obtained while the experimental setup was in the reversed layer geometry can be seen in figure 3.15. The reversed layer geometry seems to generally meet the expectations for

detected current magnitude and direction.

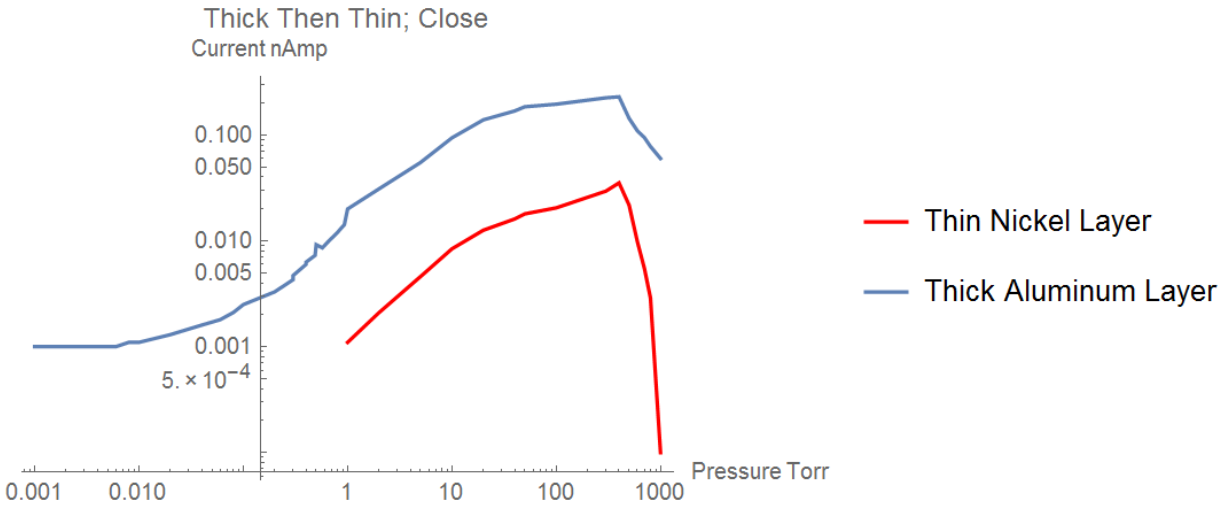

Figure 3.15: The current in both layers with the aluminum layer in front of the nickel layer

The above does not completely showcase the sets of data taken using the multi-layer detector. Combinations of the variations described above were also considered. For instance data was taken with both voltage biases applied to the detectors and with magnetic fields present. The complete collection of all of the sets of data taken with the multi-layer detector is located in appendix A. The complete sets of data obtained can be seen in appendix C

CHAPTER 4

ANALYSIS AND DISCUSSION

The many experimental setups were used to thoroughly explore the workings of both the single metal sheet type detector and the multi-layer type detector. At low pressure in both the single metal sheet style detector and the multi-layer detector the current detected dropped to a small steady value. This is thought to represent only the current collected from the flux of α particles and not from confounding ionized electrons. The increasing detected current at intermediate pressure values are due to a flux of electrons emanating from the trajectory of the α particle through the air on its way to the detector. The results from the single metal sheet type detector are discussed.

4.1 Error Propagation

Error propagation through a series of equations is given by

$$\delta_u^2 = (\frac{\delta_u}{\delta_x})^2(\delta x)^2 + (\frac{\delta_u}{\delta_y})^2(\delta y)^2 + ... \tag{4.1}$$

in which u is a function of x, y, etc. δ_u is the total error in the function u, δ_x is the error in x and δ_y is the error in y according to Ku [17]. Using equation 1.10 and the values d=.007 m and l=w=.01 m the solid angle covered by the detector is shown to be .838 radians. The error in the solid angle covered by the detector, assuming an error in l and w of .001 m, is

$$\delta_\Omega = \sqrt{\frac{\delta\Omega}{\delta l}^2 * \delta l^2 + \frac{\delta\Omega}{\delta d}^2 * \delta d^2} = .305 \tag{4.2}$$

Giving a value for the solid angle covered by the detector of .838 $\pm$ .305 radians.

4.2 Single Layer Detector With a Keithley Picoammeter

The data taken during this experiment were not expected. The current was expected to be small for pressures below a critical pressure, below which the current was expected to rise to a steady value. The α-particles produced at high pressures should have been stopped by the air between the source and the detector. When the pressure dropped enough for the α-particles to reach all the way to the aluminum sheet the current was expected to rise as α particles got collected as current. The unexpectedly high current at the higher pressures is due to α-particles ionizing electrons in the air, which are subsequently collected by the aluminum sheet as current. The stray electrons could explain why the current reduced to a small but nonzero value at low pressures; when there was no

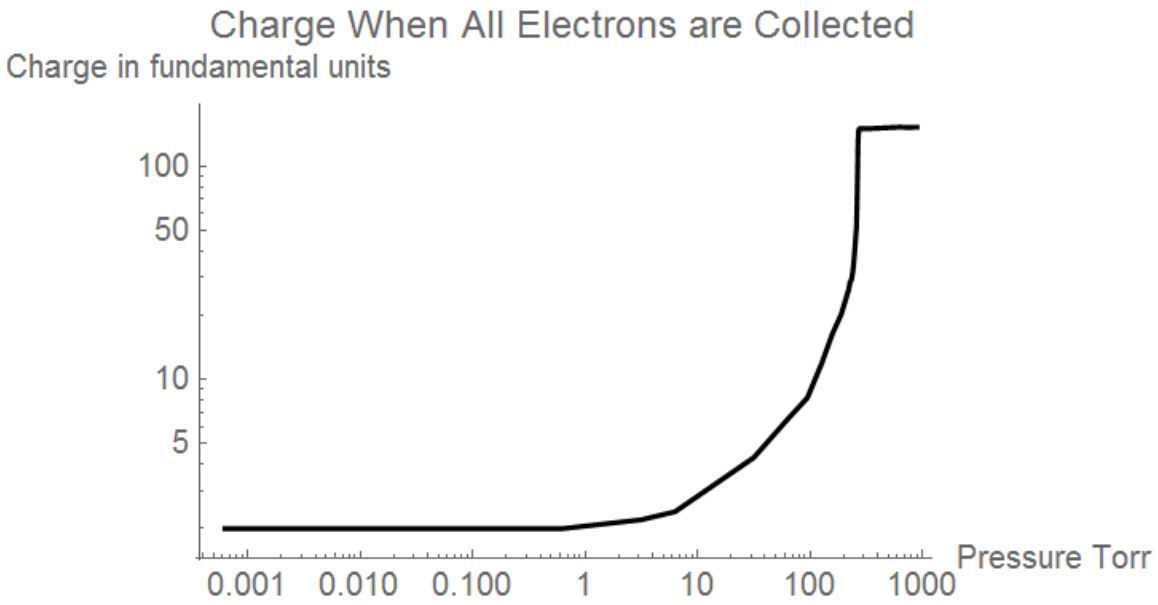

Figure 4.1: The most basic simulation of the current pressure relationship.

more air to get in the way of the α-particles the number of electrons ionized dropped to zero and only the α particles were collected as current.

To confirm that the above is accurate a simulation was performed which determined the number of electrons ionized in the intervening air at different pressures, and determined how many of them actually made it to the detector. The stopping and ranges of ions in matter program was used to find the average number of electrons which were ionized in the air between the detector and source at different pressures. Adding the average number of electrons ionized by an α particle to the portion of α particles which were not stopped before the detector gives figure 4.1. This represents the most basic simulation scheme in which all of the electrons that are ionized by the α particles journey through the air are collected by the detector. The simulation is describing the amount of charge incident on the detectors surface for one α particle at a given pressure. The amount of charge incident on the detectors surface should be directly proportional to the current detected by the detector. This simulation already has many of the major features of in the real data. The current drops to a small positive current at low pressures. The current rises in the intermediate pressure regime and levels off at high pressure. This simulation misses the drop in current that is observed in the real data at high pressure. The lack of a high pressure drop off indicates that the collection rate of ionized electrons at high pressure is not as high as the collection rate of ionized electrons at low pressure in the real system.

To improve the simulation a model of isotropic electron emission at the furthest range of the α particle was adopted. Equation 1.10, the solid angle equation, was used to determine what portion

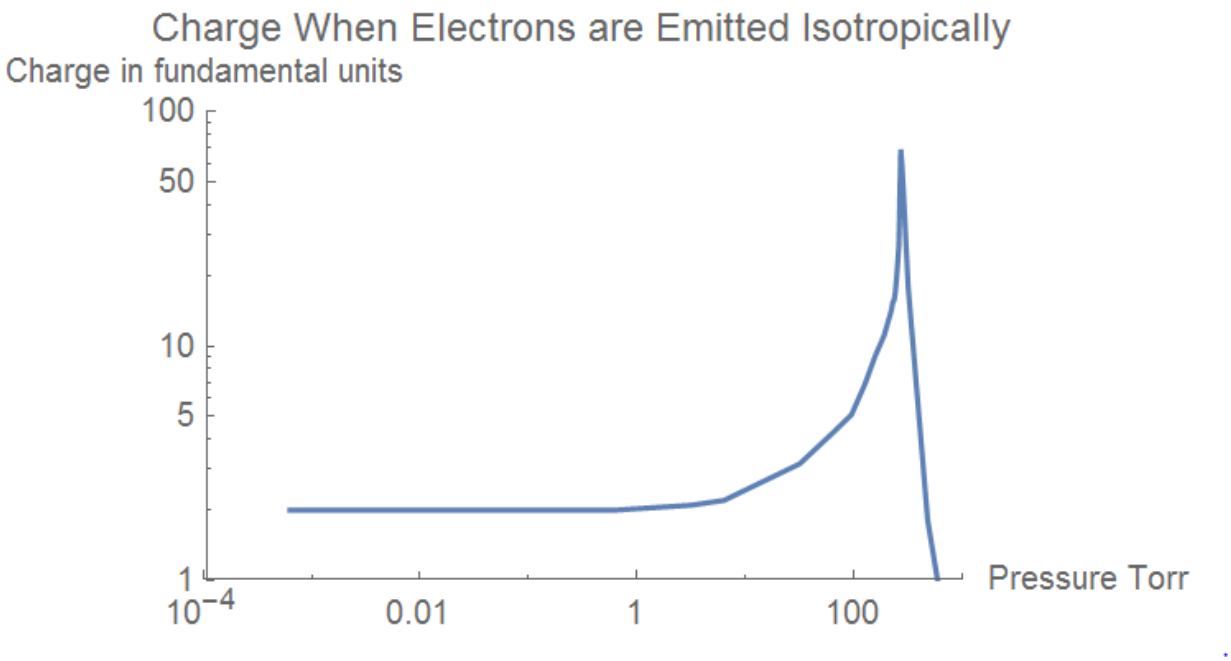

Figure 4.2: The isometric simulation.

of the ionized electrons were collected by the detector. The range of the α particle in the air between the source and detector was found using S.R.I.M. The results of this isometric simulation can be seen in figure 4.2.

This isotropic simulation captures even more of the behavior of the single metal sheet style detector. The incident charge at high pressures drops in the simulation because the range of the α particles in air is smaller at higher pressures, resulting in a small solid angle covered by the detector. In the isometric simulation all of the electrons ionized by the α particle are assumed to be emitted isotropically from only one point, namely the maximum range of the α particle. This assumption would seem to be very inaccurate, but is supported with further analysis.

Equation 1.9, called the Bethe formula, shows a relationship between the distance a heavy ion, like an α particle, has traveled in a medium and the energy which it loses. The Bethe equation was used to find the share of the energy lost by the α particles at a given distance. The energy that is lost by the α particle, as it moves through the air in the chamber, is used to ionize the electrons in the air. The amount of energy expended at a given distance is assumed to be proportional to the number of electrons ionized at that point in space. The energy which an α particle loses as it moves through the air at varying pressures can be seen in figure 4.3. The tall spikes in energy lost at the end of the α particles track is called the Bragg peak. This peak indicates that most of an α particles energy is lost at the very end of its range. This indicates that the assumption that all electrons are emitted at the very end of the α particles range may not actually be very far off.

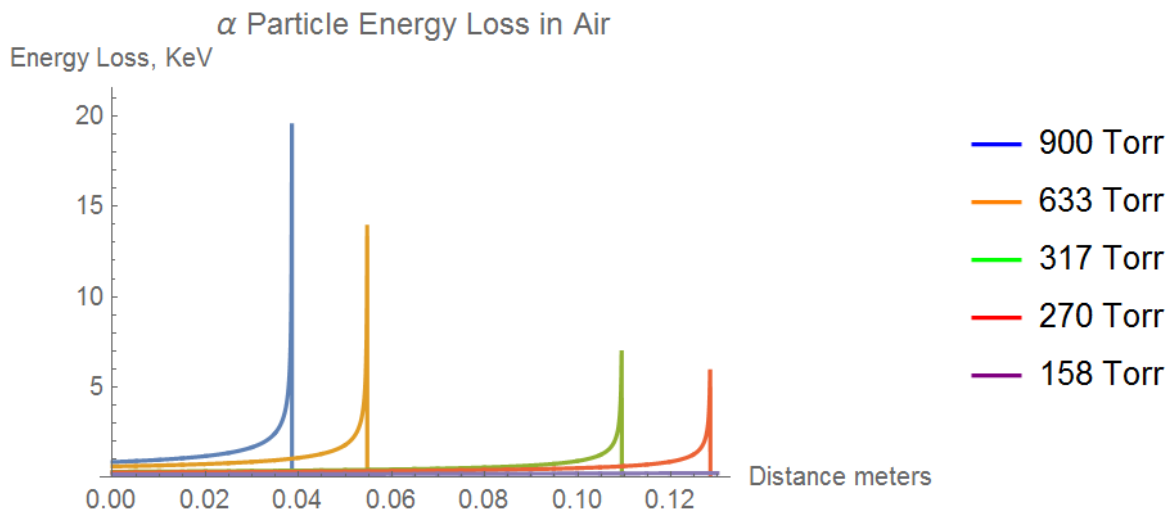

Figure 4.3: Peaks correspond to energy lost by an α particle at varying air pressures

Figure 4.4 shows a simulation in which electrons are still emitted isotropically, but the position of the emission of the electrons is determined by the Bethe formula. The simulation including the position of the emission of the electrons does not seem to influence the behavior of the system much. The total amount of charge incident on the target decreases from previous simulations at all except the lowest pressures. A comparison of all three simulation methods is shown in figure 4.5.

There is good qualitative agreement between the simulations produced and the experimental data acquired. The good agreement, particularly in the low pressure regime, indicates that the detectors low pressure current relation is most likely due to a pure α particle flux. The intermediate pressure relationship is simulated by electrons ionized in the pathway of the α particle. This is likely the source of the rise in detected current, seen at intermediate pressures in the data. The simulation and the data differ in two important ways in their shapes. The simulated data has a somewhat lower maximum value to minimum value ratio than the simulated data does. This discrepancy could be due to δ rays. δ rays are electrons that, when ionized by the α particle, have enough energy to ionize even more electrons in the medium. This would add a higher total number of electrons to the system, which could contribute to detected current. There is also a discrepancy in the widths of the pressure current relationships from simulated and actual data. One of the assumptions that was made in the simulation is the assumption of isotropic emission of ionized electrons. This assumption is likely incorrect and could be contributing to the width discrepancy. Intuitively one would expect the electrons emitted from ionization to travel in a direction similar to the direction in which the α particle traveled. The angle dependent cross section of this interaction may be possible to calculate with Fermi's golden rule. All of the analysis and simulations were done in a Mathematica notebook, which is located in appendix B

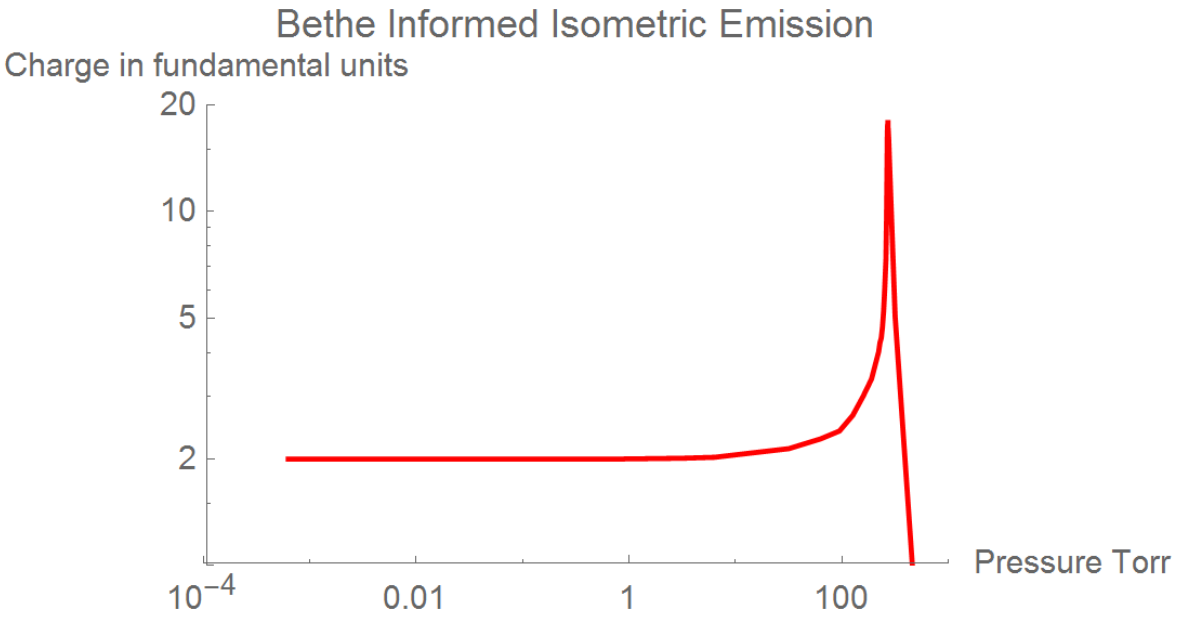

Figure 4.4: The simulation of pressure current relationship using the Bethe formula

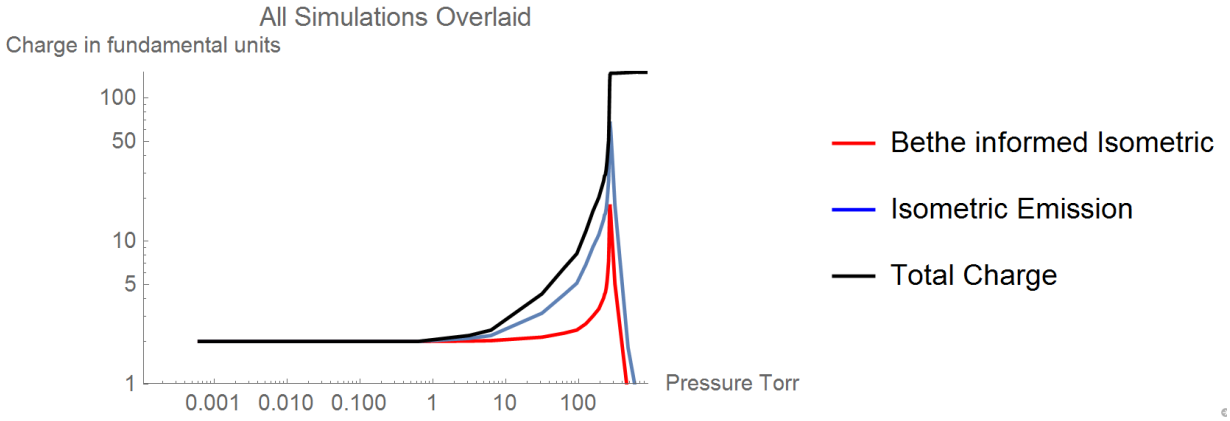

Figure 4.5: All of the simulations overlaid

4.3 Correlation Coefficient

To correlate the measurements taken with the Keithley picoammeter and measurements taken with the current detection circuit, the Pearson correlation coefficient was calculated. The Pearson correlation coefficient is given by,

$$r = \frac{\sum_{i=1}^{n}(x_i - \bar{x})(y_i - \bar{y})}{\sqrt{\sum_{i=1}^{n}(x_i - \bar{x})^2}\sqrt{\sum_{i=1}^{n}(y_i - \bar{y})^2}} \tag{4.3}$$

in which r is the coefficient, x_i and y_i are the data from the Keithley and the integrating circuit, $\bar{x}$ and $\bar{y}$ are the average values of the data, and n is the number of data points. This equation for the correlation coefficient is taken from $Pearson\ Correlation$ [12] and is equal to the covariance of the sets of data divided by the product of the data sets standard deviations.

The correlation coefficient is a scalar with values ranging from -1 to 1. A value of zero indicates that there is no linear correlation between the two sets of data. A value of negative one indicates that there is a perfectly linear relationship between the sets of data with a negative slope. A positive coefficient indicates a positive relationship between the data sets. The higher the absolute value of the correlation coefficient the better the relationship between the two sets of data can be described by a linear relationship. Ideally the absolute value of the correlation coefficient between the data from the Keithley picoammeter and the voltage output of the current integration circuit should be close to one, because this would indicate that the integration circuits output is tracking closely with the presumed correct value from the Keithley picoammeter.

4.4 Single Layer, Custom Current Integrating Circuit

The integrating circuit's measurement of current was correlated to the Keithley picoammeter's measurement of current. The correlation points to a very successful circuit design. In addition to the correlation the custom circuit improved upon the current resolution of the Keithley picoammeter. The current integration circuit had a depressed range of detectable pressure compared to the range of the Keithley picoammeter. Future versions of the circuit could be made to address this problem by extending the pressure detection range of the circuit to include measurements from 1-10 mTorr by tuning the circuit components. Interestingly the pressure in the vacuum chamber and the current turned out to be related within 1% at low pressures, with a Pearson correlation coefficient of $r = .95$. Equation 4.3 shows how the Pearson correlation coefficient was obtained. The Pearson correlation coefficient indicated a perfect correlation when it's value is 1. The correlation between the Keithley picoammeter's measurements and the measurements from the integrating circuit can be seen in figure 4.6. This relation shows that the integrating circuit was as good as the Keithley picoammeter for determining currents in the detector. The results obtained using the

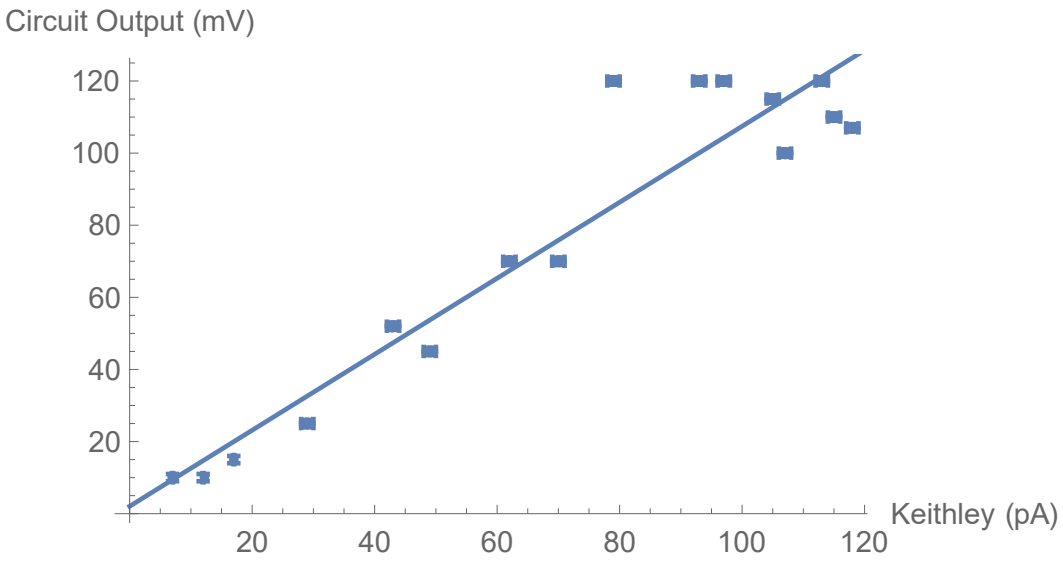

Figure 4.6: Correlation between Keithley and integrating circuit with errors shown

multi-layer detector are examined next

4.5 Multi-Layer Set Up

The multi-layer detector configuration, with a thin nickel foil in front of a thick aluminum sheet, led to some very interesting data. There was an abundance of this data so the analysis of the data will be shown in sections grouping similar experimental arrangements. The first section shows the results of the most simple multi-layer detector arrangement.

4.5.1 Simplest Case

In the simplest case the multi-layer detector is placed very close to the source of α particles. Figure 3.8 shows the data obtained in this case. The current detected in the front layer is very large compared to the current detected in the back layer. Given the model of ionized electrons contributing to current this makes sense. The ionized electrons are all collected in the front layer as current. The current in the rear layer is not expected. The back layer should not detect any current at high pressures, because the electrons are captured by the front layer, and the α particles are stopped by the air. At low pressures the current in the back layer should be small and constant, corresponding to α particle collection. Instead the trend is reversed with the back layer detecting higher current at high pressures than low pressure. This anomalous current seems to indicate that the back layer is collecting some of the flux of ionized electrons. If the back layer is indeed collecting current from ionized electrons the distribution of the flux of electrons would come into question. An analysis of the cases in which there is an applied electrical bias may help to clarify

this possible electron flux.

4.5.2 Electrical Biases

There were nine experiments run on the multi-layer detector which involved electrical biases. In all cases the magnitude of the bias applied was 18 V, produced by wiring two 9 V batteries in series. The most notable feature in all of the sets of data involving electrical biases is the increase in the magnitude of detected current observed when biasing a layer, regardless of the sign of that bias. In the nickel layer an applied bias gave an increase in current of $7.58 \pm .003$ times. This sharp increase in the magnitude of current is somewhat expected as the voltage in a circuit is equal to the resistance of the circuit multiplied by the current. The resistance of the detector will not change with the addition of an electric potential so the current should indeed be expected to increase.

The direction in which current flows through a layer of the detector is reversed in the case when a positive bias is applied to that layer, along with an increase in the magnitude of the current detected in that layer. This change in the direction of current is not particularly surprising. If the sign of the voltage is changed the sign of the current should also be changed. The biases indicate that electrons are always the current carriers, and that α particles carry no charge in this detection scheme. This can be true in the case where only α particles are incident on the surface of the detector. An α particle stopped in a layer will embed in that layer, rather than being collected as charge. The presence of this extra positive charge in the detector will push electrons through the detector. In this way the current detected from an α particle can be carried by electrons, as is indicated by the direction of detected current in the case of biased layers in the multi-layer setup. The applied electrical biases indicated that electrons carry current in the detector. Magnetic fields were applied to screen the detector from the incident electron flux.

4.5.3 Magnetic Fields

Three experiments were run with applied magnetic fields. In all of the experiments the magnetic field was oriented parallel to the surface of the detector, and had a strength of .01 T. In the simple geometry case the applied magnetic field had no noticeable affect on the current collected. The magnetic field was intended to deflect some of the electrons away from being incident on the surface of the detector. The magnetic field was clearly not strong enough to deflect the electrons paths enough to affect measured current. When experimental conditions were mixed the addition of a magnetic field to the system ended up changing the results of the experiment.

When a magnetic field was applied to a system in which one of the detectors had a negative bias applied interesting effects were observed. The presence of a magnetic field switched the direction of current flow in negatively biased layers. Figures A.9 and A.10 show this odd result.

An explanation for this switch in the direction of current is not obvious. The magnetic field should have little effect given that it could not screen electron flux in the simple geometry case. More magnetic measurements, preferably utilizing a stronger magnetic field are needed to fully explain this data.

4.5.4 Alternate Geometric Arrangements

Two alternate geometric setups were utilized. The first alternate arrangement moved the source and detector father from each other. In this setup the current detected in each of the two layers were almost equal. The current detected in the layer further from the source was slightly larger than the current detected in the closer layer. There is also a large increase in current for a small range of pressures in the back layer. The sharp increase in current is very unusual and is likely related to error in measurement. Perhaps a wire was left ungrounded during the measurements done at those pressures. The fact that the detected current is greater in the back layer than in the front layer indicates a deficit of information about the electron flux. When the source is moved farther from the detector the electrons have further to travel before they reach the detector. With this increase in distance perhaps there are more scattering events which occur, causing electron fluxes from more than one direction.

The second alternate geometry explored is a situation in which α particle flux is parallel to the surface of the detector. The exposed area of the detector is reduced, so a decrease in current should also be observed. The aluminum layer is thicker than the nickel layer so the aluminum layer has a greater exposed surface. This would suggest that the detected currents should be reduced, but the current in the aluminum layer should be greater. What was observed matched well with expectations with a greater current in the aluminum layer than in the nickel layer. All of the work done analyzing the detector data led to an interesting and unexpected relation between the chamber pressure and the detected current.

4.6 Pressure Relationship

The detector was created with the intent of measuring both the flux and energy of incoming α particles. In this regard the detector could only reliably function in a low pressure environment. In the intermediate pressure range the flux of electrons obscured the flux of α particles. The flux of electrons may obscure the α particle flux, but it is interesting on its own. The data obtained in the close range setup is plotted on a linear scale in figure 4.7 and figure 4.8. This shows a remarkably linear pressure current relationship in both the 0 to 20 Torr range and 50 to 300 Torr range. Because this relationship is linear, the α particle detector can be used to predict the pressure in the chamber by looking at the current. This technique for measuring pressure relies on the

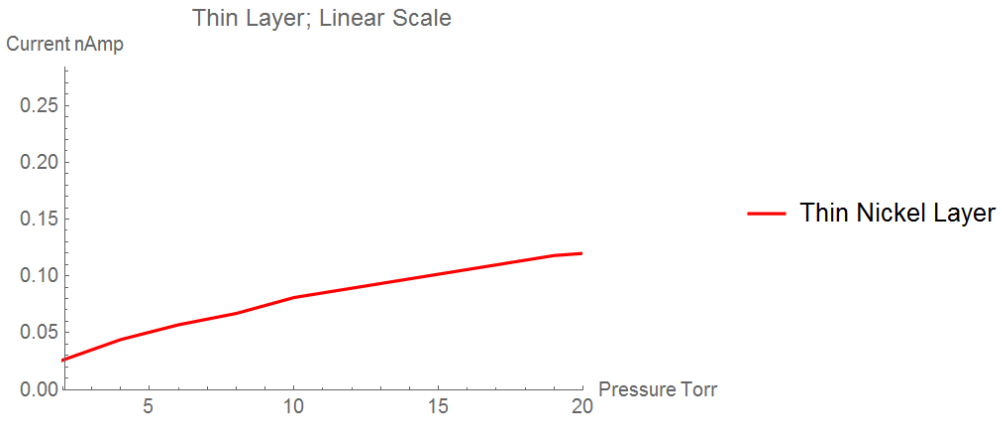

Figure 4.7: Relationship between pressure and current visualized linearly

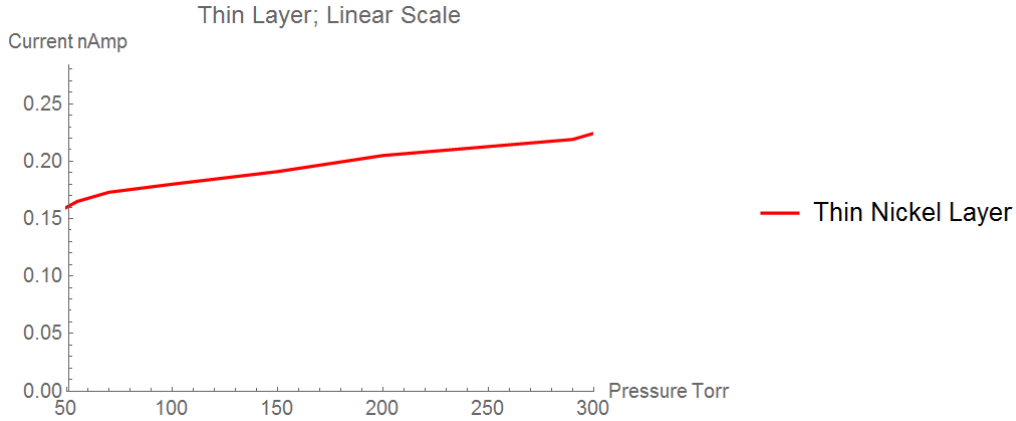

Figure 4.8: Relationship between pressure and current visualized linearly

current collected from a cascade of ionized electrons and a well known α particle source. This discovery is particularly interesting as the selection of pressure measuring devices in this range is not large. This method of detecting pressure could be tweaked by changing variables like the distance between the source and the detector, the type of source used to create the cascade of electrons and the material used in the collector.

CHAPTER 5

CONCLUSION

The α particle flux is measured accurately by both the single slab style detector and the multi-layer detector when considering low pressures. Both style of detector fail at higher pressures due to a large flux of ionized electrons. In this intermediate pressure regime the pressure in the chamber is well correlated to the current observed by the detector. This means that the current picked up by the detector can be used to accurately measure the pressure in a vessel. The flux of electrons that causes this relation at intermediate pressures is not well characterized.

Further study of this system is necessary if the detector is to work in a Tokamak fusion reactor environment. Experiments that use magnetic fields with much more strength than the ones investigated in this report would be very helpful in ensuring that the current detected in the intermediate pressure range is due to an electron flux. If a stronger magnetic field were applied the electrons would not be able to reach the detector. Another way to expand upon the research shown here would be to increase the number of layers in the detector. The behavior of particles inside of the chamber would be easier to determine with more layers. Adding more layers would also ultimately contribute to the goal of making the detector sensitive to the energy of incoming α particles. In a longer term approach the detector could be more thoroughly investigated using a particle accelerator. Using an accelerator would allow for the probing of the system with different initial α particle energies.

More simulation work could also be done in the future. The simulation of emitted electrons could be improved by using a Fermi's golden rule type calculation to find the angular cross section of reaction for the ionization of electrons in air. This would help to improve the simulation by more accurately describing the flux of electrons incident on the detectors surface. The simulation could also be continued by using the information on the energy of each of the α particles, obtained via the Bethe formula. With the energy of the α particles known at the point of contact with the detector another Bethe type simulation could be run to see how much energy the α particle would lose moving through the nickel layer. This approach could be used to solve for the position at which the α particle is stopped in the detector. The information on the stopping distance of the α particle would make it possible to model the expected current in each of the layers.

There are many directions in which this research could go moving forward. This thesis has examined the pressure dependent workings of a system comprised of a radioactive ^{244}Cm source and two different α particle detection devices. This system is meant to represent the lost α particle flux in Tokamak style fusion reactors. α particle flux in this system is shown to be readily detectable at chamber pressures on the order of mtorr and lower.

REFERENCES

[1] F.E. Cecil, P. van Belle, O.N. Jarvis and G.J. Sadler, "Development of a thin foil Faraday collector as a lost alpha particle diagnostic for high yield d-t Tokamak fusion plasmas. Proc, 21st European Physical Society Conference on Controlled Fusion and Plasma Physics (Montpelier) European Conference Abstracts, 18B (1994) 1340.

[2] M.J. Loughlin, F.E. Cecil, M.Hone, O.N. Jarvis,S. Medley and L. Roquemore,G.J. Sadler, P. V. Belle, G. Whitfield,"An ITER compatible thin foil Faraday collector as a lost alpha particle diagnostic for high yield d-t tokamak plasmas". Rev. of Sci.c Instrum. , 68 (1997) 361

[3] J.C. Barbour, F.E. Cecil, P. V. Belle, M. Hone, O.N. Jarvis, S. Kern, M. Loughlin. S. Medley, A. Nowak, A. Roquemore, G. Sadler, and Y. Takimoto, "Development of a thin foil Faraday collector as a lost alpha particle diagnostic for high yield d-t fusion plasmas" in Diagnostics for Experimental Thermonuclear Reactors,2, ed P.G. Stott, Plenum Press, New York, (1998) 525

[4] Krane, Kenneth S., and David Halliday. Introductory Nuclear Physics. New York: Wiley, 1988. Print.

[5] Plasma Science: From Fundamental Research to Technological Applications. Washington, D.C.: National Academy, 1995. Print.

[6] Ed Cecil Doug Darrow, Bob Ellis Stephan Baumel, Andreas, Vasily Kiptily, "Design of Fast Ion Loss Diagnostics for JET", Bulletin of the American Physical Society 48, 204 (2003).

[7] Herman, Mike. "Https://www.nndc.bnl.gov/sigma/index.jsp?as=58&lib=endfb7.1&nsub=10." National Nuclear Data Center. Brookhaven National Laboratory, n.d. Web.

[8] "Density of the Elements." Density for All the Elements in the Periodic Table. N.p., n.d. Web.

[9] Nuclear Data Sheets 109, 2439 (2008)

[10] "Lou Bertolini Pressure Measuring Devices - USPAS." N.p., n.d. Web. June 2002.

[11] Ziegler, J. F., J. P. Biersack, and Matthias D. Ziegler. SRIM, the Stopping and Range of Ions in Matter. Chester, MD: SRIM, 2008. Print.

[12] "Pearson Product-Moment Correlation." Https://statistics.laerd.com/statistical-guides/pearson-correlation-coefficient-statistical-guide.php. Lund Research Ltd, n.d. Web.

[13] Sigmund, Peter Particle Penetration and Radiation Effects. Springer Series in Solid State Sciences, 151. Berlin Heidelberg: Springer-Verlag. ISBN 3-540-31713-9 (2006)

[14] Carron, N.J. (2007). An Introduction to the Passage of Energetic Particles Through Matter. p. 308.

[15] Bondarenko B D ”Role played by O. A. Lavrent’ev in the formulation of the problem and the initiation of research into controlled nuclear fusion in the USSR” Phys. Usp. 44 844 (2001)

[16] ”How Strong Are Magnets?” How Strong Are Magnets? N.p., n.d. Web. http://www.coolmagnetman.com/magflux.htm

[17] Ku, H. H. (October 1966). ”Notes on the use of propagation of error formulas”. Journal of Research of the National Bureau of Standards. National Bureau of Standards. 70C (4): 262. doi:10.6028/jres.070c.025. ISSN 0022-4316.

[18] 485 Picoammeter: Keithley, Low-Current/High-Resistance Meters

[19] Schaefer, Klaus. Series 275 Digital Readout Convectron Vacuum Gauges Instruction Manual.

APPENDIX A

PLOTS OF DATA

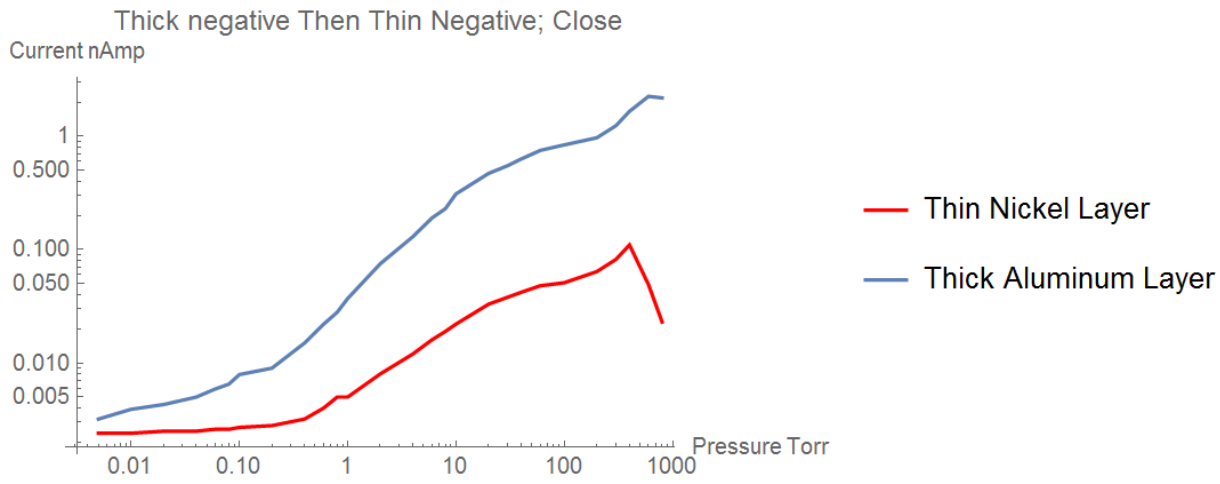

Figure A.1: Thick aluminum layer before the thin nickel layer, both with negative biases

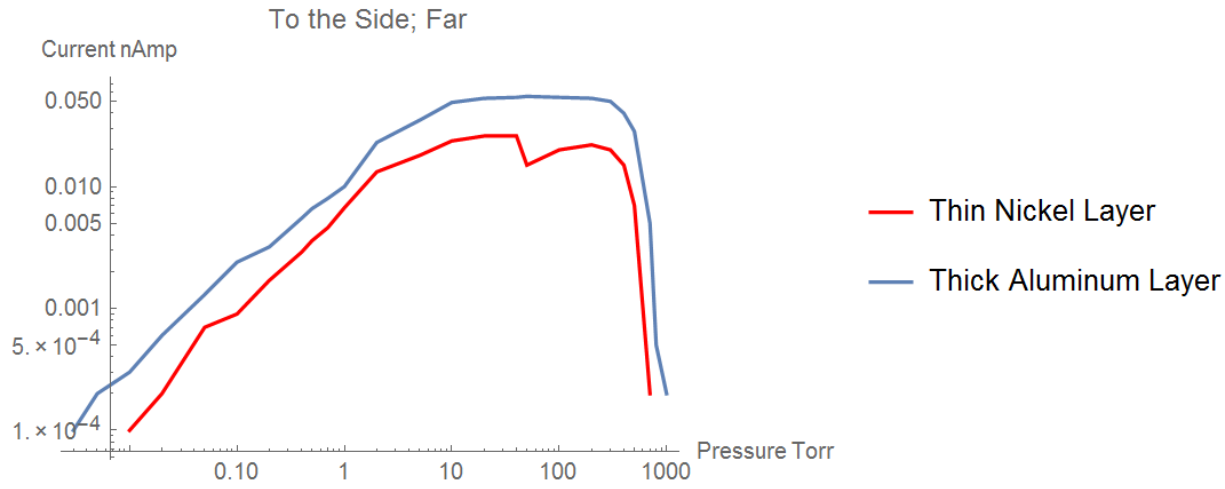

Figure A.2: Source placed on the side of the detector

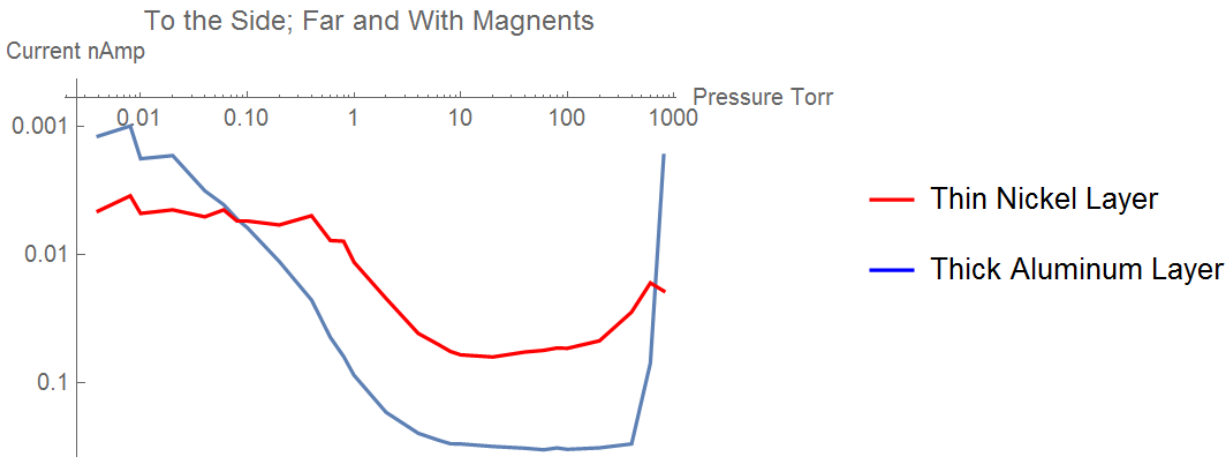

Figure A.3: Source placed on the side of the detector, magnetic field applied

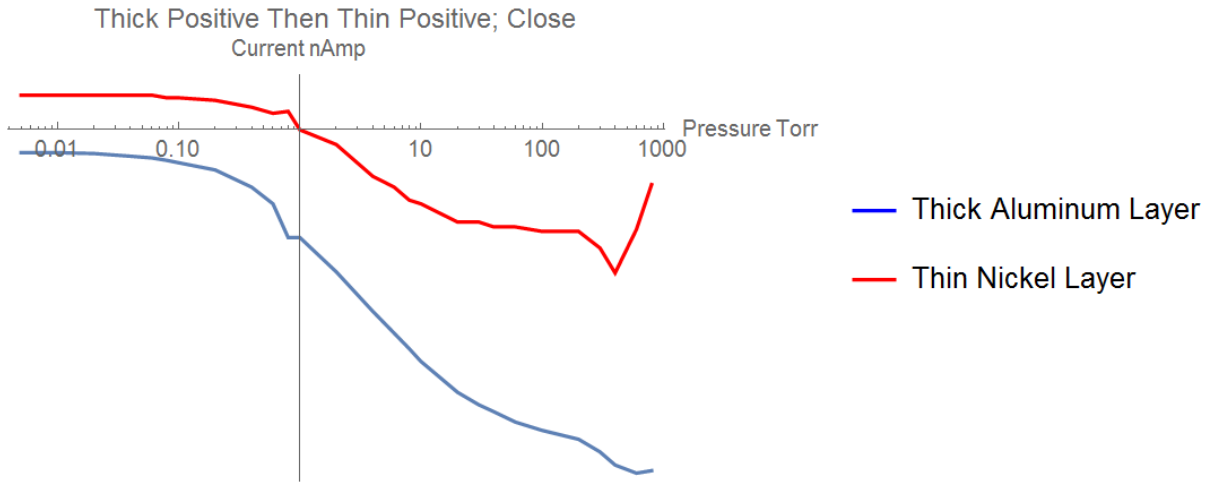

Figure A.4: Thick aluminum layer before the thin nickel layer, both with positive biases

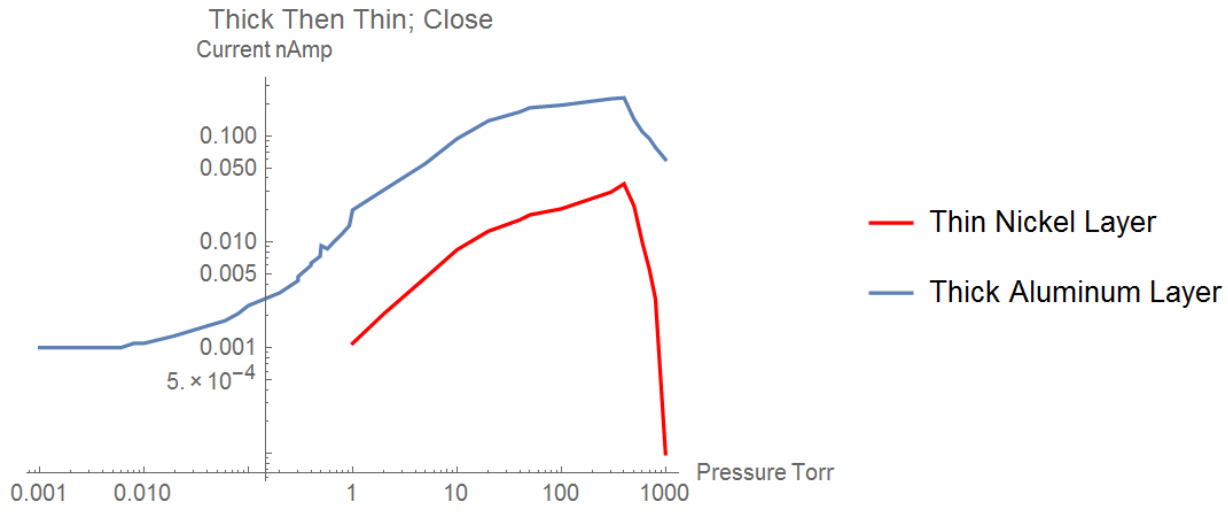

Figure A.5: Thick aluminum layer before the thin nickel layer, no biases applied

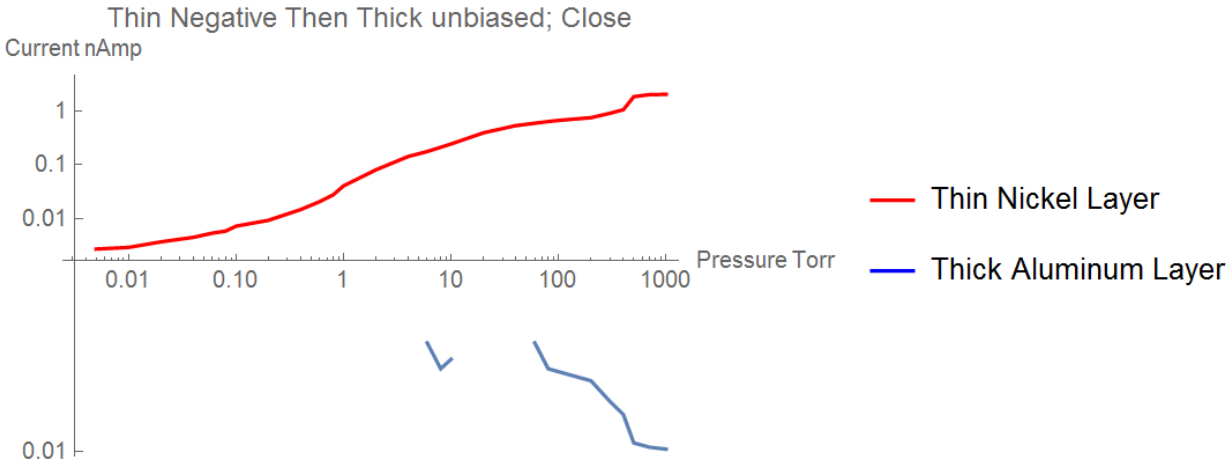

Figure A.6: Thin nickel layer before the thick aluminum layer, nickel negatively biased

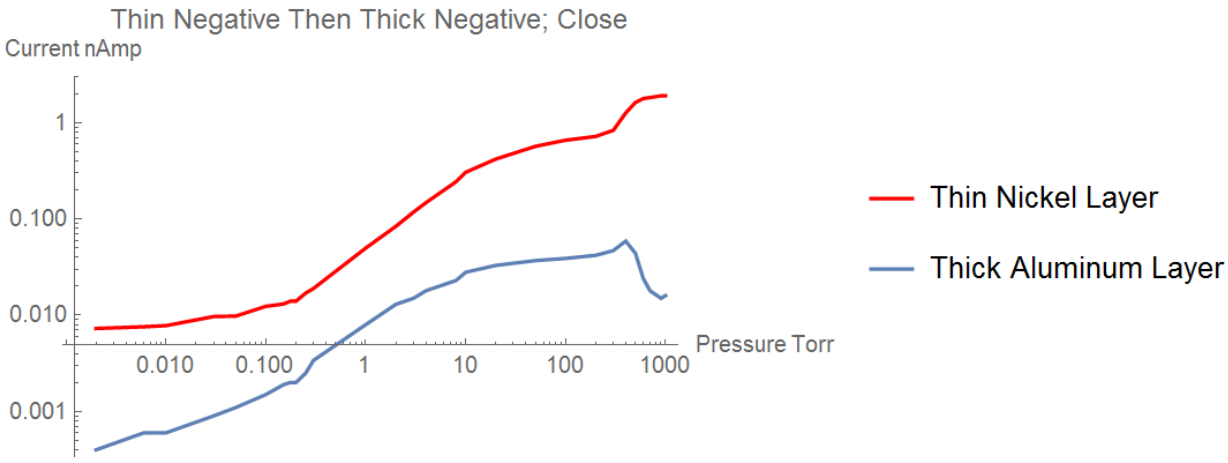

Figure A.7: Thin nickel layer before the thick aluminum layer, both with a negative bias

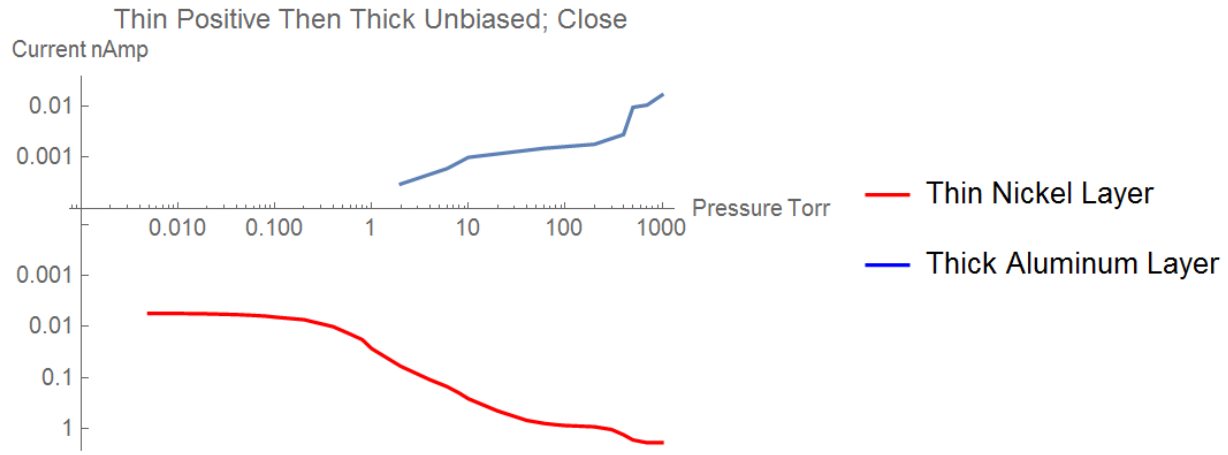

Figure A.8: Thin nickel layer before the thick aluminum layer, nickel layer positively biased

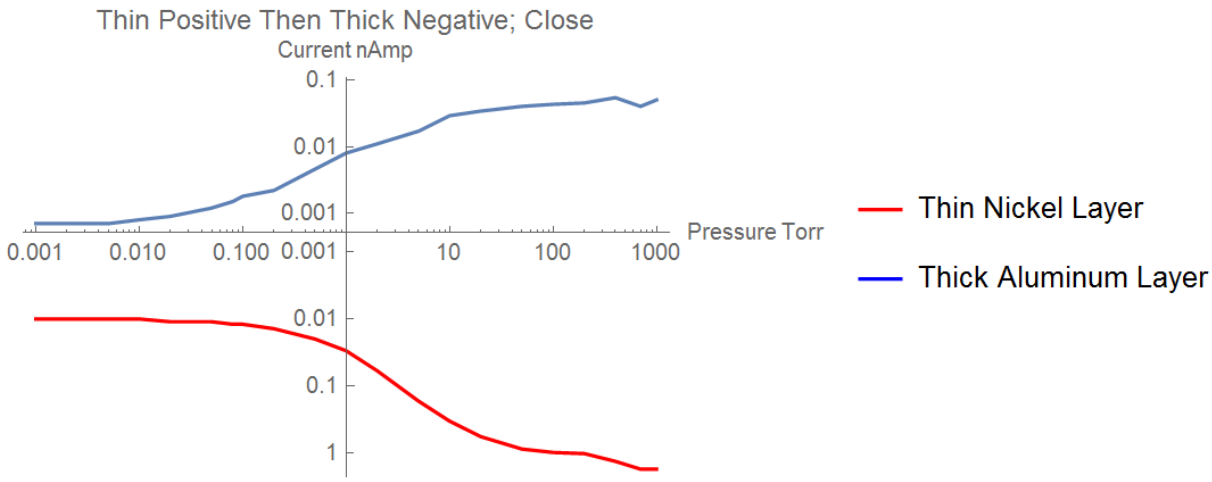

Figure A.9: Thin nickel layer before the thick aluminum layer, nickel layer with a positive bias, and aluminum layer with a negative bias

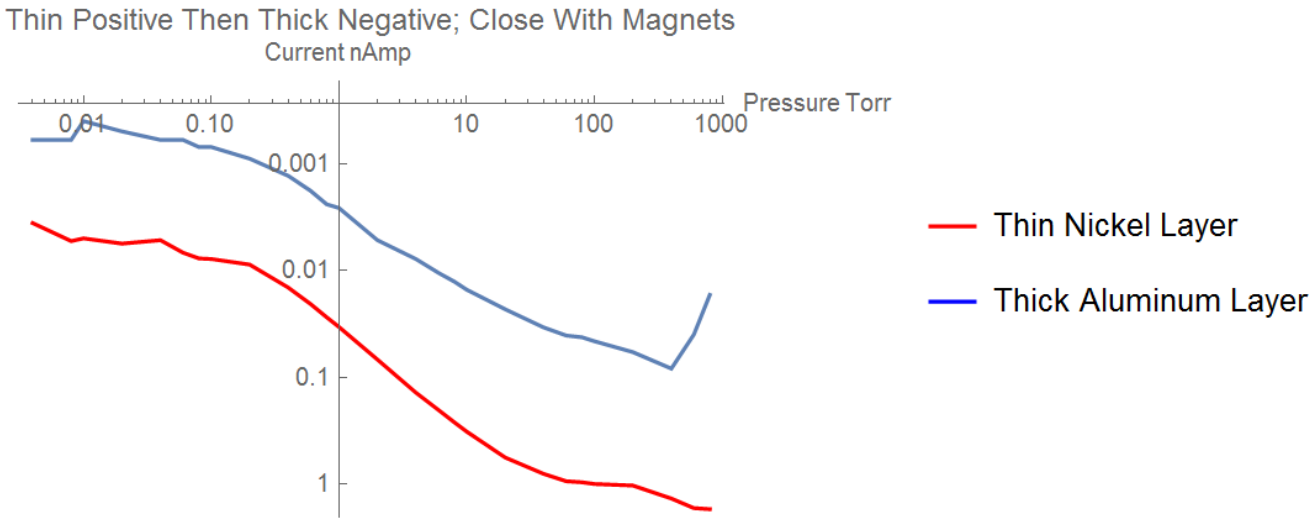

Figure A.10: Thin nickel layer before the thick aluminum layer, nickel layer with a positive bias, and aluminum layer with a negative bias, Magnetic field also applied

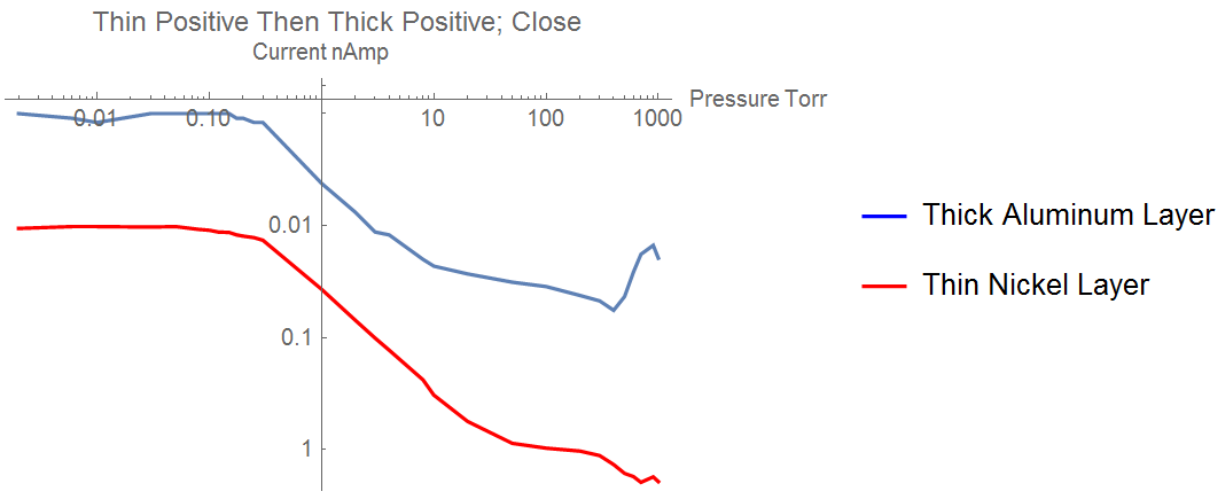

Figure A.11: Nickel layer before Aluminum layer, both layers positively biased

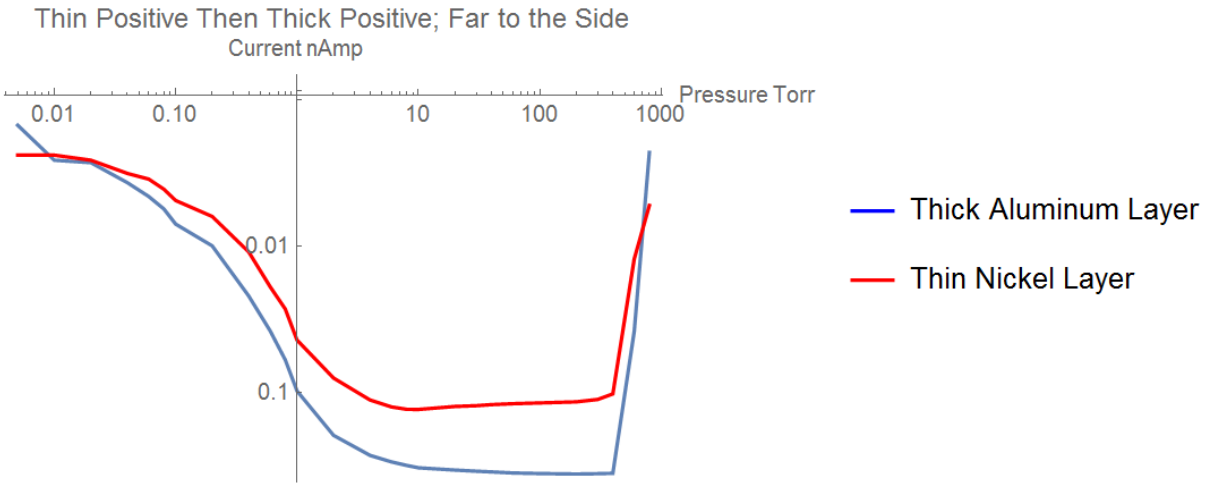

Figure A.12: Thin nickel before thick aluminum, both positively biased, source to the side

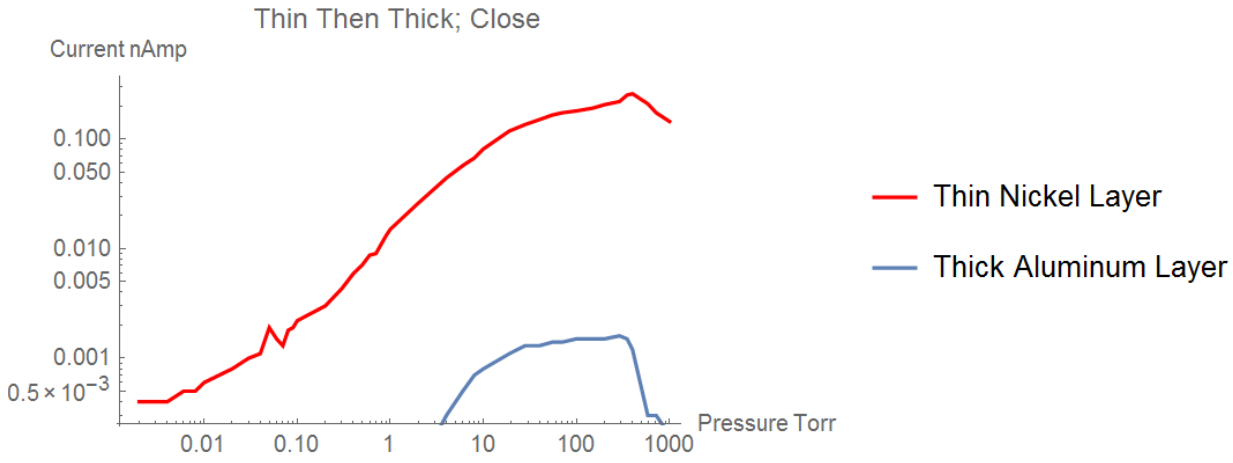

Figure A.13: Thin nickel layer before the thick aluminum layer

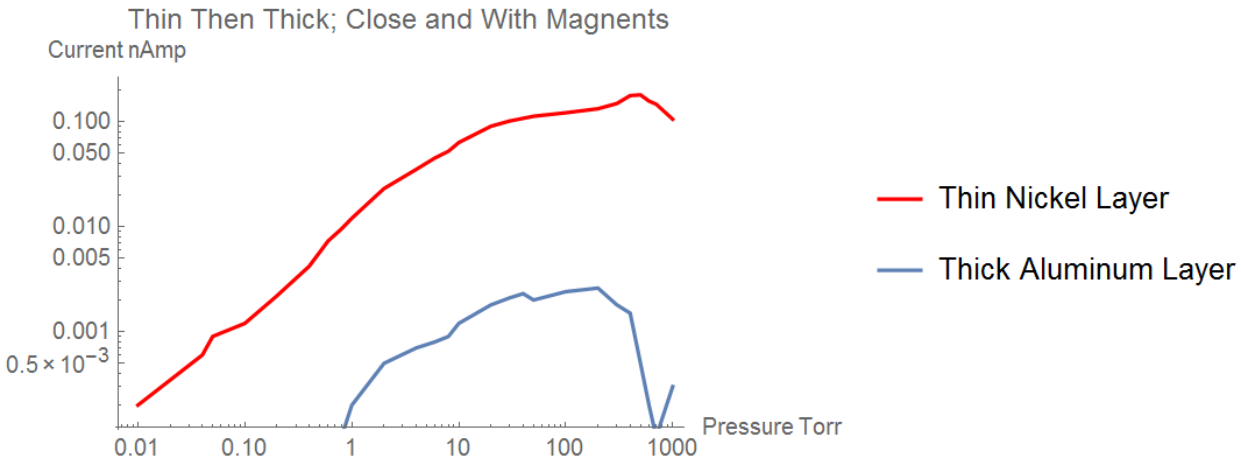

Figure A.14: Thin nickel layer before the thick aluminum layer, Magnetic field applied

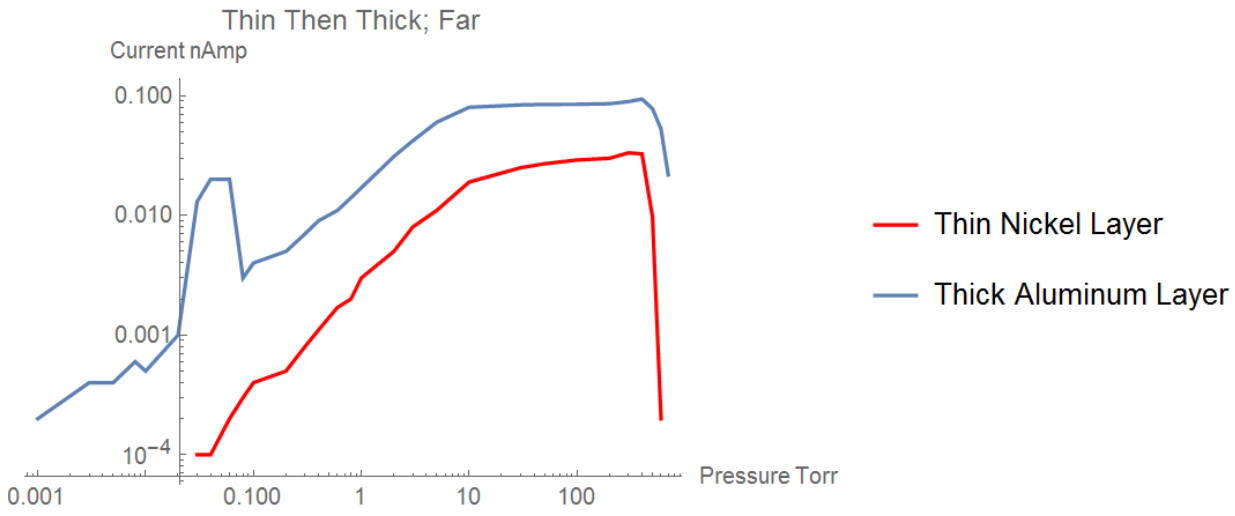

Figure A.15: Thin nickel layer before the thick aluminum layer, with the source detector distance increased

APPENDIX B

MATHEMATICA NOTEBOOK

SRIM data Analysis

13cm distance

In[620]:=
```
ClearAll["Global`*"]
data = Import["SRIMdataAirP_%trans_eper_range.txt", "Table"];
press13 = data[[2 ;;, 1]](*Torr*);
pertrans13 = data[[2 ;;, 2]](*percentage*);
epera13 = data[[2 ;;, 3]](*# e per alpha*);
range13 = data[[2 ;;, 4]] / 1000.(*m*);
```

The data from SRIM simulations is imported above. This data includes the pressure of the chamber, the percent of alpha particles that make it to the detector, the average number of electrons ionized per alpha particle and the range of the particle

In[626]:=
```
a = .04;
b = .04;
dist1 = .130;
qtot13 = epera13 + 2 * (pertrans13 / 100);
qtotplt = ListLogLogPlot[Partition[Riffle[press13, qtot13], 2],
  PlotRange → All, Joined → True, PlotStyle → Black]
```

Out[630]=

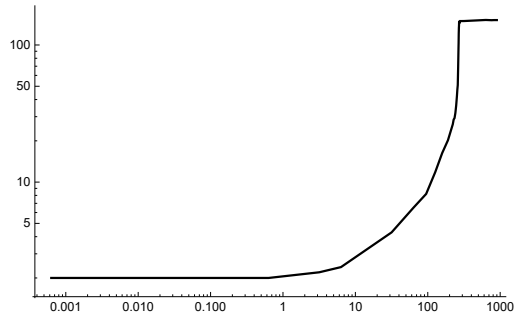

The above plot shows a simulation in which all alpha particles and ionized electrons are collected by the detector. A more realistic model would be one in which the ionized electrons are emitted isotropically from the range of the particle. This model is shown below

In[631]:=
```
Ω = {};
Do[If[dist1 - range13[[n]] == 0, AppendTo[Ω, 2 * Pi],
  AppendTo[Ω, (2 * ArcTan[a / (2 * (dist1 - range13[[n]]))]) *
    (1 - Cos[2 * ArcTan[b / (2 * (dist1 - range13[[n]]))]])]], {n, Length[press13]}]
isoeperα13 = ((Ω / (4 * Pi)) * eperα13) + 2 * (pertrans13 / 100);
pltiso = ListLogLogPlot[Partition[Riffle[press13, isoeperα13], 2],
  PlotRange → {{.0001, 1000}, {1, 100}}, Joined → True]
```

Out[634]=

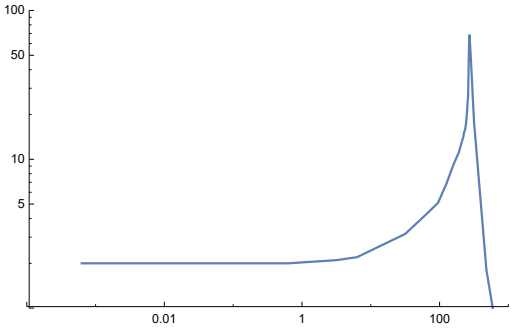

In[635]:=
```
Show[pltiso, qtotplt, PlotRange -> All]
```

Out[635]=

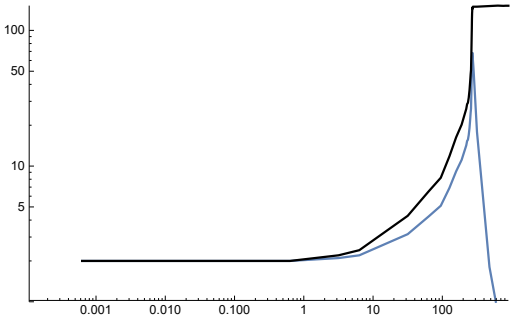

The second model seems to more accuratley capture the situation. A third approximation in which electrons are emitted based upon how far the alpha particle has moved and how much energy has been lost to ionization. isotropic emmition is still assumed. The Bethe formula is used to determine the above

Bethe no Bloch 13

The first thing to do is initialize variables and input constants.

In[636]:=
```
r = 8.314(*J K^-1 mol^-1*);
T = 294.(*K*);
av = 6.022 * 10^23;
nlist = ((press13 * (133.322)) / (r * T)) * av(*targets/m**3*);
ϵ0 = 8.854 * 10^(-12)(*F M^-1*);
zt = 7.2;
zp = 2.;
e = 1.602 * 10^(-19)(*C*);
me = 9.109 * 10^(-31)(*Kg*);
iav = .131 * 10^(-17)(*J*);
mα = 6.644 * 10^(-27)(*Kg*);
c = 299 792 458(*m/s*);
kα0 = 9.299 * 10^(-13)(*J*);
v0 = c * Sqrt[1 - (1 / (1 + kα0 / (mα * c * c))^2)](*m s^-1*);
dx = .00001(*m*);
Nrg = Table[kα0, {n, Length[press13]}, {j, 1}];
v = Table[v0, {n, Length[press13]}, {j, 1}];
x = Table[dx, {n, Length[press13]}, {j, 1}];
(*Bethe Formula from Wiki below*)
δnrg0 = dx * (4 Pi / (me c^2)) * (nlist * zp^2 * zt / (v0^2 / c^2)) * (e^2 / (4 Pi ϵ0))^2 * (Log[2 me v0^2 / (iav (1 - v0^2 / c^2))] - v0^2 / c^2);
δnrg = Partition[δnrg0, 1];
(*The Do and While loops below run the Bethe
 formula at different pressures until the ion is at rest*)
Do[
  j = 1;
  While[δnrg[[n, j]] > .5 δnrg[[n, 1]] && x[[n, j]] < dist1,
   AppendTo[Nrg[[n]], Nrg[[n, j]] - δnrg[[n, j]]];
   AppendTo[x[[n]], x[[n, j]] + dx];
   AppendTo[v[[n]], c * Sqrt[1 - (1 / (1 + Nrg[[n, j + 1]] / (mα * c * c))^2)]];
   AppendTo[δnrg[[n]], dx * (4 Pi / (me c^2)) * (nlist[[n]] * zp^2 * zt / (v[[n, j+1]]^2 / c^2)) *
     (e^2 / (4 Pi ϵ0))^2 * (Log[2 me v[[n, j + 1]]^2 / (iav (1 - v[[n, j+1]]^2 / c^2))] - v[[n, j + 1]]^2 / c^2)];
   j++]
  , {n, Length[press13]}] // AbsoluteTiming
```

Out[656]= {98.6925, Null}

In[657]:=
```
ListPlot[Partition[Riffle[x[[1]], (δnrg[[1]] / (1.602 * 10^-16))], 2],
 PlotRange → All, Joined -> True, GridLines → {{{range13[[1]], Red}}, None}]
ListPlot[{Partition[Riffle[x[[1]], δnrg[[1]] / (1.602 * 10^-16)], 2],
   Partition[Riffle[x[[4]], δnrg[[4]] / (1.602 * 10^-16)], 2],
   Partition[Riffle[x[[6]], δnrg[[6]] / (1.602 * 10^-16)], 2],
   Partition[Riffle[x[[15]], δnrg[[15]] / (1.602 * 10^-16)], 2],
   Partition[Riffle[x[[32]], δnrg[[32]] / (1.602 * 10^-16)], 2]},
 PlotRange → {0, 1.1 Max[δnrg] / (1.602 * 10^-16)}, Joined → True,
 AxesLabel → {"Distance meters", "Energy Loss, KeV"},
 PlotLabel → "α Particle Energy Loss in Air",
 PlotLegends → LineLegend[{Blue, Orange, Green, Red, Purple},
   {"900 Torr", "633 Torr", "317 Torr", "270 Torr", "158 Torr"}]]
```

Out[657]=

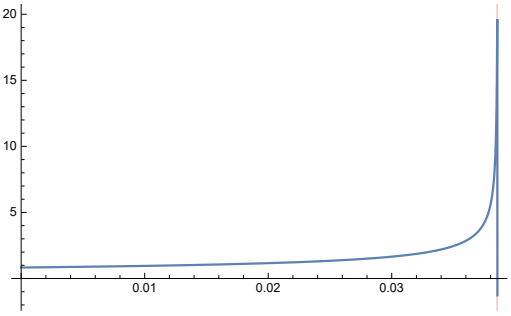

Out[658]=

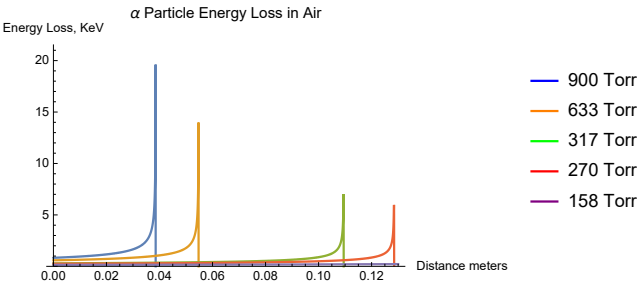

In[659]:=
```
isowdist = {}; Do[AppendTo[isowdist,
  Sum[(δnrg[[n, j]] / Total[δnrg[[n]]]) * 1/(4 Pi) (2 * ArcTan[a / (2 * (dist1 - x[[n, j]]))]) *
    (1 - Cos[2 * ArcTan[b / (2 * (dist1 - x[[n, j]]))]]) * epera13[[n]],
   {j, Length[δnrg[[n]]]}] + 2 * pertrans13[[n]] / 100.],
 {n, Length[press13]}] // AbsoluteTiming
```

Out[659]= {684.917, Null}

In[660]:=
```
isoanddist = ListLogLogPlot[Partition[Riffle[press13, isowdist], 2],
  Joined → True, PlotRange → {{.0001, 1000}, {1, 20}}, PlotStyle → Red]
```

Out[660]=

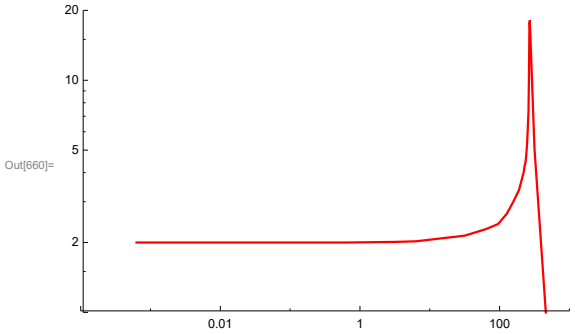

In[661]:=
```
Show[isoanddist, pltiso, qtotplt, PlotRange → All]
```

Out[661]=

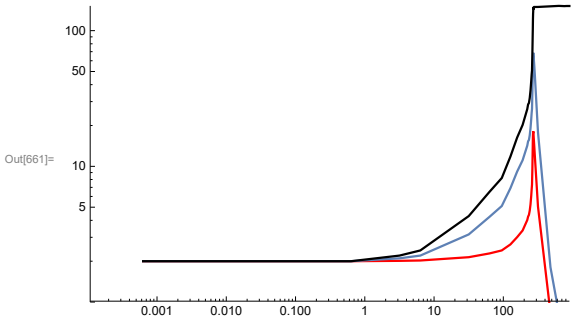

Real Data

In[850]:=
```
ClearAll["Global`*"]
Needs["ErrorBarLogPlots`"]
```

In[891]:=
```
halfthinthick = Import["HalfInchThinThick.txt", "Table"];
halftntkp = halfthinthick[[2 ;;, 1]];
halftntk3 = halfthinthick[[2 ;;, 2]];
halftntk30 = halfthinthick[[2 ;;, 3]];
plothftntk3 = ErrorListLogLogPlot[Partition[
    Riffle[Partition[Riffle[halftntkp, halftntk3], 2], ErrorBar[.001, .0001]], 2],
   Joined → True, PlotStyle → Red, PlotLegends → {"Thin Nickel Layer"}];
plothftntk30 = ErrorListLogLogPlot[Partition[
    Riffle[Partition[Riffle[halftntkp, halftntk30], 2], ErrorBar[.001, .0001]], 2],
   Joined → True, PlotLegends → {"Thick Aluminum Layer"}];
Show[plothftntk3, plothftntk30, AxesLabel → {Pressure (Torr), Current (nAmp)},
 PlotLabel → "Thin Then Thick; Close"]
Grid[halfthinthick, Frame -> All]
```

Out[897]=

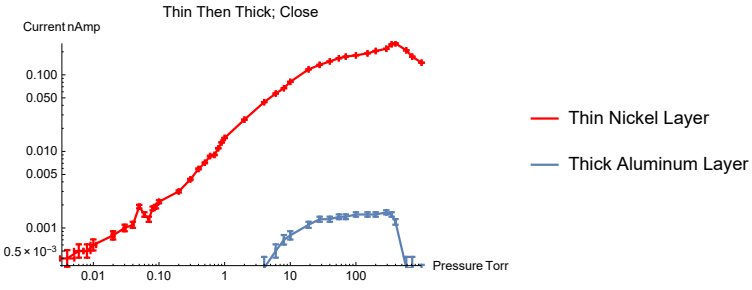

Out[896]=

Torr	Thin	Thick
999	0.1442	0.0002
720	0.173	0.0003
585	0.209	0.0003
400	0.258	0.0012
350	0.251	0.0015
290	0.219	0.0016
200	0.205	0.0015
150	0.191	0.0015
100	0.18	0.0015
70	0.173	0.0014
55	0.165	0.0014
40	0.15	0.0013
28	0.135	0.0013
19	0.118	0.0011
10	0.081	0.0008
8	0.067	0.0007
6	0.057	0.0005
4	0.044	0.0003
2	0.026	0.0001
1	0.015	0
0.9	0.0131	0
0.8	0.011	0
0.7	0.009	0
0.6	0.0087	0
0.5	0.0071	0
0.4	0.0059	0
0.3	0.0043	0
0.2	0.003	-0.0001
0.1	0.0022	-0.0002
0.09	0.0019	-0.0002
0.08	0.0018	-0.0002
0.07	0.0013	-0.0002
0.06	0.0015	-0.0003
0.05	0.0019	-0.003
0.04	0.0011	-0.0003
0.03	0.001	-0.0003
0.02	0.0008	0
0.01	0.0006	-0.0003
0.008	0.0005	-0.0003
0.006	0.0005	-0.0003
0.004	0.0004	-0.0003
0.002	0.0004	-0.0003

```
(*The error bars on the above plot are
 small and are omitted from the following plots*)
```

In[674]:=
```
halfthickthin = Import["HalfInchThickThin.txt", "Table"];
halftktnp = halfthickthin[[2 ;;, 1]];
halftktn3 = halfthickthin[[2 ;;, 2]];
halftktn30 = halfthickthin[[2 ;;, 3]];
plothftktn3 = ListLogLogPlot[Partition[Riffle[halftktnp, halftktn3], 2],
    Joined → True, PlotStyle → Red, PlotLegends → {"Thin Nickel Layer"}];
plothftktn30 = ListLogLogPlot[Partition[Riffle[halftktnp, halftktn30], 2],
    Joined → True, PlotLegends → {"Thick Aluminum Layer"}];
Show[plothftktn3, plothftktn30, AxesLabel → {Pressure (Torr), Current (nAmp)},
 PlotRange → All, PlotLabel → "Thick Then Thin; Close"]
Grid[halfthickthin, Frame -> All]
```

Out[680]=

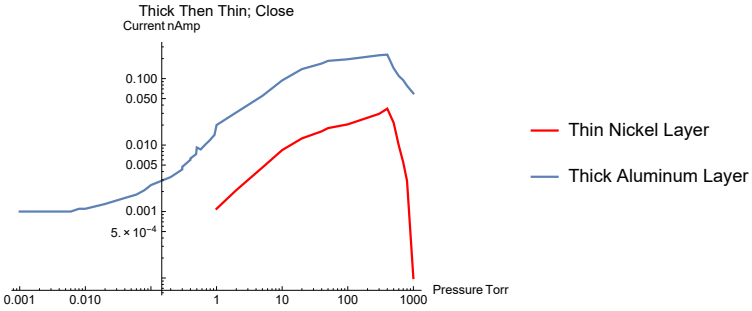

Out[681]=

Torr	Thin	Thick
999	0.0001	0.06
800	0.0029	0.078
700	0.0055	0.0947
600	0.0098	0.1093
500	0.0217	0.1433
400	0.0353	0.2296
300	0.0295	0.2245
100	0.0205	0.1954
50	0.018	0.1849
40	0.0161	0.1687
20	0.0126	0.139
10	0.0084	0.094
5	0.0046	0.055
2	0.0021	0.031
1	0.0011	0.02
0.93	na	0.0142
0.845	na	0.0128
0.8	0.0007	0.012
0.76	na	0.0114
0.675	na	0.0102
0.573	na	0.0086
0.5	0.0005	0.0092
0.488	na	0.0073
0.4	0.0003	0.0063
0.4	na	0.006
0.3	0.0002	0.0047
0.3	na	0.0043
0.2	0.0001	0.0033
0.1	0	0.0025
0.08	na	0.0021
0.06	na	0.0018
0.04	na	0.0016
0.02	na	0.0013
0.01	0	0.0011
0.008	na	0.0011
0.006	na	0.001
0.004	na	0.001
0.002	na	0.001
0.001	na	0.001

In[682]:=
```
twohalfthickthin = Import["TwoandAHalfThickThin.txt", "Table"];
twhalftktnp = twohalfthickthin[[2 ;;, 1]];
twhalftktn3 = twohalfthickthin[[2 ;;, 2]];
twhalftktn30 = twohalfthickthin[[2 ;;, 3]];
plottwtktn3 = ListLogLogPlot[Partition[Riffle[twhalftktnp, twhalftktn3], 2],
   Joined → True, PlotStyle → Red, PlotLegends → {"Thin Nickel Layer"}];
plottwtktn30 = ListLogLogPlot[Partition[Riffle[twhalftktnp, twhalftktn30], 2],
   Joined → True, PlotLegends → {"Thick Aluminum Layer"}];
Show[plottwtktn3, plottwtktn30, AxesLabel → {Pressure (Torr), Current (nAmp)},
 PlotRange → All, PlotLabel → "Thin Then Thick; Far"]
Grid[twohalfthickthin, Frame -> All]
```

Out[688]=

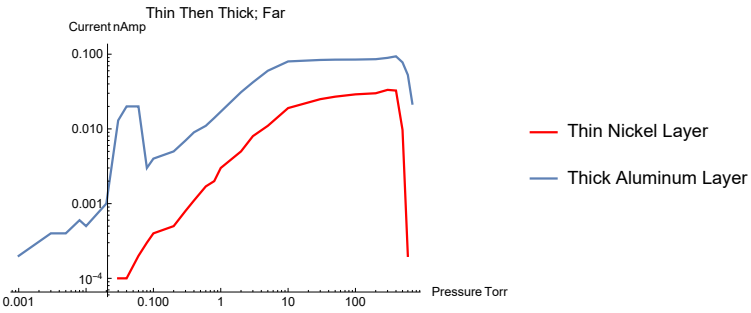

Out[689]=

Torr	Thin	Thick
999	0	na
700	na	0.0218
600	0.0002	0.0527
500	0.0097	0.0777
400	0.0326	0.0936
300	0.0333	0.0893
200	0.03	0.0857
100	0.029	0.0847
50	0.027	0.0845
30	0.025	0.0837
10	0.019	0.08
5	0.011	0.06
3	0.008	0.042
2	0.005	0.031
1	0.003	0.017
0.8	0.002	0.014
0.6	0.0017	0.011
0.4	0.0011	0.009
0.3	0.0008	0.007
0.2	0.0005	0.005
0.1	0.0004	0.004
0.08	0.0003	0.003
0.06	0.0002	0.02
0.04	0.0001	0.02
0.03	0.0001	0.013
0.02	0	0.001
0.01	0	0.0005
0.008	0	0.0006
0.005	0	0.0004
0.003	0	0.0004
0.001	0	0.0002

In[692]:=
```
side = Import["TwoandAHalfToTheSide.txt", "Table"];
sidep = side[[2 ;;, 1]];
side3 = side[[2 ;;, 2]];
side30 = side[[2 ;;, 3]];
plotside3 = ListLogLogPlot[Partition[Riffle[sidep, side3], 2],
   Joined → True, PlotStyle → Red, PlotLegends → {"Thin Nickel Layer"}];
plotside30 = ListLogLogPlot[Partition[Riffle[sidep, side30], 2],
   Joined → True, PlotLegends → {"Thick Aluminum Layer"}];
Show[plotside3, plotside30, AxesLabel → {Pressure (Torr), Current (nAmp)},
 PlotRange → All, PlotLabel → "To the Side; Far"]
Grid[side, Frame -> All]
```

Out[698]=

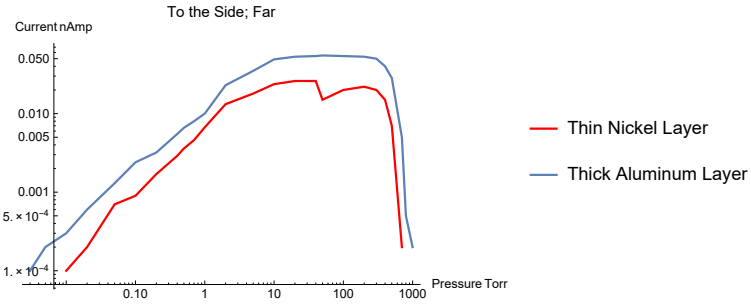

Out[699]=

Torr	Thin	Thick
999	na	0.0002
800	0	0.0005
700	0.0002	0.005
501	0.007	0.0284
400	0.015	0.04
300	0.02	0.05
200	0.022	0.053
100	0.02	0.054
50	0.015	0.055
40	0.026	0.054
20	0.026	0.053
10	0.0237	0.049
5	0.018	0.035
2	0.0132	0.023
1	0.0067	0.01
0.7	0.0046	0.008
0.5	0.0036	0.0066
0.4	0.0029	0.0055
0.2	0.0017	0.0032
0.1	0.0009	0.0024
0.05	0.0007	0.0013
0.02	0.0002	0.0006
0.01	0.0001	0.0003
0.005	0	0.0002
0.003	0	0.0001

In[700]:=
```
magthinthick = Import["HalfInchThinThickWithMag.txt", "Table"];
mtntkp = magthinthick[[2 ;;, 1]];
mtntk3 = magthinthick[[2 ;;, 2]];
mtntk30 = magthinthick[[2 ;;, 3]];
plotmtntk3 = ListLogLogPlot[Partition[Riffle[mtntkp, mtntk3], 2],
    Joined → True, PlotStyle → Red, PlotLegends → {"Thin Nickel Layer"}];
plotmtntk30 = ListLogLogPlot[Partition[Riffle[mtntkp, mtntk30], 2],
    Joined → True, PlotLegends → {"Thick Aluminum Layer"}];
Show[plotmtntk3, plotmtntk30, AxesLabel → {Pressure (Torr), Current (nAmp)},
 PlotLabel → "Thin Then Thick; Close and With Magnents"]
Grid[magthinthick, Frame -> All]
```

Out[706]=

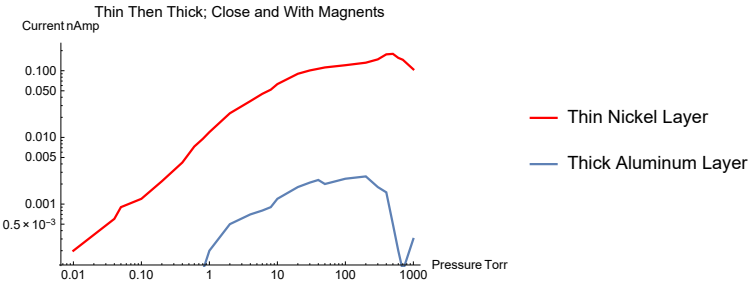

Out[707]=

Torr	Thin	Thick
999	0.105	0.0003
700	0.146	0.0001
600	0.156	0.0002
500	0.179	0.0005
400	0.176	0.0015
300	0.148	0.0018
200	0.132	0.0026
100	0.121	0.0024
50	0.112	0.002
40	0.107	0.0023
30	0.101	0.0021
20	0.09	0.0018
10	0.063	0.0012
8	0.052	0.0009
6	0.045	0.0008
4	0.035	0.0007
2	0.023	0.0005
1	0.012	0.0002
0.8	0.0095	0.0001
0.6	0.0073	0.0001
0.4	0.0042	0
0.2	0.0022	0
0.1	0.0012	0
0.05	0.0009	0
0.04	0.0006	0
0.01	0.0002	0

In[708]:=
```
magtotheside = Import["MagTwoandaHalfTotheSide.txt", "Table"];
msidep = magtotheside[[1 ;;, 1]];
mside3 = Abs[magtotheside[[1 ;;, 2]]];
mside30 = Abs[magtotheside[[1 ;;, 3]]];
plotmside3 = ListLogLogPlot[
   {Partition[Riffle[msidep, mside3], 2]}, Joined → True, PlotStyle → Red];
plotmside30 = ListLogLogPlot[Partition[Riffle[msidep, mside30], 2],
   Joined → True, Ticks → {Automatic, {.001, .01, .1, 1}}];
pivot30 = Last[AxesOrigin /. Options[plotmside30]];
pivot3 = Last[AxesOrigin /. Options[plotmside3]];
Show[plotmside3, plotmside30, PlotRange → All]
Show[Legended[MapAt[Scale[#, {1, -1}, {0, pivot30}] &, plotmside30, 1],
   LineLegend[{Red}, {"Thin Nickel Layer"}]],
  Legended[MapAt[Scale[#, {1, -1}, {0, pivot30}] &, plotmside3, 1],
   LineLegend[{Blue}, {"Thick Aluminum Layer"}]],
  AxesLabel → {"Pressure Torr", "Current nAmp"}, Joined → True,
  PlotLabel → "To the Side; Far and With Magnents",
  PlotRange → All] /. {(Ticks → {xdat_, ydat_}) :>
   Ticks → {xdat, Join[ydat, {2 * pivot30 - #, ##2} & @@@ ydat]}}
Grid[magtotheside, Frame -> All]
```

Out[716]=

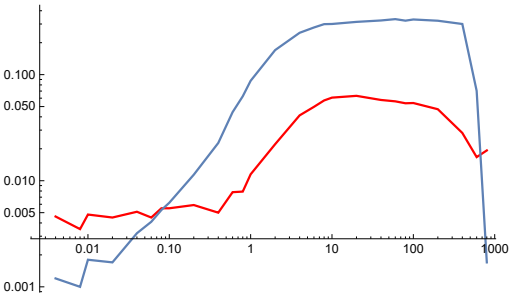

OptionValue::nodef : Unknown option Joined for Graphics. >>

Out[717]=

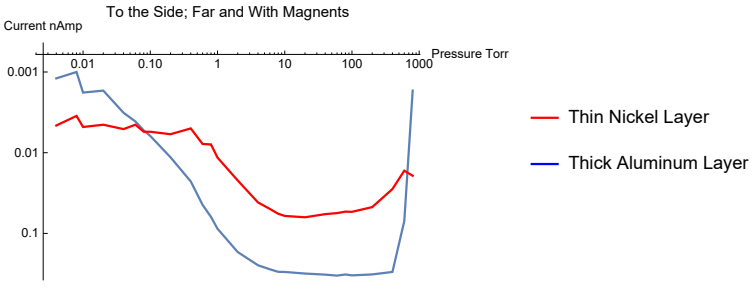

Out[718]=

Torr	Thin	Thick
800	-0.0193	-0.0017
600	-0.0167	-0.0703
400	-0.0282	-0.3001
200	-0.0472	-0.3221
100	-0.054	-0.331
80	-0.0537	-0.3226
60	-0.056	-0.3335
40	-0.0577	-0.324
20	-0.0631	-0.3142
10	-0.0607	-0.3002
8	-0.0571	-0.2991
6	-0.0497	-0.2782
4	-0.0413	-0.2479
2	-0.0221	-0.1703
1	-0.0115	-0.0875
0.8	-0.0079	-0.0625
0.6	-0.0078	-0.0443
0.4	-0.005	-0.0227
0.2	-0.0059	-0.0114
0.1	-0.0055	-0.0062
0.08	-0.0055	-0.0053
0.06	-0.0045	-0.0041
0.04	-0.0051	-0.0032
0.02	-0.0045	-0.0017
0.01	-0.0048	-0.0018
0.008	-0.0035	-0.001
0.004	-0.0046	-0.0012

In[719]:=
```
tknegtnneg = Import["ThickNegThinNeg.txt", "Table"];
tknegtnnegp = tknegtnneg[[1 ;;, 1]];
tknegtnneg3 = tknegtnneg[[1 ;;, 2]];
tknegtnneg30 = tknegtnneg[[1 ;;, 3]];
plottknegtnneg3 = ListLogLogPlot[Partition[Riffle[tknegtnnegp, tknegtnneg3], 2],
   Joined → True, PlotStyle → Red, PlotLegends → {"Thin Nickel Layer"}];
plottknegtnneg30 = ListLogLogPlot[Partition[Riffle[tknegtnnegp, tknegtnneg30], 2],
   Joined → True, PlotLegends → {"Thick Aluminum Layer"}];
Show[plottknegtnneg3, plottknegtnneg30,
 AxesLabel → {Pressure (Torr), Current (nAmp)},
 PlotLabel → "Thick negative Then Thin Negative; Close", PlotRange → All]
Grid[tknegtnneg, Frame -> All]
```

Out[725]=

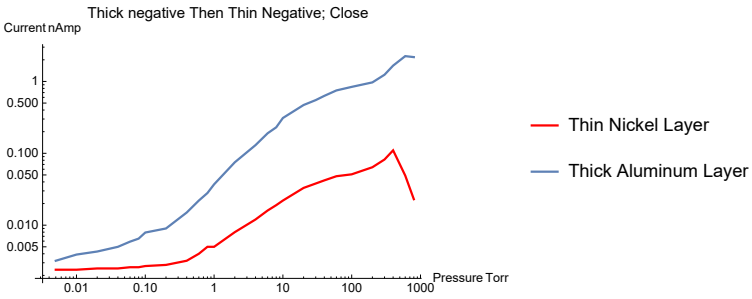

Out[726]=

Torr	Thin	Thick
800	0.023	2.18
600	0.049	2.25
400	0.11	1.66
300	0.082	1.24
200	0.064	0.97
100	0.051	0.84
60	0.048	0.75
40	0.042	0.63
30	0.038	0.55
20	0.033	0.47
10	0.022	0.31
8	0.019	0.23
6	0.016	0.19
4	0.012	0.13
2	0.008	0.075
1	0.005	0.037
0.8	0.005	0.028
0.6	0.004	0.022
0.4	0.0032	0.015
0.2	0.0028	0.009
0.1	0.0027	0.0079
0.08	0.0026	0.0065
0.06	0.0026	0.0059
0.04	0.0025	0.005
0.02	0.0025	0.0043
0.01	0.0024	0.0039
0.005	0.0024	0.0032

In[729]:=
```
tkpostnpos = Import["ThickPosThinPos.txt", "Table"];
tkptnpp = tkpostnpos[[1 ;;, 1]];
tkptnp3 = Abs[tkpostnpos[[1 ;;, 2]]];
tkptnp30 = Abs[tkpostnpos[[1 ;;, 3]]];
plottkpostnpos3 = ListLogLogPlot[
   Partition[Riffle[tkptnpp, tkptnp3], 2], Joined → True, PlotStyle → Red];
plottkpostnpos30 = ListLogLogPlot[Partition[Riffle[tkptnpp, tkptnp30], 2],
   Joined → True];
pivottkpostn3 = Last[AxesOrigin /. Options[plottkpostnpos3]];
pivotttkpostn30 = Last[AxesOrigin /. Options[plottkpostnpos30]];
Show[plottkpostnpos3, plottkpostnpos30, PlotRange → All]
Show[Legended[MapAt[Scale[#, {1, -1}, {0, pivotttkpostn30}] &, plottkpostnpos30, 1],
   LineLegend[{Blue}, {"Thick Aluminum Layer"}]],
  Legended[MapAt[Scale[#, {1, -1}, {0, pivotttkpostn30}] &, plottkpostnpos3, 1],
   LineLegend[{Red}, {"Thin Nickel Layer"}]],
  AxesLabel → {Pressure (Torr), Current (nAmp)},
  PlotLabel → "Thick Positive Then Thin Positive; Close", PlotRange → All,
  AxesOrigin → {.001, pivotttkpostn30}] /. {(Ticks → {xdat_, ydat_}) :→
   Ticks → {xdat, Join[ydat, {2 pivotttkpostn30 - #, ##2} & @@@ ydat]}}
Grid[tkpostnpos, Frame -> All]
```

Out[737]=

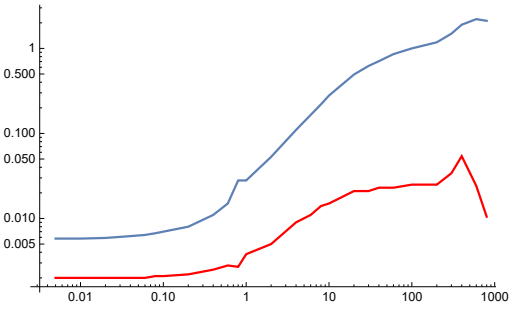

Out[738]=

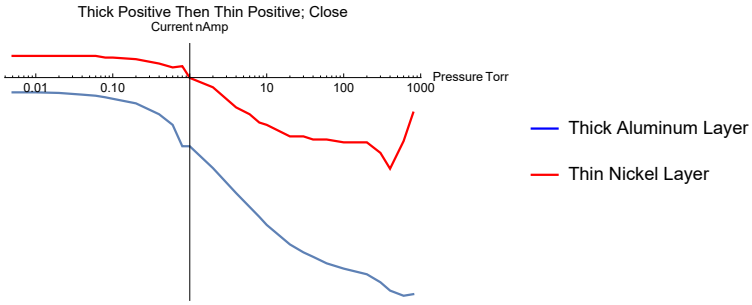

Out[739]=

Torr	Thin	Thick
800	-0.0105	-2.11
600	-0.0241	-2.21
400	-0.054	-1.9
300	-0.034	-1.49
200	-0.025	-1.18
100	-0.025	-1
60	-0.023	-0.857
40	-0.023	-0.708
30	-0.021	-0.622
20	-0.021	-0.493
10	-0.015	-0.279
8	-0.014	-0.22
6	-0.011	-0.165
4	-0.009	-0.11
2	-0.005	-0.053
1	-0.0038	-0.028
0.8	-0.0027	-0.028
0.6	-0.0028	-0.015
0.4	-0.0025	-0.011
0.2	-0.0022	-0.008
0.1	-0.0021	-0.007
0.08	-0.0021	-0.0067
0.06	-0.002	-0.0064
0.04	-0.002	-0.0062
0.02	-0.002	-0.0059
0.01	-0.002	-0.0058
0.005	-0.002	-0.0058

In[740]:=
```
tnnegtk = Import["ThinNegThick.txt", "Table"];
tnntkp = tnnegtk[[1 ;;, 1]];
tnntkp1 = tnnegtk[[1 ;;, 4]];
tnntk3 = tnnegtk[[1 ;;, 2]];
tnntk30 = tnnegtk[[1 ;;, 3]];
plottnnegtk3 = ListLogLogPlot[
    Partition[Riffle[tnntkp, tnntk3], 2], Joined → True, PlotStyle → Red,
    Ticks → {Automatic, {.01, .1, 1}}, PlotLegends → {"Thin Nickel Layer"}];
plottnnegtk30 = ListLogLogPlot[Partition[Riffle[tnntkp1, Abs[tnntk30]], 2],
    PlotRange → All, Joined → True];
pivottnnegtk3 = Last[AxesOrigin /. Options[plottnnegtk3]];
pivottnnegtk30 = Last[AxesOrigin /. Options[plottnnegtk30]];
Show[plottnnegtk3, plottnnegtk30, PlotRange → All]
Show[plottnnegtk3,
  Legended[MapAt[Scale[#, {1, -1}, {0, pivottnnegtk30}] &, plottnnegtk30, 1],
   LineLegend[{Blue}, {"Thick Aluminum Layer"}]],
  AxesLabel → {Pressure (Torr), Current nAmp},
  PlotLabel → "Thin Negative Then Thick unbiased; Close",
  PlotRange → All] /. {(Ticks → {xdat_, ydat_}) :→
   Ticks → {xdat, Join[ydat, {2 pivottnnegtk30 - #, ##2} & @@@ ydat]}}
Grid[tnnegtk, Frame -> All]
```

Last::normal : Nonatomic expression expected at position 1 in Last[AxesOrigin]. >>

Out[749]=

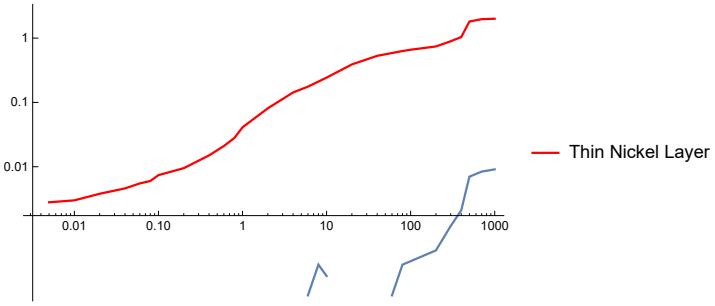

Out[750]=

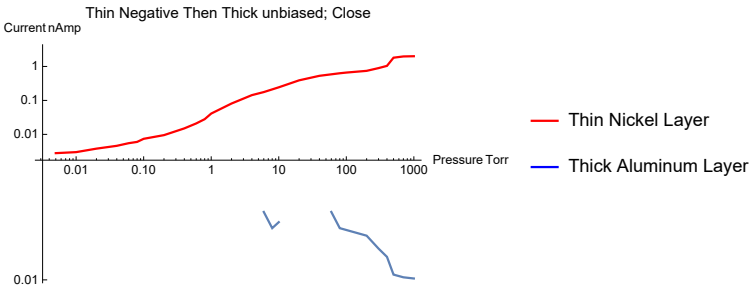

Out[751]=

Torr	Thin	Thick	Torr
999	2	-0.0091	999
700	1.97	-0.0084	700
500	1.81	0.007	500
400	1.04	-0.0021	400
300	0.894	-0.0012	300
200	0.742	-0.0005	200
100	0.66	-0.0003	80
80	0.63	-0.0001	60
40	0.53	0	40
20	0.39	0	20
10	0.243	0.0002	10
6	0.176	0.0003	8
4	0.143	0.0001	6
2	0.081	0	4
1	0.041	0	2
0.8	0.028	0	1
0.6	0.021	0	0.8
0.4	0.015	0	0.6
0.2	0.0095	0	0.4
0.1	0.0074	0	0.2
0.08	0.006	0	0.1
0.06	0.0055	0	0.08
0.04	0.0046	0	0.06
0.02	0.0038	0	0.04
0.01	0.003	0	0.02
0.005	0.0028	0	0.01
0	0	0	0.005

In[752]:= **Max[tnntk3]**

Out[752]= Max[2, Thin]

In[753]:=
```
tnnegtkneg = Import["ThinNegThickNeg.txt", "Table"];
tnntknp = tnnegtkneg[[1 ;;, 1]];
tnntkn3 = tnnegtkneg[[1 ;;, 2]];
tnntkn30 = tnnegtkneg[[1 ;;, 3]];
plottnnegtkneg3 = ListLogLogPlot[Partition[Riffle[tnntknp, tnntkn3], 2],
   Joined → True, PlotStyle → Red, PlotLegends → {"Thin Nickel Layer"}];
plottnnegtkneg30 = ListLogLogPlot[Partition[Riffle[tnntknp, tnntkn30], 2],
   Joined → True, PlotLegends → {"Thick Aluminum Layer"}];
Show[plottnnegtkneg3, plottnnegtkneg30, AxesLabel → {Pressure (Torr), Current nAmp},
 PlotLabel → "Thin Negative Then Thick Negative; Close", PlotRange → All]
Grid[tnnegtkneg, Frame -> All]
```

Out[759]=

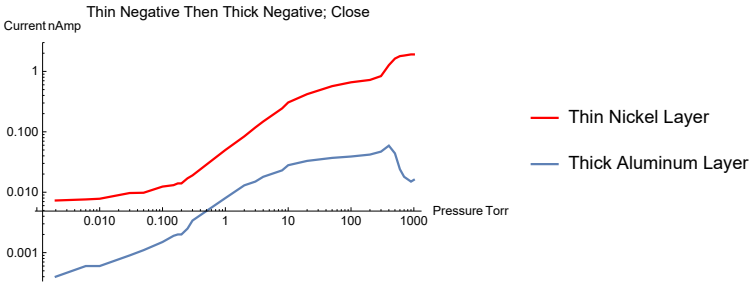

Out[760]=

Torr	Thin	Thick
999	1.91	0.016
900	1.91	0.015
700	1.83	0.018
600	1.79	0.024
500	1.63	0.044
400	1.27	0.059
300	0.836	0.047
200	0.722	0.042
100	0.66	0.039
50	0.57	0.037
20	0.42	0.033
10	0.306	0.028
8	0.244	0.023
4	0.148	0.018
3	0.118	0.015
2	0.084	0.013
1	0.05	0.008
0.3	0.019	0.0034
0.25	0.017	0.0025
0.2	0.014	0.002
0.175	0.014	0.002
0.15	0.0131	0.0019
0.1	0.0124	0.0015
0.05	0.0098	0.0011
0.03	0.0097	0.0009
0.01	0.0078	0.0006
0.006	0.0076	0.0006
0.002	0.0073	0.0004

In[761]:=
```
Max[tnntkn3]
Max[tnntkn30]
```

Out[761]= Max[1.91, Thin]

Out[762]= Max[0.059, Thick]

In[763]:=
```
tnpostk = Import["ThinPosThick.txt", "Table"];
tnptkp = tnpostk[[1 ;;, 1]];
tnptk3 = tnpostk[[1 ;;, 2]];
tnptk30 = tnpostk[[1 ;;, 3]];
tnptk30p = tnpostk[[1 ;;, 4]];
plottnpostk3 = ListLogLogPlot[
   Partition[Riffle[tnptkp, Abs[tnptk3]], 2], Joined → True, PlotStyle → Red,
   Ticks → {Automatic, {.0001, .001, .01, .1, 1}}, AxesOrigin → {.001, .0001}];
plottnpostk30 = ListLogLogPlot[Partition[Riffle[tnptk30p, tnptk30], 2],
   Joined → True];
pivottnpostk30 = Last[AxesOrigin /. Options[plottnpostk30]];
Show[Legended[MapAt[Scale[#, {1, -1}, {0, pivottnpostk30}] &, plottnpostk3, 1],
   LineLegend[{Red}, {"Thin Nickel Layer"}]],
  Legended[plottnpostk30, LineLegend[{Blue}, {"Thick Aluminum Layer"}]],
  AxesLabel → {Pressure (Torr), Current nAmp},
  PlotLabel → "Thin Positive Then Thick Unbiased; Close",
  PlotRange → All] /. {(Ticks → {xdat_, ydat_}) :→
   Ticks → {xdat, Join[ydat, {2 pivottnpostk30 - #, ##2} & @@@ ydat]}}
Grid[tnpostk, Frame -> All]
```

Out[771]=

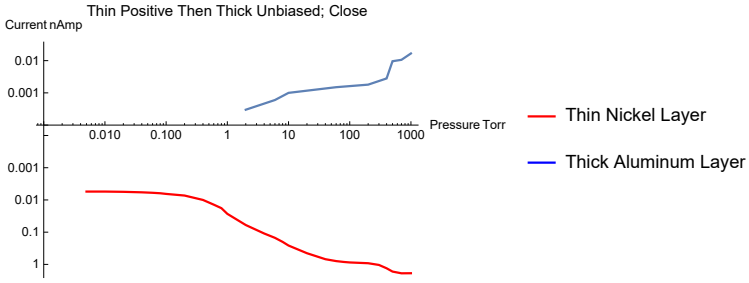

Out[772]=

Torr	Thin	Thick	Torr
999	-1.88	0.0167	999
700	-1.89	0.0106	700
500	-1.67	0.0096	500
400	-1.32	0.0028	400
300	-1.04	0.0018	200
200	-0.92	0.0015	60
100	-0.87	0.001	10
80	-0.84	0.0006	6
60	-0.79	0.0003	2
40	-0.69	0	0.8
20	-0.45	0	0.1
10	-0.26	0	0.06
8	-0.2	0.0001	0.005
6	-0.15	0	0
4	-0.11	0	0
2	-0.06	0	0
1	-0.027	0	0
0.8	-0.018	0	0
0.6	-0.014	0	0
0.4	-0.01	0	0
0.2	-0.0073	0	0
0.1	-0.0065	0	0
0.08	-0.0062	0	0
0.06	-0.006	0	0
0.04	-0.0058	0	0
0.02	-0.0056	0	0
0.01	-0.0055	0	0
0.005	0.0055	0	0

In[773]:=
```
Min[tnptk3]
```

Out[773]=
```
Min[-1.89, Thin]
```

In[774]:=
```
tnpostkneg = Import["ThinPosThickNeg.txt", "Table"];
tnptknp = tnpostkneg[[1 ;;, 1]];
tnptkn3 = tnpostkneg[[1 ;;, 2]];
tnptkn30 = tnpostkneg[[1 ;;, 3]];
plottnpostkneg3 = ListLogLogPlot[Partition[Riffle[tnptknp, Abs[tnptkn3]], 2],
   Joined → True, PlotStyle → Red, Ticks → {Automatic, {.001, .01, .1, 1}}];
plottnpostkneg30 = ListLogLogPlot[Partition[Riffle[tnptknp, tnptkn30], 2],
   Joined → True];
pivottnpostkneg30 = Last[AxesOrigin /. Options[plottnpostkneg3]];
pivottnpostkneg3 = Last[AxesOrigin /. Options[plottnpostkneg30]];
Show[Legended[MapAt[Scale[#, {1, -1}, {0, pivottnpostkneg3}] &,
    plottnpostkneg3, 1], LineLegend[{Red}, {"Thin Nickel Layer"}]],
  Legended[plottnpostkneg30, LineLegend[{Blue}, {"Thick Aluminum Layer"}]],
  AxesLabel → {Pressure (Torr), Current nAmp},
  PlotLabel → "Thin Positive Then Thick Negative; Close", PlotRange → All,
  AxesOrigin → {.002, pivottnpostkneg3}] /. {(Ticks → {xdat_, ydat_}) :→
   Ticks → {xdat, Join[ydat, {2 pivottnpostkneg3 - #, ##2} & @@@ ydat]}}
Grid[tnpostkneg, Frame -> All]
```

Out[782]=

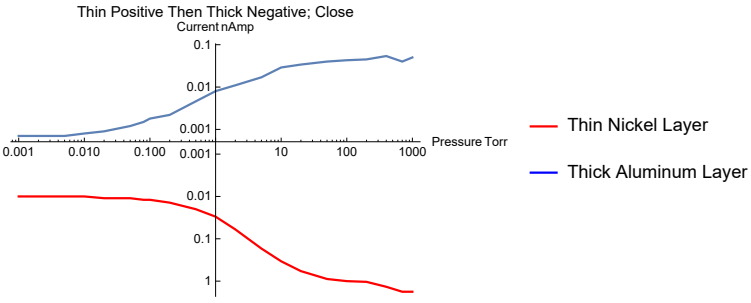

Out[783]=

Torr	Thin	Thick
999	-1.78	0.05
700	-1.78	0.04
400	-1.36	0.054
200	-1.04	0.045
100	-1	0.043
50	-0.89	0.04
20	-0.58	0.034
10	-0.34	0.029
5	-0.17	0.017
2	-0.06	0.011
1	-0.03	0.008
0.5	-0.02	0.0046
0.2	-0.014	0.0022
0.1	-0.012	0.0018
0.08	-0.012	0.0015
0.05	-0.011	0.0012
0.02	-0.011	0.0009
0.01	-0.01	0.0008
0.005	-0.01	0.0007
0.001	-0.01	0.0007

In[784]:=
```
Min[tnptkn3]
Max[tnptkn30]
```

Out[784]= Min[-1.78, Thin]

Out[785]= Max[0.054, Thick]

In[786]:=
```
tnpostkpos = Import["ThinPosThickPos.txt", "Table"];
tnptkpp = tnpostkpos[[1 ;;, 1]];
tnptkp3 = tnpostkpos[[1 ;;, 2]];
tnptkp30 = tnpostkpos[[1 ;;, 3]];
plottnpostkpos3 = ListLogLogPlot[
    Partition[Riffle[tnptkpp, Abs[tnptkp3]], 2], Joined → True, PlotStyle → Red];
plottnpostkpos30 = ListLogLogPlot[Partition[Riffle[tnptkpp, Abs[tnptkp30]], 2],
    Joined → True, Ticks → {Automatic, {.001, .01, .1, 1}}];
pivottnpostkpos30 = Last[AxesOrigin /. Options[plottnpostkpos30]];
pivottnpostkpos3 = Last[AxesOrigin /. Options[plottnpostkpos3]];
Show[Legended[MapAt[Scale[#, {1, -1}, {0, pivottnpostkpos30}] &,
     plottnpostkpos30, 1], LineLegend[{Blue}, {"Thick Aluminum Layer"}]],
  Legended[MapAt[Scale[#, {1, -1}, {0, pivottnpostkpos30}] &, plottnpostkpos3, 1],
   LineLegend[{Red}, {"Thin Nickel Layer"}]],
  AxesLabel → {Pressure (Torr), Current nAmp},
  PlotLabel → "Thin Positive Then Thick Positive; Close", PlotRange → All,
  AxesOrigin → {.001, pivottnpostkpos30}] /. {(Ticks → {xdat_, ydat_}) :→
   Ticks → {xdat, Join[ydat, {2 pivottnpostkpos30 - #, ##2} & @@@ ydat]}}
Grid[tnpostkpos, Frame -> All]
```

Out[794]=

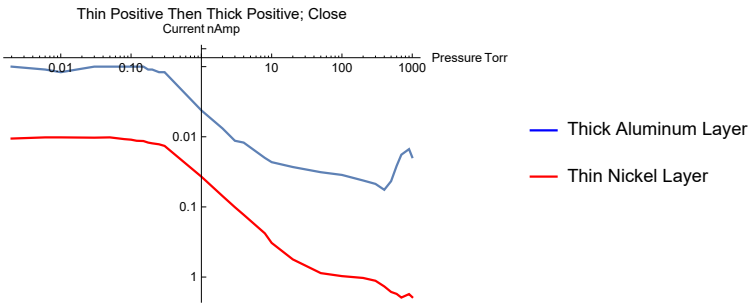

Out[795]=

Torr	Thin	Thick
999	-1.93	-0.0195
900	-1.75	-0.015
700	-1.96	-0.018
600	-1.74	-0.026
500	-1.63	-0.043
400	-1.36	-0.057
300	-1.13	-0.047
200	-1.03	-0.042
100	-0.97	-0.035
50	-0.879	-0.032
20	-0.56	-0.027
10	-0.326	-0.023
8	-0.238	-0.02
4	-0.1294	-0.0121
3	-0.101	-0.0114
2	-0.07	-0.0076
1	-0.037	-0.0042
0.3	-0.0135	-0.0012
0.25	-0.0128	-0.0012
0.2	-0.0124	-0.0011
0.175	-0.0121	-0.0011
0.15	-0.0115	-0.001
0.12	-0.0114	-0.001
0.1	-0.011	-0.001
0.08	-0.0108	-0.001
0.05	-0.0102	-0.001
0.03	-0.0103	-0.001
0.01	-0.0102	-0.0012
0.006	-0.0102	-0.0011
0.002	-0.0106	-0.001

In[796]:=
```
Min[tnptkp3]
Min[tnptkp30]
```

Out[796]= Min[-1.96, Thin]

Out[797]= Min[-0.057, Thick]

In[798]:=
```
tnpostkposmag = Import["ThinPosThickPosMag.txt", "Table"];
tnptkpmp = tnpostkposmag[[1 ;;, 1]];
tnptkpm3 = tnpostkposmag[[1 ;;, 2]];
tnptkpm30 = tnpostkposmag[[1 ;;, 3]];
plottnpostkposmag3 = ListLogLogPlot[Partition[Riffle[tnptkpmp, Abs[tnptkpm3]], 2],
   Joined → True, PlotStyle → Red, Ticks → {Automatic, {.001, .01, .1, 1}}];
plottnpostkposmag30 = ListLogLogPlot[Partition[Riffle[tnptkpmp, Abs[tnptkpm30]], 2],
   Joined → True, Ticks → {Automatic, {.001, .01, .1, 1}}];
pivottnpostkposmag30 = Last[AxesOrigin /. Options[plottnpostkposmag30]];
Show[Legended[MapAt[Scale[#, {1, -1}, {0, pivottnpostkposmag30}] &,
    plottnpostkposmag3, 1], LineLegend[{Red}, {"Thin Nickel Layer"}]],
  Legended[MapAt[Scale[#, {1, -1}, {0, pivottnpostkposmag30}] &,
    plottnpostkposmag30, 1], LineLegend[{Blue}, {"Thick Aluminum Layer"}]],
  AxesLabel → {Pressure (Torr), Current nAmp}, PlotLabel →
   "Thin Positive Then Thick Negative; Close With Magnets", PlotRange → All,
  AxesOrigin → {0, pivottnpostkposmag30}] /. {(Ticks → {xdat_, ydat_}) :→
   Ticks → {xdat, Join[ydat, {2 pivottnpostkposmag30 - #, ##2} & @@@ ydat]}}
Grid[tnpostkposmag, Frame -> All]
```

Out[805]=

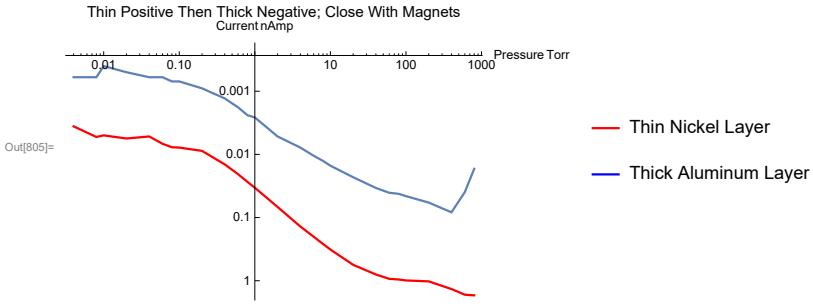

Out[806]=

Torr	Thin	Thick
800	-1.703	-0.0169
600	-1.6645	-0.0397
400	-1.3541	-0.0826
200	-1.0245	-0.0579
100	-0.99	-0.0458
80	-0.9554	-0.0421
60	-0.9333	-0.0405
40	-0.7965	-0.034
20	-0.5602	-0.023
10	-0.3209	-0.0151
8	-0.2624	-0.0127
6	-0.201	-0.0105
4	-0.1386	-0.0078
2	-0.068	-0.0052
1	-0.0337	-0.0026
0.8	-0.0273	-0.0024
0.6	-0.0206	-0.0018
0.4	-0.0144	-0.0013
0.2	-0.0088	-0.0009
0.1	-0.0078	-0.0007
0.08	-0.0077	-0.0007
0.06	-0.0068	-0.0006
0.04	-0.0052	-0.0006
0.02	-0.0056	-0.0005
0.01	-0.005	-0.0004
0.008	-0.0053	-0.0006
0.004	-0.0036	-0.0006

In[807]:=
```
twotnpostkposside = Import["ThinPosThickPosTwoandaHalfToTheSide.txt", "Table"];
twtnptkpsidep = twotnpostkposside[[1 ;;, 1]];
twtnptkpside3 = twotnpostkposside[[1 ;;, 2]];
twtnptkpside30 = twotnpostkposside[[1 ;;, 3]];
plottwotnpostkposside3 =
  ListLogLogPlot[Partition[Riffle[twtnptkpsidep, Abs[twtnptkpside3]], 2],
   Joined → True, PlotStyle → Red];
plottwotnpostkposside30 = ListLogLogPlot[
   Partition[Riffle[twtnptkpsidep, Abs[twtnptkpside30]], 2],
   Joined → True, Ticks → {Automatic, {.001, .01, .1, 1}}];
pivottwotnpostkposside30 = Last[AxesOrigin /. Options[plottwotnpostkposside30]];
Show[Legended[MapAt[Scale[#, {1, -1}, {0, pivottwotnpostkposside30}] &,
    plottwotnpostkposside30, 1], LineLegend[{Blue}, {"Thick Aluminum Layer"}]],
  Legended[MapAt[Scale[#, {1, -1}, {0, pivottwotnpostkposside30}] &,
    plottwotnpostkposside3, 1], LineLegend[{Red}, {"Thin Nickel Layer"}]],
  AxesLabel → {Pressure (Torr), Current nAmp},
  PlotLabel → "Thin Positive Then Thick Positive; Two and a Half to the Side",
  PlotRange → All, AxesOrigin → {0, pivottwotnpostkposside30}] /.
 {(Ticks → {xdat_, ydat_}) :→
   Ticks → {xdat, Join[ydat, {2 pivottwotnpostkposside30 - #, ##2} & @@@ ydat]}}
Grid[twotnpostkposside, Frame -> All]
```

Out[814]=

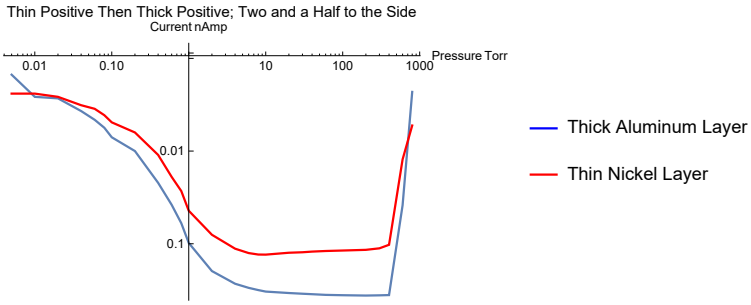

Out[815]=

Torr	Thin	Thick
800	-0.0053	0.0023
600	-0.0123	-0.0384
400	-0.1026	-0.3577
300	-0.112	-0.36
200	-0.1163	-0.362
100	-0.1183	-0.359
60	-0.1197	-0.356
40	-0.1215	-0.35
30	-0.1235	-0.346
20	-0.125	-0.34
10	-0.131	-0.328
8	-0.1307	-0.316
6	-0.126	-0.299
4	-0.113	-0.27
2	-0.08	-0.197
1	-0.044	-0.098
0.8	-0.027	-0.06
0.6	-0.019	-0.038
0.4	-0.011	-0.022
0.2	-0.0063	-0.01
0.1	-0.0049	-0.0071
0.08	-0.0041	-0.0056
0.06	-0.0035	-0.0046
0.04	-0.0032	-0.0037
0.02	-0.0026	-0.0027
0.01	-0.0024	-0.0026
0.005	-0.0024	-0.0015

APPENDIX C

COLLECTED DATA

All of the current values in the following data sets are in nAmps. The error in all of the current measurements with values less than 2 nA is $\pm$ .0001 nA. The error in the current range of 2 nA to 20 nA is $\pm$ .001 nA, according to Keithley [18]. The error in the pressure measurement at varying pressures can be seen in the first data set, according to Schaefer [19]

Error in Pressure Measurement

Measured Pressure Range	Error in Measurement
0-48 mTorr	1 mTorr
48-193 mTorr	2 mTorr
193-290 mTorr	3 mTorr
290-400 mTorr	4 mTorr
400-850 mTorr	5 mTorr
850-995 mTorr	6 mTorr
1-2 Torr	.01 Torr
2-3.64 Torr	.02 Torr
3.64-4.4 Torr	.03 Torr
4.4-5.6 Torr	.04 Torr
5.6-8 Torr	.05 Torr
8-8.4 Torr	.06 Torr
8.4-9 Torr	.07 Torr
9-9.95 Torr	.08 Torr
10-12.3 Torr	.1 Torr
12.3-18.2 Torr	.2 Torr
18.2-22 Torr	.3 Torr
22-24 Torr	.4 Torr
24-33 Torr	.5 Torr
33-50 Torr	1 Torr
50-64 Torr	2 Torr
64-76 Torr	3 Torr
76-90 Torr	4 Torr
90-95 Torr	5 Torr
100-240 Torr	10 Torr

240-535 Torr	5 Torr
535-960 Torr	10 Torr

Single Thick Aluminum Sheet

Torr	Aluminum Current nA
800	0.0182
750	0.0206
700	0.0225
650	0.0244
600	0.0265
550	0.0287
500	.0314
450	0.0353
400	0.0409
350	.0572
300	0.0909
250	0.1137
200	0.1254
150	0.1332
100	0.1378
90	0.1384
80	0.1398
70	0.1399
60	0.1401
50	0.1416
40	0.1412
30	0.1365
20	0.1240
10	0.0916
9	0.0852
8	0.0779
7	0.0701
6	0.0618
5	0.0531
4	0.0437

3	0.0336
2	0.0219
1	0.0104
0.954	0.0097
0.9	0.0092
0.85	0.0086
0.8	0.008
0.75	0.0067
0.7	0.0062
0.65	0.0057
0.6	0.005
0.55	0.005
0.5	0.0046
0.45	0.0043
0.4	0.0039
0.35	0.0035
0.3	0.0031
0.25	0.0028
0.2	0.0026
0.15	0.0023
0.1	0.002
0.09	0.002
0.08	0.002
0.07	0.002
0.06	0.0019
0.05	0.0019
0.04	0.0018
0.03	0.0018
0.02	0.0018
0.01	0.0018
0.009	0.0017
0.008	0.0017
0.007	0.0018
0.006	0.0019
0.005	0.0018
0.004	0.0019

0.003	0.002
0.002	0.0019
0.001	0.002

Thin Then Thick; Close

Torr	Thin	Thick
999	0.1442	0.0002
720	0.173	0.0003
585	0.209	0.0003
400	0.258	0.0012
350	0.251	0.0015
290	0.219	0.0016
200	0.205	0.0015
150	0.191	0.0015
100	0.18	0.0015
70	0.173	0.0014
55	0.165	0.0014
40	0.15	0.0013
28	0.135	0.0013
19	0.118	0.0011
10	0.081	0.0008
8	0.067	0.0007
6	0.057	0.0005
4	0.044	0.0003
2	0.026	0.0001
1	0.015	0
0.9	0.0131	0
0.8	0.011	0
0.7	0.009	0
0.6	0.0087	0
0.5	0.0071	0
0.4	0.0059	0
0.3	0.0043	0
0.2	0.003	-0.0001
0.1	0.0022	-0.0002

0.09	0.0019	-0.0002
0.08	0.0018	-0.0002
0.07	0.0013	-0.0002
0.06	0.0015	-0.0003
0.05	0.0019	-0.003
0.04	0.0011	-0.0003
0.03	0.001	-0.0003
0.02	0.0008	0
0.01	0.0006	-0.0003
0.008	0.0005	-0.0003
0.006	0.0005	-0.0003
0.004	0.0004	-0.0003
0.002	0.0004	-0.0003

Thick Then Thin; Close

Torr	Thin	Thick
999	0.0001	0.06
800	0.0029	0.078
700	0.0055	0.0947
600	0.0098	0.1093
500	0.0217	0.1433
400	0.0353	0.2296
300	0.0295	0.2245
100	0.0205	0.1954
50	0.018	0.1849
40	0.0161	0.1687
20	0.0126	0.139
10	0.0084	0.094
5	0.0046	0.055
2	0.0021	0.031
1	0.0011	0.02
0.93	na	0.0142
0.845	na	0.0128
0.8	0.0007	0.012
0.76	na	0.0114

0.675	na	0.0102
0.573	na	0.0086
0.5	0.0005	0.0092
0.488	na	0.0073
0.4	0.0003	0.0063
0.4	na	0.006
0.3	0.0002	0.0047
0.3	na	0.0043
0.2	0.0001	0.0033
0.1	0	0.0025
0.08	na	0.0021
0.06	na	0.0018
0.04	na	0.0016
0.02	na	0.0013
0.01	0	0.0011
0.008	na	0.0011
0.006	na	0.001
0.004	na	0.001
0.002	na	0.001
0.001	na	0.001

Thin Then Thick; Far

Torr	Thin	Thick
999	0	na
700	na	0.0218
600	0.0002	0.0527
500	0.0097	0.0777
400	0.0326	0.0936
300	0.0333	0.0893
200	0.03	0.0857
100	0.029	0.0847
50	0.027	0.0845
30	0.025	0.0837
10	0.019	0.08
5	0.011	0.06

3	0.008	0.042
2	0.005	0.031
1	0.003	0.017
0.8	0.002	0.014
0.6	0.0017	0.011
0.4	0.0011	0.009
0.3	0.0008	0.007
0.2	0.0005	0.005
0.1	0.0004	0.004
0.08	0.0003	0.003
0.06	0.0002	0.02
0.04	0.0001	0.02
0.03	0.0001	0.013
0.02	0	0.001
0.01	0	0.0005
0.008	0	0.0006
0.005	0	0.0004
0.003	0	0.0004
0.001	0	0.0002

To the Side; Far

Torr	Thin	Thick
999	na	0.0002
800	0	0.0005
700	0.0002	0.005
501	0.007	0.0284
400	0.015	0.04
300	0.02	0.05
200	0.022	0.053
100	0.02	0.054
50	0.015	0.055
40	0.026	0.054
20	0.026	0.053
10	0.0237	0.049
5	0.018	0.035

2	0.0132	0.023
1	0.0067	0.01
0.7	0.0046	0.008
0.5	0.0036	0.0066
0.4	0.0029	0.0055
0.2	0.0017	0.0032
0.1	0.0009	0.0024
0.05	0.0007	0.0013
0.02	0.0002	0.0006
0.01	0.0001	0.0003
0.005	0	0.0002
0.003	0	0.0001

Thin Then Thick; Close and With Magnets

Torr	Thin	Thick
999	0.105	0.0003
700	0.146	0.0001
600	0.156	0.0002
500	0.179	0.0005
400	0.176	0.0015
300	0.148	0.0018
200	0.132	0.0026
100	0.121	0.0024
50	0.112	0.002
40	0.107	0.0023
30	0.101	0.0021
20	0.09	0.0018
10	0.063	0.0012
8	0.052	0.0009
6	0.045	0.0008
4	0.035	0.0007
2	0.023	0.0005
1	0.012	0.0002
0.8	0.0095	0.0001
0.6	0.0073	0.0001

0.4	0.0042	0
0.2	0.0022	0
0.1	0.0012	0
0.05	0.0009	0
0.04	0.0006	0
0.01	0.0002	0

To the Side; Far and With Magnets

Torr	Thin	Thick
800	-0.0193	-0.0017
600	-0.0167	-0.0703
400	-0.0282	-0.3001
200	-0.0472	-0.3221
100	-0.054	-0.331
80	-0.0537	-0.3226
60	-0.056	-0.3335
40	-0.0577	-0.324
20	-0.0631	-0.3142
10	-0.0607	-0.3002
8	-0.0571	-0.2991
6	-0.0497	-0.2782
4	-0.0413	-0.2479
2	-0.0221	-0.1703
1	-0.0115	-0.0875
0.8	-0.0079	-0.0625
0.6	-0.0078	-0.0443
0.4	-0.005	-0.0227
0.2	-0.0059	-0.0114
0.1	-0.0055	-0.0062
0.08	-0.0055	-0.0053
0.06	-0.0045	-0.0041
0.04	-0.0051	-0.0032
0.02	-0.0045	-0.0017
0.01	-0.0048	-0.0018
0.008	-0.0035	-0.001
0.004	-0.0046	-0.0012

Thick Negative Then Thin Negative; Close

Torr	Thin	Thick
800	0.023	2.18
600	0.049	2.25
400	0.11	1.66
300	0.082	1.24
200	0.064	0.97
100	0.051	0.84
60	0.048	0.75
40	0.042	0.63
30	0.038	0.55
20	0.033	0.47
10	0.022	0.31
8	0.019	0.23
6	0.016	0.19
4	0.012	0.13
2	0.008	0.075
1	0.005	0.037
0.8	0.005	0.028
0.6	0.004	0.022
0.4	0.0032	0.015
0.2	0.0028	0.009
0.1	0.0027	0.0079
0.08	0.0026	0.0065
0.06	0.0026	0.0059
0.04	0.0025	0.005
0.02	0.0025	0.0043
0.01	0.0024	0.0039
0.005	0.0024	0.0032

Thick Positive Then Thin Positive; Close

Torr	Thin	Thick
800	-0.0105	-2.11
600	-0.0241	-2.21

400	-0.054	-1.9
300	-0.034	-1.49
200	-0.025	-1.18
100	-0.025	-1
60	-0.023	-0.857
40	-0.023	-0.708
30	-0.021	-0.622
20	-0.021	-0.493
10	-0.015	-0.279
8	-0.014	-0.22
6	-0.011	-0.165
4	-0.009	-0.11
2	-0.005	-0.053
1	-0.0038	-0.028
0.8	-0.0027	-0.028
0.6	-0.0028	-0.015
0.4	-0.0025	-0.011
0.2	-0.0022	-0.008
0.1	-0.0021	-0.007
0.08	-0.0021	-0.0067
0.06	-0.002	-0.0064
0.04	-0.002	-0.0062
0.02	-0.002	-0.0059
0.01	-0.002	-0.0058
0.005	-0.002	-0.0058

Thin Negative Then Thick Unbiased; Close

Torr	Thin	Thick	Torr
999	2	-0.0091	999
700	1.97	-0.0084	700
500	1.81	0.007	500
400	1.04	-0.0021	400
300	0.894	-0.0012	300
200	0.742	-0.0005	200
100	0.66	-0.0003	80

80	0.63	-0.0001	60
40	0.53	0	40
20	0.39	0	20
10	0.243	0.0002	10
6	0.176	0.0003	8
4	0.143	0.0001	6
2	0.081	0	4
1	0.041	0	2
0.8	0.028	0	1
0.6	0.021	0	0.8
0.4	0.015	0	0.6
0.2	0.0095	0	0.4
0.1	0.0074	0	0.2
0.08	0.006	0	0.1
0.06	0.0055	0	0.08
0.04	0.0046	0	0.06
0.02	0.0038	0	0.04
0.01	0.003	0	0.02
0.005	0.0028	0	0.01
0	0	0	0.005

Thin Negative Then Thick Negative; Close

Torr	Thin	Thick
999	1.91	0.016
900	1.91	0.015
700	1.83	0.018
600	1.79	0.024
500	1.63	0.044
400	1.27	0.059
300	0.836	0.047
200	0.722	0.042
100	0.66	0.039
50	0.57	0.037
20	0.42	0.033
10	0.306	0.028

8	0.244	0.023
4	0.148	0.018
3	0.118	0.015
2	0.084	0.013
1	0.05	0.008
0.3	0.019	0.0034
0.25	0.017	0.0025
0.2	0.014	0.002
0.175	0.014	0.002
0.15	0.0131	0.0019
0.1	0.0124	0.0015
0.05	0.0098	0.0011
0.03	0.0097	0.0009
0.01	0.0078	0.0006
0.006	0.0076	0.0006
0.002	0.0073	0.0004

Thin Positive Then Thick Unbiased; Close

Torr	Thin	Thick	Torr
999	-1.88	0.0167	999
700	-1.89	0.0106	700
500	-1.67	0.0096	500
400	-1.32	0.0028	400
300	-1.04	0.0018	200
200	-0.92	0.0015	60
100	-0.87	0.001	10
80	-0.84	0.0006	6
60	-0.79	0.0003	2
40	-0.69	0	0.8
20	-0.45	0	0.1
10	-0.26	0	0.06
8	-0.2	0.0001	0.005
6	-0.15	0	0
4	-0.11	0	0
2	-0.06	0	0

1	-0.027	0	0
0.8	-0.018	0	0
0.6	-0.014	0	0
0.4	-0.01	0	0
0.2	-0.0073	0	0
0.1	-0.0065	0	0
0.08	-0.0062	0	0
0.06	-0.006	0	0
0.04	-0.0058	0	0
0.02	-0.0056	0	0
0.01	-0.0055	0	0
0.005	0.0055	0	0

Thin Positive Then Thick Negative; Close

Torr	Thin	Thick
999	-1.78	0.05
700	-1.78	0.04
400	-1.36	0.054
200	-1.04	0.045
100	-1	0.043
50	-0.89	0.04
20	-0.58	0.034
10	-0.34	0.029
5	-0.17	0.017
2	-0.06	0.011
1	-0.03	0.008
0.5	-0.02	0.0046
0.2	-0.014	0.0022
0.1	-0.012	0.0018
0.08	-0.012	0.0015
0.05	-0.011	0.0012
0.02	-0.011	0.0009
0.01	-0.01	0.0008
0.005	-0.01	0.0007
0.001	-0.01	0.0007

Thin Positive Then Thick Positive; Close

Torr	Thin	Thick
999	-1.93	-0.0195
900	-1.75	-0.015
700	-1.96	-0.018
600	-1.74	-0.026
500	-1.63	-0.043
400	-1.36	-0.057
300	-1.13	-0.047
200	-1.03	-0.042
100	-0.97	-0.035
50	-0.879	-0.032
20	-0.56	-0.027
10	-0.326	-0.023
8	-0.238	-0.02
4	-0.1294	-0.0121
3	-0.101	-0.0114
2	-0.07	-0.0076
1	-0.037	-0.0042
0.3	-0.0135	-0.0012
0.25	-0.0128	-0.0012
0.2	-0.0124	-0.0011
0.175	-0.0121	-0.0011
0.15	-0.0115	-0.001
0.12	-0.0114	-0.001
0.1	-0.011	-0.001
0.08	-0.0108	-0.001
0.05	-0.0102	-0.001
0.03	-0.0103	-0.001
0.01	-0.0102	-0.0012
0.006	-0.0102	-0.0011
0.002	-0.0106	-0.001

Thin Positive Then Thick Negative; Close With Magnets

Torr	Thin	Thick
800	-1.703	-0.0169
600	-1.6645	-0.0397
400	-1.3541	-0.0826
200	-1.0245	-0.0579
100	-0.99	-0.0458
80	-0.9554	-0.0421
60	-0.9333	-0.0405
40	-0.7965	-0.034
20	-0.5602	-0.023
10	-0.3209	-0.0151
8	-0.2624	-0.0127
6	-0.201	-0.0105
4	-0.1386	-0.0078
2	-0.068	-0.0052
1	-0.0337	-0.0026
0.8	-0.0273	-0.0024
0.6	-0.0206	-0.0018
0.4	-0.0144	-0.0013
0.2	-0.0088	-0.0009
0.1	-0.0078	-0.0007
0.08	-0.0077	-0.0007
0.06	-0.0068	-0.0006
0.04	-0.0052	-0.0006
0.02	-0.0056	-0.0005
0.01	-0.005	-0.0004
0.008	-0.0053	-0.0006
0.004	-0.0036	-0.0006

Thin Positive Then Thick Positive; Far to the Side

Torr	Thin	Thick
800	-0.0053	0.0023
600	-0.0123	-0.0384
400	-0.1026	-0.3577
300	-0.112	-0.36

200	-0.1163	-0.362
100	-0.1183	-0.359
60	-0.1197	-0.356
40	-0.1215	-0.35
30	-0.1235	-0.346
20	-0.125	-0.34
10	-0.131	-0.328
8	-0.1307	-0.316
6	-0.126	-0.299
4	-0.113	-0.27
2	-0.08	-0.197
1	-0.044	-0.098
0.8	-0.027	-0.06
0.6	-0.019	-0.038
0.4	-0.011	-0.022
0.2	-0.0063	-0.01
0.1	-0.0049	-0.0071
0.08	-0.0041	-0.0056
0.06	-0.0035	-0.0046
0.04	-0.0032	-0.0037
0.02	-0.0026	-0.0027
0.01	-0.0024	-0.0026
0.005	-0.0024	-0.0015

APPENDIX D

CIRCUIT DIAGRAMS

The circuit diagram for the off board custom charge amplifier. The amplifier used is an IVC102

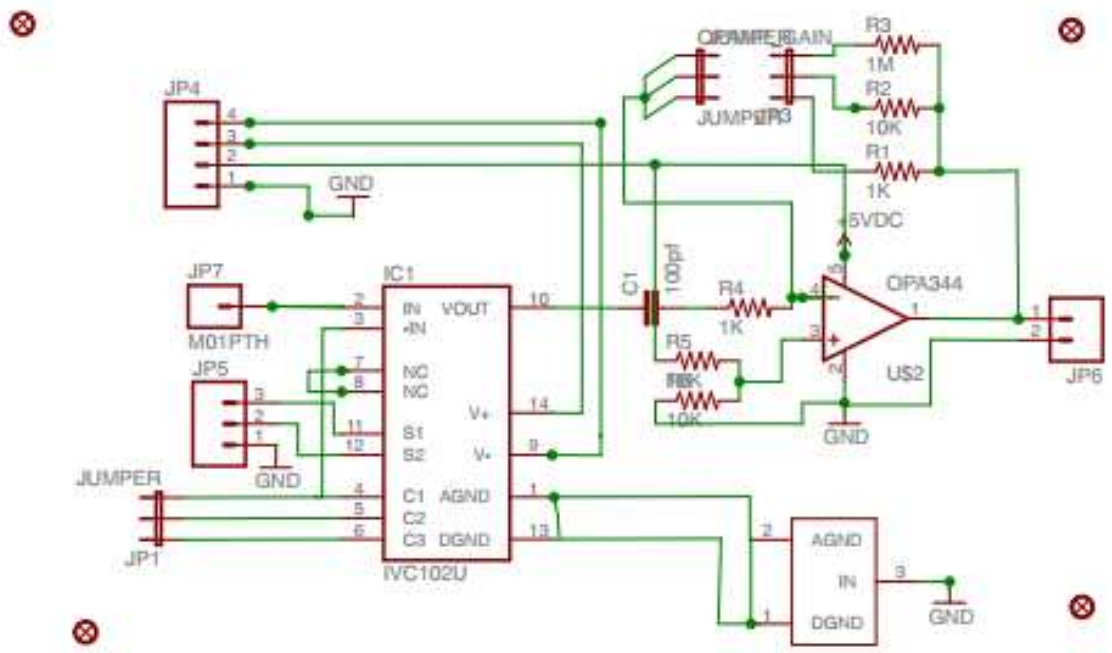

Figure D.1: Off board custom charge integrator

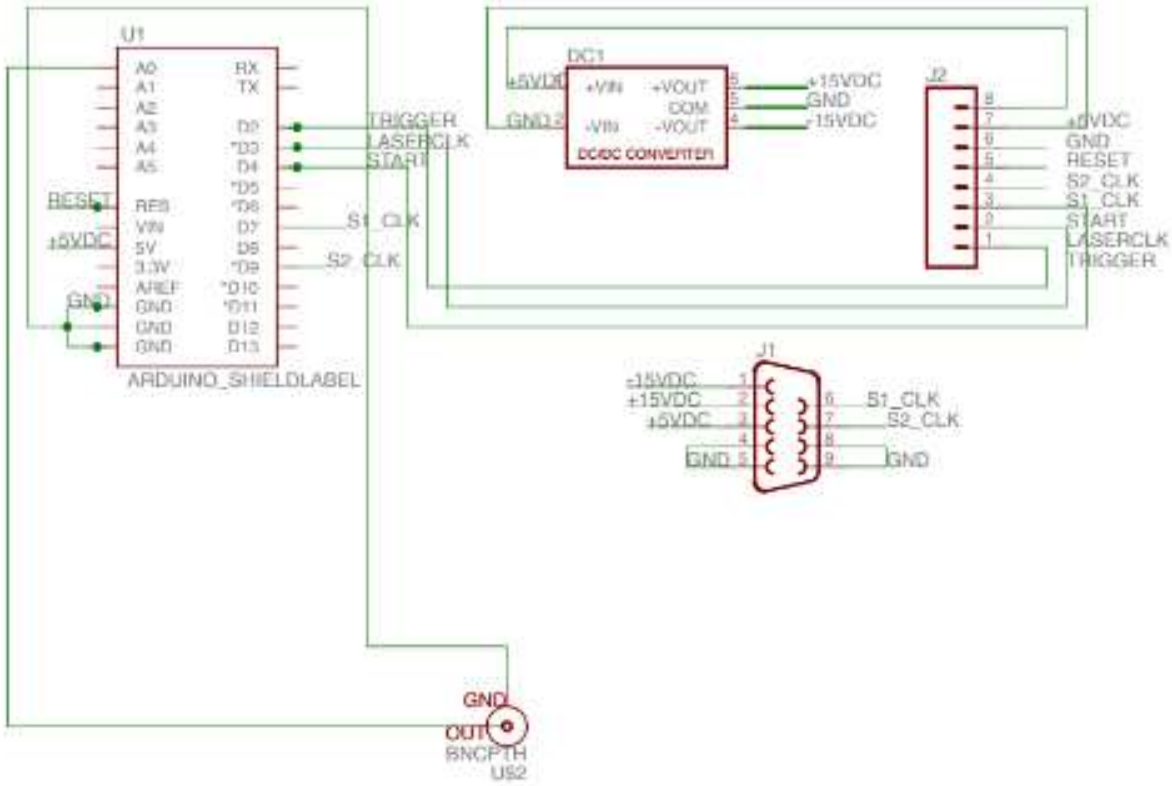

Figure D.2: The connection of the basic circuit to the Arduino